Investigating the role of the Hippo pathway in epithelial-mesenchymal transition and drug resistance

Andrew Bondesson

A dissertation

submitted in partial fulfillment of the

requirements for the degree of

Doctor of Philosophy

University of Washington

2021

Reading Committee:

Taranjit S. Gujral, Chair

David Hockenbery

Jason Bielas

Program Authorized to Offer Degree:

Molecular and Cellular Biology

University of Washington

Abstract

Investigating role of the Hippo pathway in epithelial-mesenchymal transition and drug resistance

Andrew Bondesson

Chair of the Supervisory Committee:

Taranjit S. Gujral

The Hippo pathway is an evolutionarily conserved signaling cascade and comprises the core Hippo kinases MST1/2 and LATS1/2, which phosphorylate the transcriptional YES associated protein (YAP), promoting its nuclear exclusion and degradation. Excess YAP activity is oncogenic and is commonly observed in various human malignancies. Despite increased understanding of phenotypes associated with Hippo aberration and excess YAP activity, specific mediators of YAP-driven phenotypic changes remain elusive. In this thesis, I present two projects investigating the kinome signaling downstream of YAP and a survey of YAP-activity mediated changes to drug response. In the first project, I describe the first comprehensive survey of kinome signaling downstream of YAP. YAP hyper-activity results in widespread changes to the activity state of the kinome. I identified the ZAK kinase as highly phosphorylated in YAP-driven cells and identified a strong correlation with this kinase in mesenchymal-like cells. Inhibition of ZAK reversed the mesenchymal phenotype, and overexpression of ZAK resulted in epithelial-mesenchymal transition (EMT). Analysis of The Cancer Genome Atlas (TCGA) data shows a strong correlation between ZAK expression and mesenchymal-characterized tumors and Hippo pathway output. These data implicate the ZAK kinase as a critical mediator of YAP-driven EMT and provide an in-depth look at

kinome signaling changes resulting from YAP activity. In the second project, I investigated YAP-mediated changes to the cellular response to a collection of >2000 compounds. To uncover therapeutic vulnerabilities caused by increased YAP activity, I analyzed results from a quantitative, high-throughput chemical screen in Panc02.13 cells, a pancreatic ductal adenocarcinoma (PDAC) cell line. I confirmed previously annotated resistances and sensitivities conferred by YAP-activity and identified a significant resistance to MEK inhibition (MEKi) in YAP-driven cells. This resistance was robust; YAP-driven cells survived MEKi treatment even with a combined inhibition of common compensatory signaling through pro-survival kinase, AKT and receptor tyrosine kinase, AXL. Follow-up studies identified alterations in the expression of at least four apoptotic regulators and EMT transcription factors. Thus, I posit that YAP-induced EMT enables resistance to MEK inhibitors through kinome re-wiring and apoptotic re-programming changes. These results may help explain the failure of MEKi targeted therapy in clinical trials treating PDAC. Overall, these studies provide a comprehensive overview of the signaling landscape downstream of aberrant YAP activity and may be useful in understanding how aberrant Hippo signaling results in resistance to targeted therapy.

Acknowledgements

I thank firstly the present and former members of the Gujral lab for providing a fantastic environment in which to conduct this work. I thank Dr. Taran Gujral for his mentorship and patience while I rose to the demands of graduate school and in becoming a research scientist. I thank Drs. Marina Chan and Nao Naoki for their time and conversation during my constant question asking. I also thank Stella Shin for her incredible organization, attitude and skills in the lab. I would like to extend a special thank you and a deep respect for my lab mate Dr. Thomas Bello, who for the past 4 years has been a reliable companion through the trials of the Molecular and Cell Biology Program at the University of Washington. Having a partner to share successes and failures with was an enormous boon throughout these studies. I sincerely appreciate all of the advice, editing and scientific input he has provided, all of which has had a serious beneficial impact on this dissertation.

I would like to thank my many collaborators: Dr. Martin Golkowski, who's expertise in phosphoproteomics was an invaluable resource in gathering and interpreting data that forms the backbone of this thesis. I also thank Dr. Michele Ceribelli who was very helpful in performing the MIPE screen and who's conversations provided valuable insight into Hippo influences on drug response. I also am very thankful for the skills of Andrew Xue who's statistical and computational efforts helped to broaden the scope of this work significantly.

I thank my parents, Jeff, and Kelly Bondesson, for their unwavering support through graduate school and in the rest of my life. I have always relied on them for advice in all manners of my life, science notwithstanding. I thank my brother and sister for their encouragement and perspective, as well as for their visits, which have brought a lasting brightness to living in Seattle. I thank my friends in Seattle, and particularly Ian Bloom, who's arrival heralded some of the best (and continuing) times I've had living in the northwest.

I thank my girlfriend Ashley Anderson, whose presence and companionship has made the last year infinitely better. There is nothing finer than being with you. You are an amazing person

and I continue to be amazed at how lucky I am to be your partner. I love you and I hope our days will continue to be long and joyful together.

Finally, I acknowledge that this work was carried out on the unceded ancestral lands of the Duwamish people, and honor with gratitude the land and the Duwamish tribe.

Specific contributions

Chapter 2

The phosphoproteomic screens and data processing were performed by Dr. Martin Golkowski at the University of Washington in Seattle.

The HCC line correlation matrix (Figure 2.2.3D) was generated by Dr. Taran Gujral at the Fred Hutchinson Cancer Research Center.

The FZD2 knockdown experiments and associated figure (Figure 2.2.3F) were performed and generated, respectively, by Dr. Taran Gujral at the Fred Hutchinson Cancer Research Center.

The TCGA analysis (Figure 2.2.6) was performed by Andrew Xue at the Fred Hutchinson Cancer Research Center.

Some of the results shown in this chapter here are in whole or part based upon data generated by the TCGA Research Network: https://www.cancer.gov/tcga.

Chapter 3

The MIPE screen was performed by Dr. Michelle Ceribelli at the National Center for the Advancement of Translational Science in Bethesda Maryland.

The western blot of Figure 3.2.2A was performed by Aya Miyaki.

Funding sources

The Fred Hutchinson Cancer Research Center Chromosome Metabolism and Cancer Training Grant, Fred Hutchinson Cancer Research Center New Investigator Startup Fund.

Table of Contents

List of Figures

Chapter 1: Introduction

The Hippo pathway is an evolutionarily conserved signaling pathway composed of several kinases that modify the activity of the transcriptional co-activators Yes-assocaited protein (YAP) and Tafazzin (TAZ). The Hippo signaling pathway touches many areas of biology, from the earliest stages of development, to the later stages of cancer metastasis. This dissertation describes results from systems-based projects investigating YAP-mediated effects on kinase signaling and cancer drug response. This chapter will serve as an introduction to these topics and the motivation for this work.

In part 1 of this introduction, I will provide a brief history of the discovery of the Hippo pathway, followed by a non-exhaustive description of the various signaling phenomena that serve as upstream regulators of Hippo pathway signaling. I will conclude with a description of the output of the Hippo pathway as mediated by YAP and TAZ with a focus on their effects in mammalian contexts and in promoting cancer. Part 2 will introduce the epithelial-to-mesenchymal transition (EMT)—a critical cellular state change associated with development and cancer progression—and Hippo pathway involvement in EMT signaling. Finally, part 3 will discuss mechanisms of resistance to anticancer drugs and the relationship between dysregulated Hippo signaling and altered drug response.

1.1 The Hippo pathway: an overview

1.1.1 Discovery of the core components of the Hippo signaling pathway

The initial discovery of the Hippo pathway's core components took place in the 1990s and 2000s in *Drosophila melanogaster,* where several groups used mutagenesis screens to identify genes causing tissue overgrowth. The *Drosophila* gene Warts (*Wts*) was the first such gene discovered in 1995 and was named due to the wart-like overgrowth of affected tissues[1,2]. Years later, the rest of the core signaling cassette was identified via similar mutagenesis screens searching for genes that phenocopied *Wts* disruption: Salvador (*Sav*)[3,4] in 2002, followed by Hippo

(*Hpo*)[5-9], the pathway's namesake, in 2003. Mob as tumor suppressor (*Mats*)[10] was later identified in 2005 as a scaffolding protein partner to *Wts*. *Hpo*, *Wts,* and their associated scaffolding proteins comprise what is known as the "core" Hippo signaling module. This module was finally tied to transcriptional output when *Yki* was discovered as the penultimate effector of Hippo pathway signaling in 2005[11]. However, *Yki* is a transcriptional coactivator that must bind to a transcriptional effector. This transcriptional partner (in the context of driving the Hippo phenotype) was found to be Scalloped (*Sd*) in 2008[12-14].

The Hippo pathway is highly evolutionarily conserved and has direct orthologs in humans. *Hpo* is homologous to the mammalian sterile 20-like 1, and 2 kinases (*MST1/2*, also called *STK3/4*), *Sav* to salvador family WW domain-containing protein 1 (*SAV1*), *Wts* to large tumor suppressor kinase 1 and 2 (*LATS1/2*), *Mats* to MOB kinase activator 1A/B (*MOB1a/b*), *Yki* to Yes-associated protein (*YAP*)/transcriptional co-activator with PDZ binding motif (*TAZ*)[15] and *Sd* is homologous to tea domain-containing protein 1-4 (*TEAD1-4*)[16]. The core signaling module of the hippo pathway functions similarly in mammals as it does in the fly[17] as seen in the similar organ overgrowth phenotypes observed in mice with deficiencies in MST1/2[18-20], SAV1[20], or with overexpression of YAP[21,22]. Mechanistically, activation of MST1/2 by upstream signaling promotes MST1/2 phosphorylation and activation of LATS1/2, which in turn phosphorylates YAP on several serine residues, including serine-127. Phosphorylated serine-127 creates a docking site for 14-3-3 proteins, which simultaneously results in the competitive exclusion of TEADs and promotes YAP nuclear exclusion[22,23]. Additional phosphorylation by LATS on YAP serine-381 primes YAP for phosphorylation via casein kinase 1 alpha 1 (CK1), which in turn creates a phosphodegron sequence recognized by the F-box protein β-TRCP, leading to ubiquitination and degradation of the YAP protein[24]. These two processes—nuclear-cytoplasmic shuttling and protein degradation—comprise the primary mechanisms through which YAP activity is controlled (Figure 1.1.1).

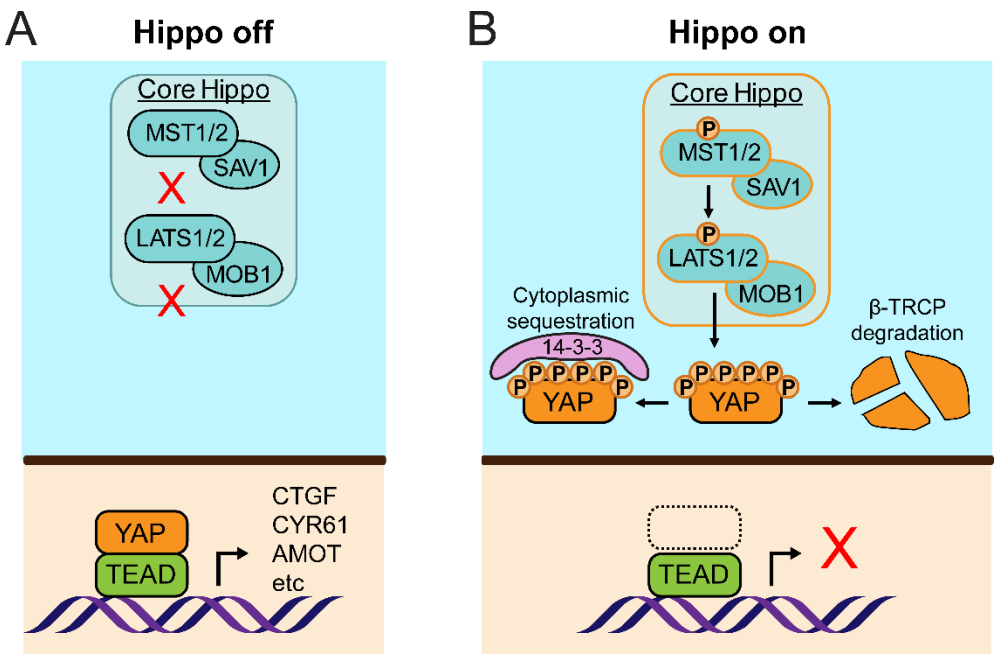

Figure 1.1.1 Schematic of the core Hippo pathway
The core of the Hippo pathway (teal box containing MST1/2, SAV1, LATS1/2 and MOB1), when deactivated allows the nuclear accumulation of YAP where it binds to TEADS, triggering expression of YAP/TEAD target genes such as CYR61, CTGF, etc (**A**). Activation of the Hippo pathway causes LATS1/2 mediated phosphorylation of YAP, causing its nuclear exclusion, sequestration by 14-3-3 proteins, and β-TRCP mediated degradation (**B**).

1.1.2 Regulation of the hippo pathway: upstream factors

Since the initial discovery of the core Hippo pathway kinases, there has been a concerted effort in identifying upstream molecular drivers that feed into Hippo pathway signaling. This has come to encompass at least 35 discrete regulators, which can broadly be categorized by their associated cell processes, including apical-basal polarity, cell-cell contact, cytoskeletal and mechanical cues, and soluble factor signaling (Figure 1.1.2)[25].

Apical-basal polarity

Apical-basal polarity is the establishment of specific membrane domains and intercellular contacts and is a critical aspect of organized epithelial tissue[26]. Components of apical-basal polarity machinery were identified early in *Drosophila* as regulators of Hippo signaling with the apically located Merlin (Mer, also *NF2* in mammals), Expanded (Ex) and Kibra[27,28]. These three proteins

enhance Hippo signaling by physically binding with Hippo components, localizing them to the apical domain, and activating downstream signaling[29]. Furthermore, Crumbs (Crb) is a critical transmembrane component involved in apical domain formation that binds to Ex in *Drosophila*, helping to localize Ex and its associated Hippo organizing capability to the apical domain[30,31]. While Ex is not well-conserved in mammals, mammalian Crumbs3 can nevertheless bind YAP/TAZ, promoting their cytoplasmic association[32]. This function is further aided through the activity of angiomotin (AMOT) proteins, which coordinate YAP and LATS1/2 binding at the Crumbs complex, fulfilling a similar role in apically organizing Hippo signaling to Ex in the fly[32-37]. The basolateral domain also potentiates Hippo signaling through Scribble (SCRIB), enhancing the association between MST and LATS[38]. Other components of the basolateral domain, such as lethal giant larvae (Lgl) and discs large homolog 5 (DLG5) have also been found to enhance Hippo signaling[39,40]. Additionally, liver kinase B1 (LKB1, also STK11) was shown to be essential in promoting the association between LATS1, MST1, and the basolateral complex[41].

Cell-cell contact

The Hippo pathway exhibits a striking ability to mediate cell-contact-mediated inhibition of growth, where cells cease to proliferate once growth conditions become crowded and cellular contact increases[23,42,43]. This process is likely aided by the formation of intercellular junctional complexes, one of the hallmarks of polarized epithelial cells[44]. Tight junctions are one such complex and are comprised of the transmembrane proteins claudins and occludins which form intercellular contacts that are connected to the actin cytoskeleton via ZO-1/2[44]. Tight junction protein ZO-2 binds YAP directly via its PDZ domain[45]. Furthermore, AMOT, in addition to its role in the Crumbs complex, is also capable of sequestering YAP and TAZ at tight junctions, binding to NF2 and enhancing NF2's activation of LATS1/2[35,36,46,47]. Adherens junctions are formed by cadherin transmembrane proteins that are connected to the cytoskeleton via β- and α-catenin[44]. Adherens junctions have also been implicated in Hippo signaling and were found to be a critical component

mediating cell-contact inhibition of growth—a Hippo phenotype[42]. For example, the adherens junction proteins E-cadherin[43], β-catenin[43] and α-catenin[48,49] have all been implicated as negative regulators of YAP. Interestingly, the inhibitory influence of E-cadherin and β-catenin on YAP were found to rely on Hippo signaling[43], whereas α-catenin was Hippo-independent[48,49], indicating multiple avenues for adherens junctions to control YAP activity.

Mechanical and cytoskeletal signaling

In addition to cell polarity and cell-cell contact, mechanical forces and the physical architecture of cells also affect YAP activity. Mechanotransduction was initially connected to YAP activity in 2011 when it was observed that cells grown on a stiff extra-cellular matrix (ECM) had increased nuclear YAP activity[50,51]. Moreover, cellular contexts in which the actin cytoskeleton can generate stress fibers and contractile force have higher YAP activity[50,51]. The role of the Hippo kinases in controlling YAP activity downstream of cytoskeletal cues is debated as various groups have reported LATS1/2 signaling as essential[51,52] or dispensible[50,53] for this effect. Thus it has been argued that Hippo pathway kinases are the major regulators of YAP activity only in the context of a baseline amount of cytoskeletal tension[54]. In any case, filamentous actin and high contractile force have a powerful effect on increasing YAP activity[54]. Mechanical sensing and force generation also occurs through the focal adhesion kinase (FAK) downstream of integrin attachment to fibronectin[55]. Activation of FAK has been shown in several studies to increase the nuclear localization of YAP[55-57]. Interestingly, in one such study, PDK1 was implicated as a scaffolding/organizing center for Hippo signaling, which is deactivated in response to FAK signaling[55], a system identified by the same authors to similarly influence YAP activity in response to mitogenic growth signaling[58].

Soluble factors

Several soluble factors have been implicated in Hippo pathway regulation. Notably, the effect of these factors on the Hippo pathway is contingent on their downstream signaling apparatus. For example, G-protein coupled receptors are a broad class of receptors that can activate and

inhibit YAP activity depending on which Gα subunit the individual receptor is bound to[59]. Lysophosphatidic acid (LPA)[58-60], sphingosine 1-phosphoate[59,60], and thrombin[61] were some of the first ligands identified to activate YAP through GPCRs coupled to $G\alpha_{12/13}$ specific subunits. Similarly, the $G\alpha_{q\text{-}11}$ subunit has been implicated as a positive regulator of YAP in estrogen[62] and angiotensin II[63] GPCRs. In contrast, ligands that activate GPCRs coupled to $G\alpha_s$ subunits such as glucagon and epinephrine have the opposite effect, increasing the phosphorylation of YAP[59]. This is underscored by findings that PKA signaling—a major downstream effector of $G\alpha_s$—activates LATS1/2 to increase YAP phosphorylation[64,65].

Other soluble factors can influence YAP activity independently of GPCRs, including EGF[58,66], IGF[67], glucocorticoids[68], WNT [69-71], and VEGF[72,73]. These ligands generally inhibit the Hippo pathway resulting in an increased transcriptional output of their associated genes through increased YAP activity. However, proposed mechanisms for these effects are diverse, even among papers reporting Hippo deactivation downstream of the same ligand. For instance, in EGFR signaling, Reddy *et al.* [66] implicate AJUBA family proteins in negative regulation of LATS1, whereas Fan and colleagues[58] identify activation of PI3K/PDK1 as the necessary negative regulator of LATS[58]. The influence of WNT ligands on the Hippo pathway is likewise controversial, where Azzolin *et al.* [70] report YAP as a member of the β-catenin destruction complex which is released upon WNT binding, in contrast to Park *et al.* [69], who report YAP activation occurs through non-canonical WNT signaling. Therefore, individually proposed mechanisms linking extracellular ligands to altered YAP activity may depend on cell-type specific contexts. Disparities in mechanistic underpinnings may also reflect overlapping and non-mutually exclusive regulatory machinery governing the control of YAP activity. Regardless of the upstream signaling mechanism, the crucial signaling point common to all is the control of YAP and TAZ activity within the nucleus.

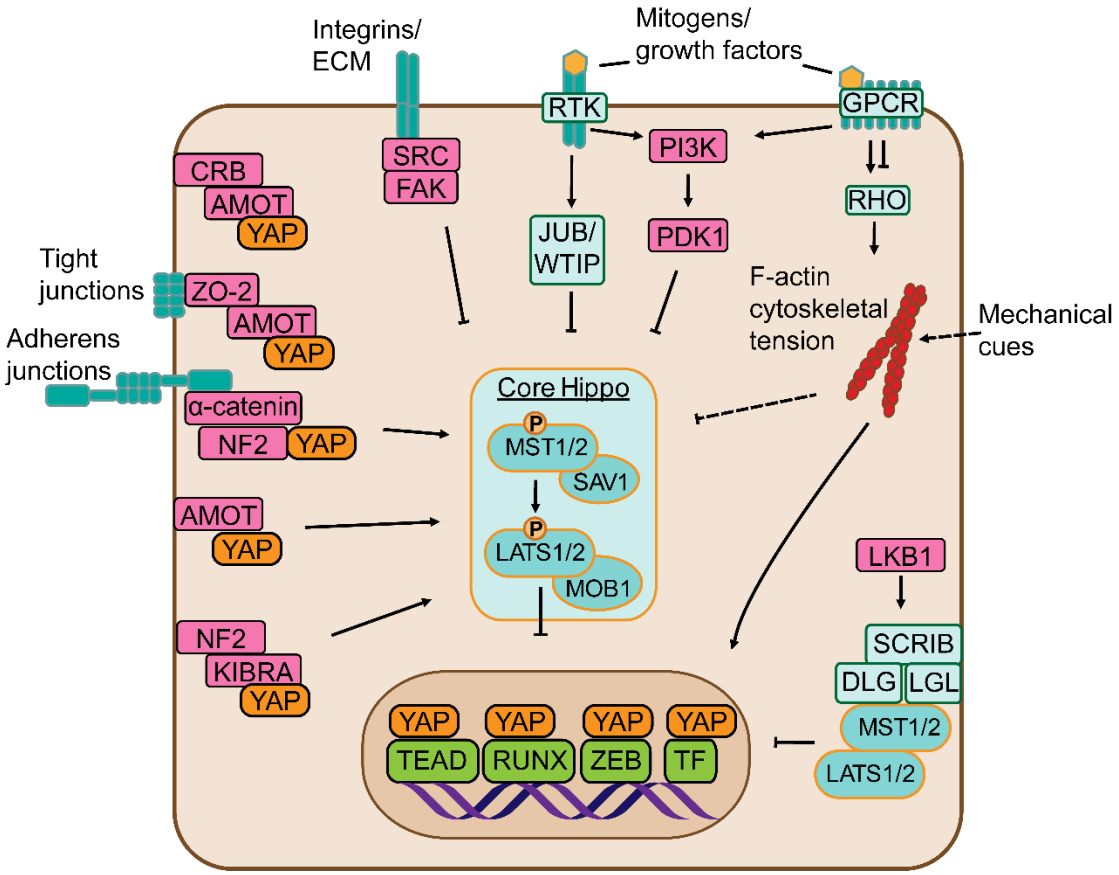

Figure 1.1.2 Upstream regulation of the Hippo pathway in mammals
Upstream activation of the Hippo pathway (teal box, center) is induced by mechanisms of cell adhesion (tight junctions, adherens junctions), apical-basal polarity complexes (CRB, SCRIB). The same core pathway is antagonized by integrin attachment and ECM interaction, mitogenic signaling through RTKs and PCRS, as well as mechanical cues mediated by the actin cytoskeleton. Modulations in Hippo pathway activity change the ability of YAP to bind to transcription factors (TEAD, RUNX, ZEB and others) in the nucleus.

1.1.3 Transcriptional output of the Hippo pathway

While the mechanics of upstream Hippo signaling are diverse and complex, they generally all lead to modifications of YAP and TAZ activity, positioning the two as the central watersheds of Hippo signaling[74]. YAP and TAZ cannot activate transcription themselves and therefore rely on binding to other transcription factors to promote the expression of target genes[54]. In the context of the Hippo pathway, TEAD1-4, homologs of the *Drosophila* Sd, are the primary mediators of YAP/TAZ transcriptional output in mammals[13,14,16,75-77]. This is supported by the fact that Sd and TEAD inhibition reverses the effect of Hippo mutation and are necessary for many Hippo-associated

phenotypes mediated by YAP[12-14]. TEADs are typically held in a default repressed state by VGLL4, which YAP and TAZ displace to activate gene transcription[78-80]. YAP/TAZ bind to TEADs via their TEAD binding domains[54], but they are capable of binding to a multitude of other transcription factors via their WW domains. These include, P73[81,82], WBP2[83,84], RUNX2[85-87], ERBB4[88,89], SMADS[32,90,91], ZEB1[92], SNAIL/SLUG [93] and others[54]. TEADs mediate a majority of the transcriptional output of YAP/TAZ within the nucleus[94,95]. However, functional studies have indicated the WW-domains are also essential in mediated the full transformational effects driven by YAP/TAZ activity[77,83].

Numerous studies have identified a common set of YAP-TEAD target genes, which include *CTGF, CYR61, ANKRD1, BIRC5,* and *AXL*, which have become *de facto* measures of YAP/TAZ transcriptional activity[54,96]. In addition to these genes, YAP can increase the expression of cell cycle-related genes and the DNA-replication machinery required by actively dividing cells[97]. Outside of this core set, YAP can alter the expression of thousands of genes across the genome[94,95]. Among these thousands, enrichment studies have consistently identified sets of genes associated with proliferation, epithelial-mesenchymal transition, migration, extracellular matrix organization, apoptosis, and other signaling pathways[94,96,98]. Many of these enriched features strongly overlap with the hallmarks of cancer[99]. Moreover, with few exceptions, YAP and TAZ driven gene expression is associated with oncogenic potential and worse prognosis in human cancers[96,100]. Indeed, Hippo mutation and YAP activity have been implicated in specifically driving several cancer hallmarks, including increased proliferation, increased cell survival, promoting cancer stem cell development, alterations to drug sensitivity, and increased metastasis (Figure 1.1.3)[100]. While many studies have focused on molecular regulators that drive YAP-mediated transcription, there have been comparatively fewer studies comprehensively examining signaling effectors downstream of YAP. This has resulted in a relative lack of information regarding YAP's specific effectors in a cell state change.

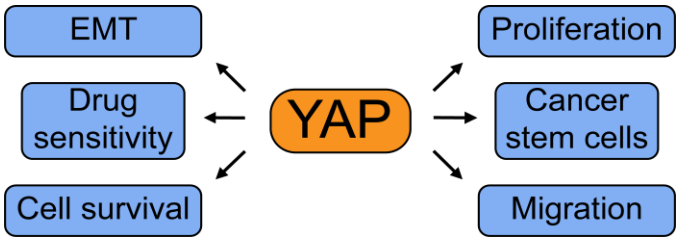

Figure 1.1.3 YAP-mediated oncogenic phenotypes
Excess yap activity motivates several oncogenic phenotypes including increases in EMT; alterations to drug sensitivity; increased proliferation, migration, cell survival and the generation of cancer stem cells.

1.2 Hippo, YAP, and the epithelial to mesenchymal transition

The epithelial-mesenchymal transition (EMT) is an important cellular transdifferentiation process that takes place at several stages in development, wound healing, and in cancer[101-103]. Epithelial cells are non-motile and are defined by their intercellular contact and apical-basal polarity. In contrast, mesenchymal cells are highly motile, have reduced cell-cell junctional complexes, and do not exhibit apical-basal polarity[101]. EMT represents the physical and behavioral transition from epithelial to mesenchymal cell states. EMT is an important process in normal development; however, dysregulation of EMT is a critical feature in invasion and metastasis in cancer[103].

1.2.1 Roles in development and cancer

EMT has been classified broadly into three different subtypes: 1) EMT involved in development, 2) inflammation and fibrosis, and 3) cancer-associated EMT. Developmental EMT occurs at several stages in development, including embryo implantation, the formation of the primitive streak, and the generation of neural crest cells that migrate throughout the developing embryo, eventually undergoing differentiation into neural, adrenal, and craniofacial connective tissue in the developing animal[102,104]. EMT is also important in wound healing in the adult animal, where cellular migration is necessary for reconstituting damaged epithelium[105]. Similarly, matrix remodeling in response to TGFβ signaling underlies a crucial aspect of the fibrotic response[105]. Finally, EMT is notoriously involved in cancer, and its dysregulation is thought to be a major

contributor to metastasis[103,106]. During metastasis, cellular dissemination from the primary tumor involves invasion and extravasation, both influenced by many of the same signaling pathways governing EMT in developmental and wound healing contexts. The plasticity induced by EMT is also a contributing factor in cancer stem cells' development, a subpopulation of tumor cells noted for their high tumor initiation capacity and metastatic ability[106,107].

1.2.2 Mechanisms of epithelial-to-mesenchymal transition

The epithelial cell state is defined by cell junctional and polarity complexes, which are the same as those described as positive regulators of the Hippo pathway *supra*. Cell-cell contact allows epithelial cells to adhere to each other and is accomplished primarily by tight junctions, adherens junctions, and desmosomes[101]. Desmosomes are similar to cadherins in structure and function; however, their constituent proteins and cytoskeletal linkages differ. Desmoglein and desmocollin form the extracellular contact points between cells and are linked to cytokeratin intermediate filaments via plakoglobin and plakophilin[44]. The combined work of adherens junctions, tight junctions, and desmosomes helps maintain an epithelial tissue's physical form and function.

Apical-polarity is maintained by three complexes: Crumbs, PAR, and Scribble[101]. The Crumbs and PAR complexes are responsible for defining the apical compartment and antagonizing the Scribble complex's activity, which defines the basolateral compartment[101]. These polarity defining complexes are integrally linked with the junctional architecture, forming a stable, polarized gestalt common to most epithelial tissue[101]. As cells transition from epithelial to mesenchymal cell state, junctional complexes dissolve, and expression of their components is reduced, leading to a collapse of the adhesive properties of cells and in the ability of polarity complexes to efficiently organize[108]. The dissolution of these complexes also imparts a major structural change to the cytoskeleton of cells undergoing EMT.

Mesenchymal cells have dramatically different cytoskeletal structures compared to epithelial cells. Several GTPases are involved in mesenchymal cell cytoskeletal dynamics and have

discrete functions. The GTPase RHOA is involved in reorganizing cortical actin to generate stress fibers, which are crucial in producing contractile forces necessary for motility[109]. Additionally, CDC42 and RAC1 are responsible for lamellipodia and filopodia (respectively)—actin organized membrane extensions that aid in migration and invasiveness of mesenchymal cells[109]. Notably, the same structures responsible for apical-basal polarity can be coopted by mesenchymal cells in determining front-rear polarity. The PAR complex and Crumbs complex are located at the front of migrating cells and aid in the organization of actin cytoskeletal dynamics of directional travel[109]. Migrating mesenchymal cells also express integrins on their leading-edge, enabling them to interact with and bind to the extracellular matrix (ECM) present in the stroma[101]. Cellular travel through tissue is also aided by the expression of matrix metalloproteinases (MMPs), which degrade the extracellular matrix, allowing easier passage for migrating cells[105]. The actin cytoskeleton's coordination with MMP and integrin expression allows mesenchymal cells to travel through stromal tissue. Such a dramatic change in cell behavior requires coordination at the transcriptional level to maintain the mesenchymal state.

The transcription factors SNAIL, TWIST, and ZEB are the three most prominent EMT transcription factors and function as master EMT regulators[110]. All three have complimentary and dual roles in reducing the expression of epithelial genes and increasing the expression of mesenchymal genes. Canonical epithelial genes downregulated by these factors include the very structures responsible for intercellular contact and apical-basal polarity, including ECAD, claudins, CRUMBS etc. Mesenchymal genes increased by these transcription factors have the mesenchymal specific N-cadherin (NCAD), MMPs, and ECM components such as fibronectin and collagen[101]. EMT transcription factors are activated in response to signaling pathway input, the most well characterized being TGFβ-SMAD signaling. SNAIL is activated in response to SMAD activity downstream of TGFβ, both in terms of SMAD increasing SNAIL expression, and in enhancing SNAIL-dependent transcription[111]. Numerous other signaling pathways feed into EMT at the level of

promoting SNAIL/TWIST/ZEB, including RTKs, NOTCH signaling, and inflammation[101]. These diverse inputs allow the EMT program to be activated at appropriate stages of development and in response to insult, however, they also provide avenues for dysregulation in the context of cancer.

1.2.3 Hippo regulation of EMT and *vice versa*

The Hippo pathway has a reciprocal relationship with EMT, being able to influence and be influenced by EMT. As has been elaborated previously, the Hippo pathway is activated by epithelial cell characteristics such as apical-basal polarity and cell junctional complexes. These serve to activate the Hippo kinases and directly sequester YAP in the cytoplasm and at the cell membrane. During the process of EMT, these complexes are downregulated, freeing YAP from phosphorylation and physical restraint, allowing it to enter the nucleus to increase transcription[43,48]. While the epithelial cell state downregulates YAP activity, YAP and the Hippo pathway are more well known for their ability to induce EMT.

Early studies quickly recognized YAP as a potent driver of EMT[112-114]. YAP was found to promote classic hallmarks of the transition, such as reduced expression of epithelial markers, increased expression of mesenchymal markers, disrupted adherens junctions, and increased migratory and invasive potential[75]. Mechanistic studies have strongly implicated TEADs as the major transcriptional partner of YAP involved in promoting EMT[16,75,115]. However, it remains unclear if YAP-TEAD transcription is solely responsible for EMT or whether YAP-TEAD activity increases downstream EMT transcription factors responsible for the state change. While the canonical EMT transcription factors are not typically included in core YAP-driven gene signatures, they have nonetheless been observed to be upregulated in some model systems downstream of active YAP[116]. Further complicating this are findings that YAP can bind to both SNAIL[93] and ZEB[92] in a TEAD-dependent manner. While these studies indicate diverse YAP involvement with EMT transcription factors, they all point towards YAP as a powerful driver of EMT phenotypic change. Therefore, it is a crucial research question to identify specific mechanisms downstream of YAP that

influence EMT in cancer. This is of particular importance due to the influence of EMT on cancer metastasis—one of the deadliest aspects of the disease. The relationship between EMT, the Hippo pathway, and cancer extends beyond just metastasis, as EMT has also been associated with increased drug resistance.

1.3 Hippo pathway and drug resistance

1.3.1 Mechanisms of drug resistance

Cytotoxic and targeted therapy are two of the major forms of drug-based treatment of cancer. Cytotoxic therapy is the oldest and still the most common form of cancer treatment. Most cytotoxic therapies act systemically and are effective in cancer by disrupting the essential processes of cell division[117]. Some examples that illustrate common targets include anti-microtubule agents such as taxol, which disrupt mitotic spindle dynamics; antimetabolites such as gemcitabine which inhibit nucleotide biosynthesis, preventing proper DNA replication; DNA-damaging agents such as cisplatin which cause DNA damage by cross-linking, or doxorubicin, a topoisomerase inhibiter that prevents proper DNA unwinding[118-122]. In contrast to the broadly acting cytotoxic therapies, targeted therapies have much more specific mechanisms of action. For example, many targeted therapies are directed towards inhibition of kinases, signaling proteins that often harbor critical cancer-driving mutations[123]. However, despite advancements in drug design and administration, relapse due to acquired resistance is a consistent problem in both targeted and cytotoxic cancer therapies[124].

Cellular based mechanisms of drug resistance can occur through many mechanisms: alterations in drug uptake or efflux; changes to drug activation or increased inactivation of the drug; increased tolerance and repair of drug-induced damage; deactivation of apoptosis and cell death signaling[124]. Additionally, in the case of targeted therapy, drug tolerance can occur through mutation or amplification of the drug target and modification or activation of compensatory signaling, either within the targeted pathway or in parallel signaling pathways[124]. The Hippo

pathway has been implicated in nearly all of these processes in some form, making it a dangerously adaptable signaling pathway in the context of drug resistance.

1.3.2 Hippo and drug resistance

The landscape of Hippo signaling and its effects on cytotoxic drug response are complex, although YAP activity has generally been associated with increased drug resistance. Hippo and YAP activity have been reported in driving resistance to microtubule targeting drugs such as taxol through various mechanisms involving CYR61 and CTGF[125], altered drug transporter expression[126], resisting CDK1 mediated phosphorylation of YAP[126], and many others[127]. YAP has also been reported to increase resistance to DNA damaging agents such as cisplatin[128-130], doxorubicin[130,131], and others[127]. Additionally, YAP has been implicated in altering resistance to antimetabolites, namely gemcitabine, and Fluorouacil (5-FU)—the anti-metabolite analogs of cytidine and uracil respectively[127]. Although much of this work defined a pro-resistance role for YAP in response to antimetabolite treatment[127,132], work from Kirschner and Gujral has found contrasting evidence, implicating YAP activity in causing sensitivity to some of these drugs[133]. Mechanistically, Kirschner and Gujral found YAP decreases the expression of cytidine deaminase (CDA)—the enzyme responsible for converting gemcitabine to its uracil derivative [2′,2′- difluorodeoxyuridine] (dFdU)—and several drug efflux pumps, cumulatively lowering the intracellular concentration of gemcitabine[133]. These conflicting results add to an already complicated landscape of interactions between the Hippo pathway and cytotoxic therapy. On the one hand, there is good evidence to suggest that YAP increases resistance to these drugs. However, under carefully controlled experimental conditions such as those in Gujral, 2017, the resistance-relationship reverses, signaling a clear need for further study into Hippo mediated drug sensitivity studies.

Hippo effects on targeted therapy are equally numerous and complex. YAP activity and Hippo de-activation have been commonly seen in resistance to therapies targeting the MAPK pathway. In particular, YAP upregulation has been observed in resistant cell outgrowth

downstream of BRAF inhibition in melanoma and non-small-cell lung cancers[134-136]. Similar results were observed in pancreatic ductal adenocarcinoma (PDAC) models and colon cancer, where YAP upregulation provides a survival escape mechanism to KRAS inhibition[116,137,138]. YAP activity has also been shown to increase resistance to targeted inhibition of signaling nodes upstream of the MAPK pathway, particularly to drugs targeting the receptor tyrosine kinases (RTKs) such as the epidermal growth factor receptor (EGFR)[127,139]. Importantly, YAPs ability to induce resistance to MAPK and RTK inhibition is robust and can withstand intra-[140] and parallel-pathway[141] combination therapy. What is surprising about these findings is that there is a large diversity in how not only YAP is activated but also in the survival pathways activated by YAP to induce resistance. For instance, YAP activates AKT as a parallel survival pathway in some pancreatic cancer models[138], whereas in non-small cell lung cancer, YAP is capable of reprogramming apoptosis to induce resistance[135,140]. Of note, some studies have implied that YAP driven EMT is a major contributor to MAPK inhibition resistance[116,137]. Mechanisms activating YAP in the context of MAPK therapy resistance are equally diverse, including actin remodeling downstream of TESK1[136], NF2 depletion[134], and amplification of the YAP genomic locus[137]. The diversity in mechanistic input to- and output from YAP in the context of MAPK therapy resistance underscores YAP's adaptability as a pro-survival signal.

1.4 Concluding remarks

Although still a relatively young field, work surrounding the Hippo pathway has quickly expanded to include many areas of biology. While the race to discover the upstream regulation of Hippo signaling has been a significant focus of the field, there have been fewer efforts to characterize signaling cascades downstream of YAP systematically. This is of particular importance concerning YAPs involvement in cancer. YAP is a potent oncogene that drives several cancer phenotypes, yet, the underlying signaling effectors of YAP-driven oncogenesis are largely unknown. There have been efforts to drug YAP-TEAD binding; however, this interface is difficult to inhibit

pharmacologically due to the inherent difficulty in designing molecules that disrupt protein-protein interactions[142]. Due to this difficulty in targeting the YAP-TEAD activity itself, it therefore becomes essential to target the effectors of YAP function within the cell. Confounding this search for druggable effectors of YAP function is the added difficulty of YAPs effects on drug resistance. This dissertation attempts to address these challenges simultaneously.

Firstly, in collaboration with Martin Golkowski and the Ong Lab at the University of Washington, we performed the first survey of YAP-driven changes to the kinome. Kinases are essential signaling proteins that function by phosphorylating substrates. They are ubiquitous in regulating diverse cellular phenomena and are common targets for anti-cancer drugs. This survey led me to discover the ZAK kinase as an effector of YAP activity in driving EMT. Secondly, in collaboration with Michelle Ceribelli of the National Center for the Advancement of Translational Science (NCATS), we performed a medium scale, cancer-focused drug screen in YAP driven cells. These results showed a powerful resistance to pharmacological inhibition of the MAPK pathway that is possibly driven by EMT. Together these results elaborate on the mechanism of how YAP drives EMT, as well as describe the potent advantages this transition may confer in building resistance to targeted therapies. The data generated by this work will aid the field in further identifying and characterizing YAP involvement in cancer and cancer treatment.

Chapter 2: Mixed lineage kinase ZAK drives YAP-mediated epithelial-mesenchymal transition

2.1 Introduction

The Hippo pathway is an evolutionarily conserved kinase signaling pathway that is involved in development, tissue homeostasis and oncogenesis[15]. The core Hippo kinases MST1/2 and LATS1/2 phosphorylate the transcriptional co-activator yes associated peptide 1 (YAP), promoting its nuclear exclusion and degradation[5-9,11,23,112,143]. In addition to the Hippo kinases, YAP activity is modulated by other kinases such as AMPK, LKB1 and receptor tyrosine kinases (RTKs)[41,144,145]. Dysregulation of Hippo pathway components is associated with specific malignancies and increased YAP nuclear localization is common in many tumors, especially in late stage metastatic disease[94,100]. YAP accomplishes much of its oncogenic function by binding to and activating TEAD transcription factors, although other factors such as RUNX are involved[94,146]. Despite large efforts in identifying YAP downstream effectors, specific mediators of YAP driven phenotypes remain elusive.

Kinases are important regulators of virtually every cell process and are deeply involved in Hippo pathway regulation[98,147]. Protein kinases are master cell state regulators and play active roles in virtually every cell signaling pathway, however, in comparison to kinase regulation upstream of YAP, the kinome downstream of YAP has been comparatively understudied[148]. Due to their central role in cell signaling, kinases position themselves as potentially critical regulators of YAP driven cell phenotypic change. I sought to survey kinase signaling changes driven by YAP by using kinome focused mass spectrometry[147,148]. To accomplish this, I worked in collaboration with Dr. Martin Golkowski to employ kinobead liquid chromatography-mass spectrometry (LC-MS), which improves upon standard mass spectrometry through the use of kinobeads, a kinase affinity enrichment reagent using nonselective kinase inhibitors bound to agarose beads[149]. This protocol overcomes traditional limitations of low relative abundance of kinases in cell lysates and is capable of profiling > 200 kinases and their attendant phosphorylation state with as little as 5ul of

kinobeads and 300ug of starting material[150]. Golkowski and colleagues have previously used this technique to identify a FZD2-AXL-NUAK1/2 signaling module that drives epithelial to mesenchymal transition and drug resistance in hepatocellular carcinoma[151]. I sought to apply this technique to identify kinase mediators of YAP-driven phenotypic change.

In this study I used kinobead LC-MS and transcriptomic profiling to build a systems level view of YAP driven changes to the kinome. I discovered large changes to the kinome in YAP-driven cells both in kinase abundance and in phosphorylation, and I identified the leucine-zipper and sterile-α-motif kinase (ZAK, also known as MAP3K20) as the most significantly upregulated kinase. ZAK was originally identified in the early 2000s as a mixed lineage kinase termed MRK[152], MLTK[153] and ZAK[154], capable of activating the MAPK signaling cascade. Since then, ZAK has been purported to have roles in both pro-[155-157] and anti-tumorigenic properties[158-162], with recent work suggesting that its role in EMT[163-165] may underlie these differential roles. I found ZAK overexpression is capable of inducing epithelial to mesenchymal transition (EMT) and ZAK knockdown is able to reverse this effect in our cell model system. I investigated the molecular relationship between YAP and ZAK expression and found that YAP-mediated transcriptional control of ZAK is not dependent on TEAD transcription factors. Finally, with Andrew Xue, we explored the clinical relevance in data sourced from The Cancer Genome Atlas (TCGA) and found increased ZAK expression is significantly correlated with 13/17 mesenchymal classified tumors and is significantly correlated with high YAP activity in every tumor type within TCGA. This work represents a critical next step in the study of the Hippo pathway by providing a comprehensive survey of the signaling network that YAP induces in pancreatic cells. Moreover, this profiling may help elucidate druggable targets in YAP driven cancers, which has historically been notoriously difficult due to the difficulty in targeting YAP directly[166].

2.2 Results

2.2.1 Whole transcriptome profiling of YAP driven cells reveals enrichment in proliferation and EMT-associated gene sets

I set out to study the altered signaling landscape downstream of hyper-active YAP by first investigating transcriptomic changes in Panc02.13 cells driven by YAPS6A, a constitutively active, permanently nuclear localized version of YAP that does not respond to Hippo[21,23,100,113]. Over 3,000 genes exhibited altered expression in response to YAPS6A (Figure 2.2.1A). These data show large increases in well-characterized YAP/TEAD targets such as *RBMS3*, *CTGF*, *CYR61*, *NUAK2*, *CCDC80*, *AXL, ANKRD1,* and *LATS2* (log2 fold change > 2, p-value < 0.05), confirming the activity of YAP in this experimental context (Figure 2.2.1B, C)[96]. To gain better insight into specific pathways that YAP influences, I performed Gene-set enrichment analysis (GSEA) on the whole transcriptome sequencing data[167]. As a first pass I profiled the Hallmark gene sets from the Molecular Signatures Database and found sets associated with cell proliferation were top hits, including MYC targets (NES: 2.77, FDR q-value: 0) , E2F targets (NES: 2.59, FDR q-value: 0) as well as the G2M checkpoint (NES: 2.44, FDR q-value: 0) (Figure 2.2.1D)[168]. In particular, there was a high enrichment of genes associated with epithelial to mesenchymal transition (EMT) (NES: 1.59, FDR q-value: 0.01), a cellular phenomenon that YAP has been previously implicated in mediating (Figure 2.2.1D, E)[75,113,115].

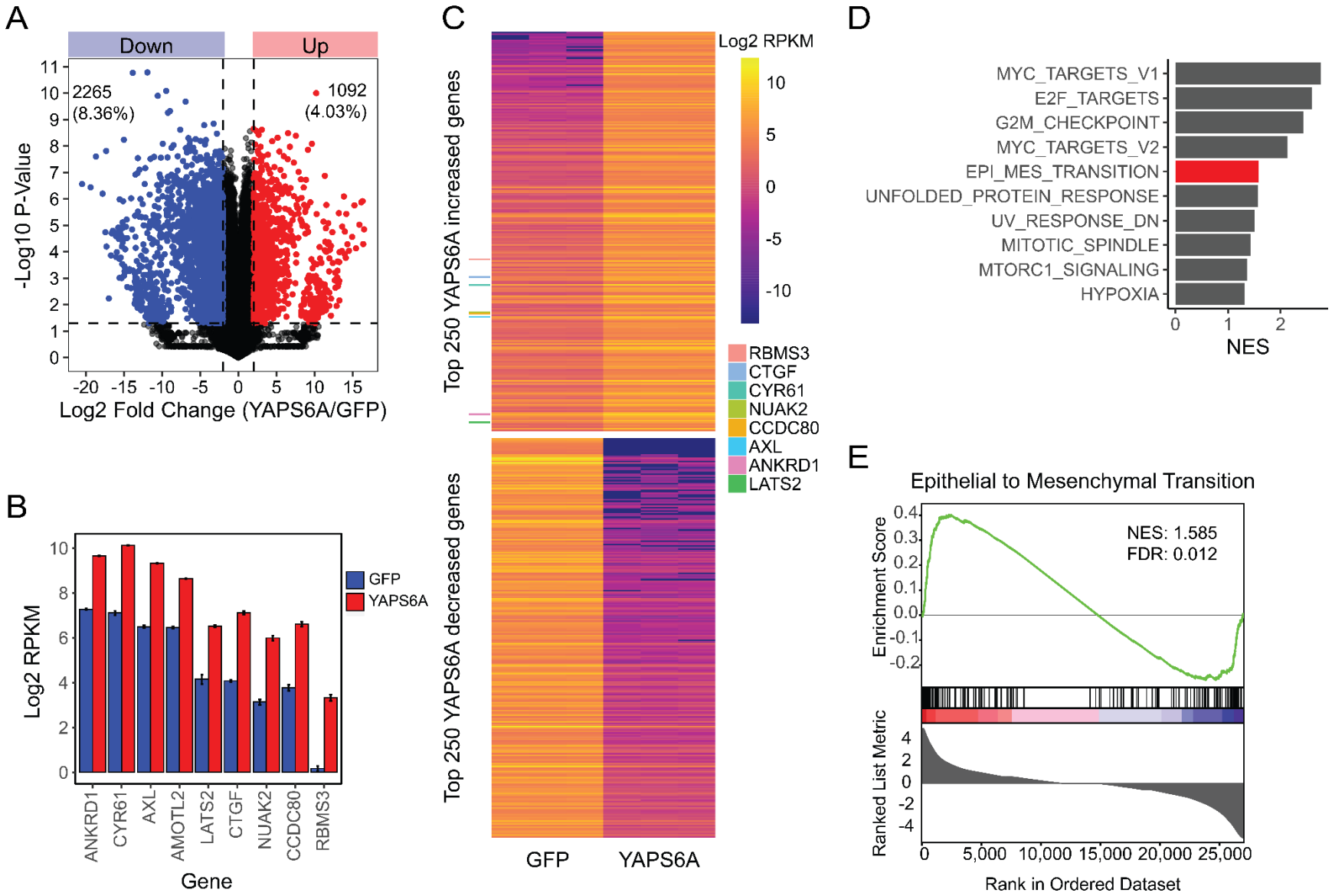

Figure 2.2.1 *Figure legend on following page.*

Figure 2.2.1 Nuclear YAP causes large changes to the transcriptome of Panc02.13 cells
A) Volcano plot of whole transcriptome RNA sequencing in YAPS6A versus GFP transfected Panc02.13 cells. Log2 fold change (YAPS6A/GFP) vs. -log10 P-values (two-sample T-test). **B)** Log 2 reads per kilobase per million mapped reads (RPKM) gene expression of YAP/TAZ target score genes identified in [96], ranked by total expression in Panc02.13 expressing YAPS6A. **C)** Heatmap of top/bottom 250 most increased genes in Panc02.13 cells expressing YAPS6A or GFP, ranked by log2 fold change (YAPS6A/GFP) of RPKM. Highlighted genes are members of the YAP/TAZ target score gene-set from [96]. **D)** Gene set enrichment analysis of YAPS6A effect on transcriptome of Panc02.13 cells. Top ten Hallmark gene sets ranked by normalized enrichment score (NES). **E)** The Hallmark Epithelial to Mesenchymal Transition gene set enrichment plot. NES: normalized enrichment score, FDR: false discovery ratio.

2.2.2 YAP activity causes re-wiring of the kinome

Having identified broad changes in the transcriptome downstream of YAP activity, I next surveyed the YAP-driven kinome. I began a collaboration with Dr. Martin Golkowski at the University of Washington to use kinobead/MS and label-free quantitation (LFQ) to profile abundance and activity state changes in the kinome of Panc02.13 cells expressing GFP (control) or YAPS6A[149]. Overall, we quantified the abundance of 1,464 proteins of which 216 were kinases (Figure 2.2.2A,B). YAPS6A caused a significant increase in the abundance of 137 proteins (absolute $\log_2$ ratio > 1, p-value < 0.05) including 22 kinases, and significant decrease in 186 proteins including 50 kinases. The four most significantly increased kinases were LATS2, NUAK1, NUAK2, and CDK6 (log 2 ratio > 2.5, p-value < 0.05). The four most significantly decreased kinases were MST1R, SYK, CDKL5, and DDR1 (log2 ratio < -2, p-value <0.05) (Figure 2.2.2A,B). We conclude that YAP activity induced by the YAPS6A construct causes large shifts in the abundance of many kinases and their associated interactors.

Our kinobead/MS approach allowed us to quantify not only protein abundance, but also phosphorylation, one of the critical post-translational modifications affecting kinase activity[169,170]. In total, we quantified 4695 phospho-peptides across 1,267 unique protein identifiers. YAPS6A expression caused significant changes in 560 phosphosites compared with GFP control (Figure 2.2.2C, D). The Hippo kinase LATS2 was among the top most upregulated kinases by number of increased phosphosites, showing significant increases in 11 phosphosites, five of which were

mainly detected in YAPS6A expressing cells including Thr-1079, the putative site of MST1/2 phosphorylation responsible for increasing the activation of LATS2[171] (Figure 2.2.2D). We observed increased phosphorylation on NUAK1 (5 increased phosphosites, plus 1 site mainly detected in YAPS6A) as well as ZAK (10 sites increased, plus 2 sites mainly detected in YAPS6A). Furthermore, we observed increased phosphorylation on the Hippo kinase MST2 on Ser-15 (log_2 ratio: 2.61, p-value: 1.98×10^{-3}). We also observed downregulation of several phosphorylation sites, with four of the top hits being CDC42bpa (6 sites decreased), STK10 (6 sites decreased), MARK2 (12 sites decreased), and RIPK2 (6 sites decreased) (Figure 2.2.2D). These data confirm YAP activity has a profound effect on the activation state of the kinome.

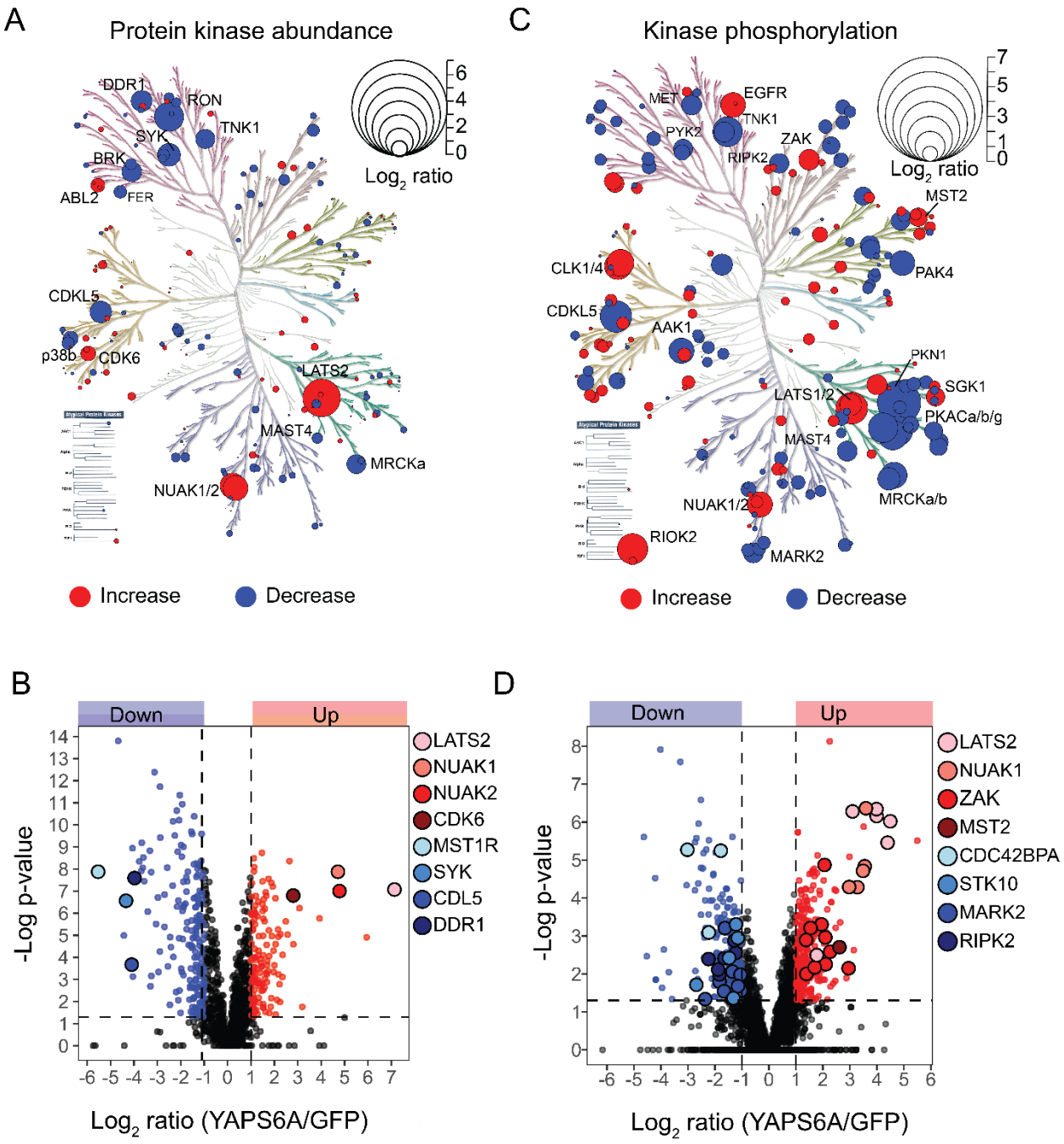

Figure 2.2.2 *Figure legend on following page.*

Figure 2.2.2 Kinobead/LC-MS profiling of YAP mediated changes to the kinome in Panc02.13 cells
A) Human kinome dendrogram overlaid with absolute log2 LFQ intensity ratios of quantified kinases (n = 214 circles) from Panc02.13 cells transfected with YAPS6A or control (GFP). **B)** Scatter plot of protein abundance changes measured by kinobead/LC-MS profiling in Panc02.13 cells transfected with YAPS6A or control (GFP). Log2 LFQ intensity ratio vs. -log10 P-values (two-sample T-test). Larger circles represent specific protein abundance changes. **C)** As in **A**, but circle size represents the single largest absolute magnitude log2 LFQ intensity ratio phosphorylation site per kinase gene symbol. **D)** As in **B**, but each circle represents abundance change of all quantified phosphorylation sites as measured by kinobead/LC-MS profiling. Larger circles represent all quantified phosphorylation sites related to each specific gene symbol.

2.2.3.1 YAP activity promotes expression and activation of the ZAK kinase

Armed with a detailed view of the kinome I next investigated individual signaling nodes that were likely to have major impacts on controlling YAP-mediated phenotypes. I identified thirteen upregulated kinases (>2-fold expression and >1 log2 LFQ ratio; $p<0.05$) and 21 downregulated kinases (<2-fold expression and <1 log2 LFQ ratio; $p<0.05$) that were at the confluence of increased expression and protein abundance (Figure 2.2.3A). I then ranked these kinases by number of significantly altered phosphosites, using significance criteria of absolute log2 ratio greater than 1 and p-value less than 0.05 (Figure 2.2.3B). This ranking revealed ZAK as the most heavily phosphorylated kinase, with significant increases in 12 unique phosphorylation sites resulting from YAP activity (Figure 3B). Conversely, MARK2 was the most heavily de-phosphorylated kinase, showing significant reduction in 10 separate phosphorylation sites resulting from YAP activity (Figure 2.2.3B). I chose to pursue ZAK because of recent reports implicated ZAK in promoting EMT and because the EMT hallmark gene-set was a top hit from our gene set enrichment analysis[163-165]. Quantitative real-time PCR confirms YAPS6A increases *ZAK* transcript levels and, conversely, *ZAK* mRNA expression was reduced by high cell density, a well-documented method of reducing the nuclear localization of endogenous YAP (Figure 2.2.3C)[23,42]. Collectively these data show that increased YAP activity increases expression, protein abundance and phosphorylation of ZAK.

2.2.3.2 ZAK kinase expression correlates with mesenchymal cells state

With help with Dr. Taran Gujral and using data generated by Dr. Martin Golkowski, I

analyzed expression data from 28 hepatocellular carcinoma cell (HCC) lines gathered from The Cancer Cell Line Encyclopedia and compared ZAK expression with several common mesenchymal and epithelial cell markers to determine the relationship between ZAK expression and EMT state[172] (Figure 2.2.3D). ZAK expression is strongly correlated with mesenchymal cell markers and anti-correlated to epithelial markers across the 28 HCC cell lines (Figure 2.2.3D). Previously, Golkowski *et al.* selected 18 representative HCC lines and used hierarchal clustering to classify each representative line as mesenchymal or epithelial based on the expression of common EMT markers[151]. Using this classification system, we found that mesenchymal-type HCC cells had significantly (2.9-fold) higher ZAK abundance levels than epithelial-type HCC cells, further confirming higher ZAK correlation with the mesenchymal cell state (Figure 2.2.3E).

EMT is reversible (termed the mesenchymal to epithelial transition, MET), and Dr. Gujral has previously used FZD2 knockdown to induce MET in mesenchymal FOCUS cells[102,173]. Additionally, FZD2 has been demonstrated to be an activator of YAP/TAZ and thus knockdown should decrease nuclear YAP[69]. Confirming this, knockdown of FZD2 performed by Dr. Gujral reduced nuclear localization of YAP in FOCUS cells (Figure 2.2.3F). Knockdown of FZD2 also caused a sharp reduction in the expression of *ZAK* mRNA (3.3-fold), as well as a significant reduction in the phosphorylation of four different phosphosites on the ZAK protein. I conclude from these data that ZAK is highly correlated with the mesenchymal cell state.

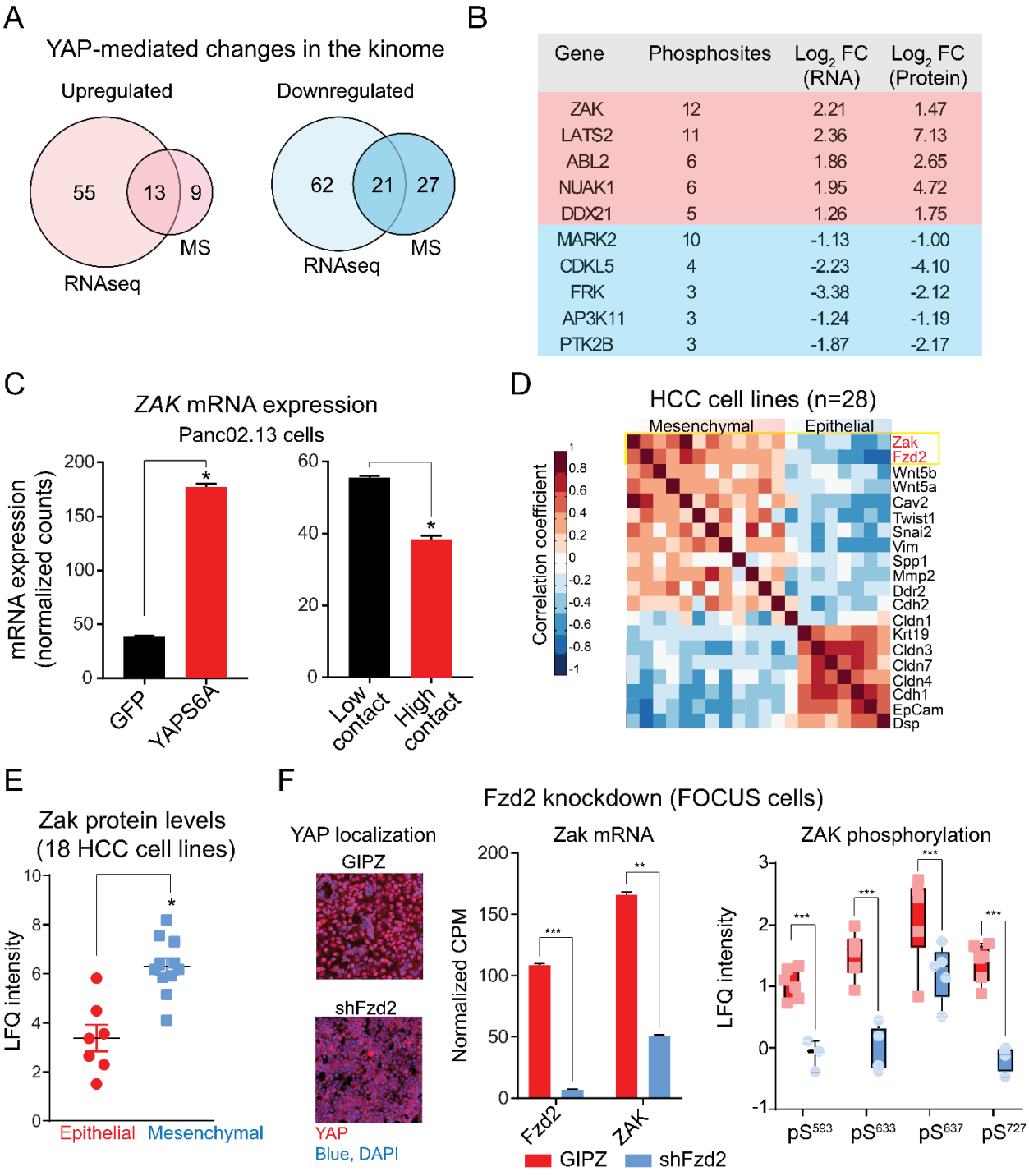

Figure 2.2.3 *Figure legend on following page*

Figure 2.2.3 ZAK is upregulated in nuclear YAP-expressing and mesenchymal cancer cells
A) Venn-diagrams of number of up- and downregulated kinase gene symbols from mass spectrometry (MS) and whole transcriptome (RNAseq) datasets in cells transfected with YAPS6A versus control (GFP). Upregulated/downregulated correspond to gene symbols with absolute log2 LFQ ratio > 1 (MS) or with absolute log2 reads per kilobase per million mapped reads (RPKM), fold changes > 1 (RNAseq), and p-values < 0.05 (two-sample T-test, both). **B)** Top and bottom five gene symbols from intersections of **A**, ranked by number of significantly (absolute log2 LFQ ratio > 1, p-value < 0.05) increased/decreased phosphorylation sites. **C**) *ZAK* mRNA expression is correlated with higher YAP activity. Overexpression of nuclear YAP (YAPS6A) or low cell-cell contact (nuclear YAP) showed relative high *ZAK* mRNA expression (* denotes p-value < 0.05). **D)** ZAK kinase expression is correlated with mesenchymal cellular state markers. Pairwise correlation of expression of common epithelial/mesenchymal markers across 28 HCC cell lines. **E)** ZAK protein levels are increased in mesenchymal cancer cells. LFQ intensity values for ZAK protein across 18 HCC cell lines. **F)** Fzd2 knockdown is correlated with YAP nuclear exclusion and decreased ZAK protein and phosphorylation levels. Left: immunofluorescence micrographs of Fzd2 knockdown (shFzd2) or control (GIPZ) transfected FOCUS cells stained with anti-YAP antibody (red) and DAPI (blue). Middle: *ZAK* mRNA expression in Fzd2 knockdown (shFzd2) or control (GIPZ) transfected FOCUS cells. Right: LFQ intensity of several ZAK phosphorylation sites in Fzd2 knockdown (shFzd2) or control (GIPZ) transfected FOCUS cells

2.2.4 ZAK expression promotes EMT

Having confirmed ZAK association with the mesenchymal cell state, I next began a functional validation of ZAK involvement in EMT by overexpressing ZAK in epithelial cells or knocking down ZAK in mesenchymal cells (Figure 2.2.4.1A). ZAK has two alternatively spliced isoforms, ZAKα, and ZAKβ[153]. Both isoforms have identical N-terminal kinase domains, followed by a leucine zipper, but the c-terminal region of ZAKα contains a sterile α-motif which is lacking in ZAKβ[153] (Figure 2.2.7A). I established stable Panc02.13 ZAKα/β overexpression lines by transfecting overexpression constructs containing full-length cDNA of either ZAKα or V5-tagged ZAKβ (Figure 2.2.4.1B, left, middle). I was able to achieve significant, stable knockdown of total ZAK by transfecting shRNAs that were antagonistic to *ZAKA* and *ZAKB,* the mRNA isoforms of ZAKα/β, into FOCUS cells (Figure 2.2.4.1B, right). I confirmed the expression and subcellular localization of ZAKα and V5-ZAKβ in Panc02.13 cells by immunofluorescence microscopy using anti-ZAKα and V5 specific antibodies. I found ZAKα to be primarily cytosolic, while ZAKβ was localized to both the cytosol and the nucleus (Figure 2.2.4.1C). Having confirmed the overexpression and knockdown of ZAK, I next stained cells with antibodies against the common epithelial markers E-cadherin (ECAD)

and Occludin (OCLN), and the mesenchymal markers N-cadherin (NCAD) and Vimentin (VIM)[102]. Overexpression of ZAKβ caused a large reduction in ECAD as measured by the total fluorescence of ECAD and a smaller reduction in OCLN (Figure 2.2.4.1D). I also observed large increases in VIM and NCAD staining in response to ZAKβ overexpression (Figure 2.2.4.1D). I could not detect any ECAD, OCLN or NCAD staining in FOCUS cells regardless of ZAK knockdown, however, I did detect a reduction in VIM staining (Figure 2.2.4.1D). These immunofluorescence data indicate that ZAK promotes EMT in epithelial cells, and ZAK knockdown promotes MET in mesenchymal cells.

To gain further insight into ZAK mediated EMT phenotypic change I performed qPCR on a larger array of EMT markers. Overexpression of ZAKβ in epithelial Panc02.13 cells had a profound effect on the expression of many EMT related genes. I observed significant increases in the mesenchymal markers *MMP-3, MMP-2, MMP-9, SPARC, GNG11, VIM, ZEB2,* and *SNAI1,* (log2 fold change > 2, p-value < 0.05)[101,102] (Figure 2.2.4.1E). I also saw increased expression of several genes involved in enhancing migration including *COL5A2*, *SPP1, SERPINE1,* and *ITGA5* (log2 fold change > 1.9, p-value < 0.05)[101,102,174-176] (Figure 2.2.4.1E). Additionally, ZAK overexpression increased expression of the mesenchymal mitogens *PDGFRB*, *IGFBP4,* and *WNT11* (log 2 fold change > 2.5, p-value < 0.05)[101,177,178] (Figure 2.2.4.1E). I observed similar EMT gene expression profiles in both ZAKα and ZAKβ overexpressing cells, however, ZAKβ produced a much stronger effect (Figure 2.2.4.2, compare to Figure 2.2.4.1E). Knockdown of ZAK in FOCUS was able to reduce expression of a portion of the same genes increased by ZAKβ overexpression. The mesenchymal markers *MMP-2, MMP-9, GNG11* (log2 fold change < -1.4, p-value < 0.05); and migration enhancers *COL5A2*, and *SPP1* (log2 fold change < -3, p-value < 0.05) all showed significantly reduced expression (Figure 2.2.4.1E). I next tested how ZAK overexpression affected the migration of cells. To this end, I used the scratch wound assay to evaluate cell migratory potential[179]. ZAK knockdown severely reduced the migratory ability of FOCUS cells (Figure 2.2.4.1F). These data collectively describe a role for the ZAK kinase as a potent EMT regulator by increasing mesenchymal cell characteristics both

transcriptionally and functionally.

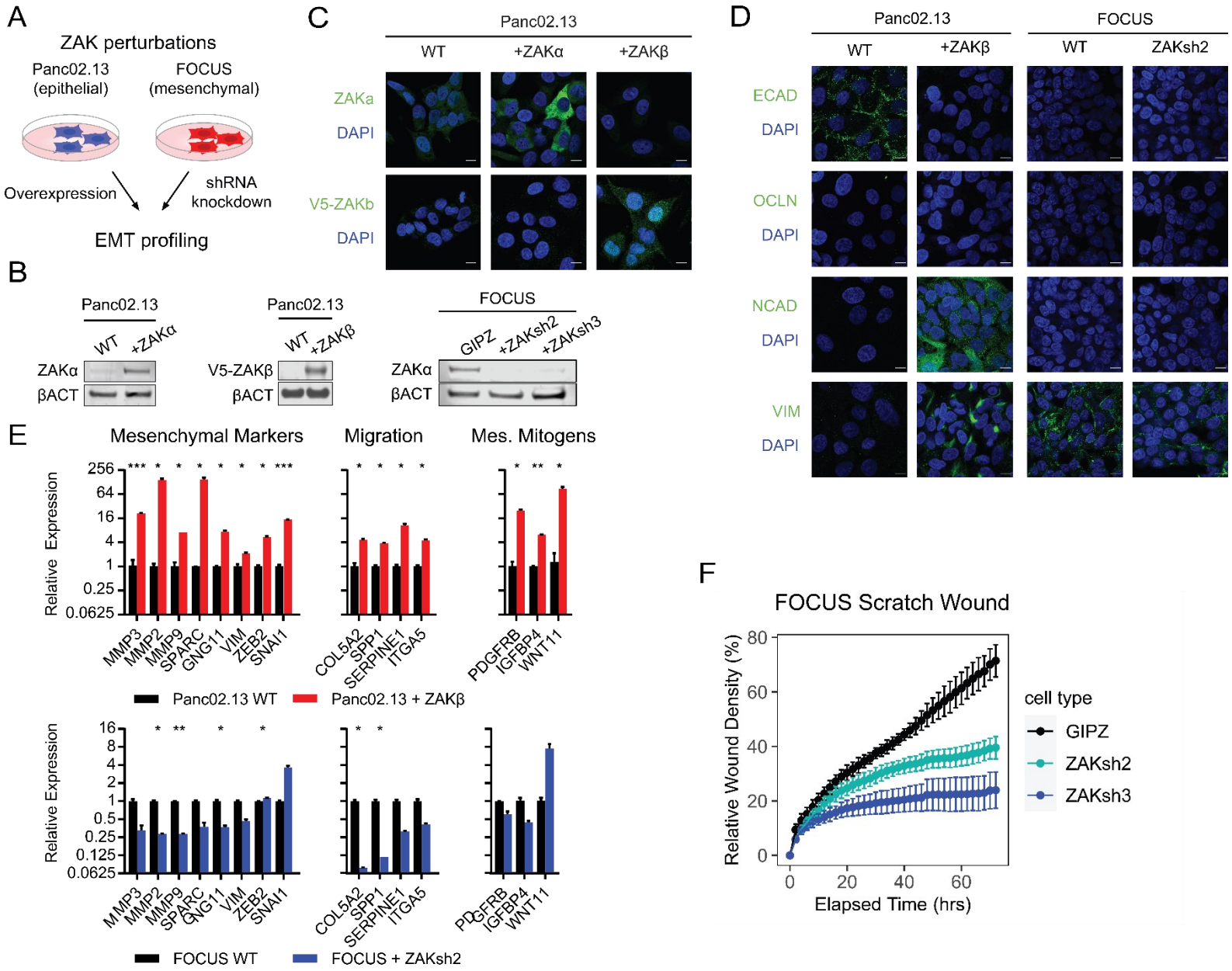

Figure 2.2.4.1 *Figure legend on following page*

Figure 2.2.4.1 ZAK overexpression and knockdown induce and inhibit EMT characteristics respectively in vitro
A) Schematic of ZAK experimental manipulations in Panc02.13 and FOCUS cells. **B)** Left, middle: western blot showing efficient overexpression of ZAKα and V5-ZAKβ in Panc02.13 cells. Right: efficient knockdown of ZAKα in FOCUS cells expressing short hairpins against total ZAK (ZAKsh2, ZAKsh3) or non-targeting control (GIPZ). **C)** Immunofluorescence micrographs of Panc02.13 cells expressing ZAKα (+ZAKα, middle), ZAKβ (+ZAKβ, right) or un-transfected control (WT, left) stained with anti-ZAKα (top), and anti-V5 (bottom) antibodies. Cells counterstained with Hoechst 33342. **D)** Immunofluorescence micrographs of Panc02.13 wild type cells (WT, far left), Panc02.13 cells overexpressing ZAKβ (+ZAKβ, middle left), wild type FOCUS cells (WT, middle right) and FOCUS cells with total ZAK knockdown (ZAKsh2, far right). Top: cells stained with anti-E-Cadherin (ECAD) antibody (green) and DAPI (blue). Middle top: cells stained with anti-occludin (OCLN) antibody (green) and DAPI (blue). Middle bottom: cells stained with anti-N-cadherin (NCAD) antibody (green) and DAPI (blue). Bottom: Cells stained with anti-vimentin (VIM) antibody (green) and DAPI (blue). **E**) Top: relative expression of epithelial to mesenchymal transition marker mRNAs in Panc02.13 cells overexpressing ZAKβ versus un-transfected control (WT). Bottom: relative expression of epithelial to mesenchymal transition markers in FOCUS cells with total ZAK knockdown (ZAKsh2) versus un-transfected control (WT). **F)** Left: scratch wound migration assay of FOCUS cells with ZAK knockdown (ZAKsh2, ZAKsh3) or control (GIPZ). Right: scratch wound migration assay of Panc02.13 cells expressing ZAKα, ZAKβ or YAPS6A compared to un-transfected control (WT). Data shown are mean ± SEM. Significance was calculated using unpaired t test with Holm-Sidak correction method for multiple comparisons (* denotes p-value < 0.05, ** denotes p-value < 0.01 and *** denotes p-value < 0.001).

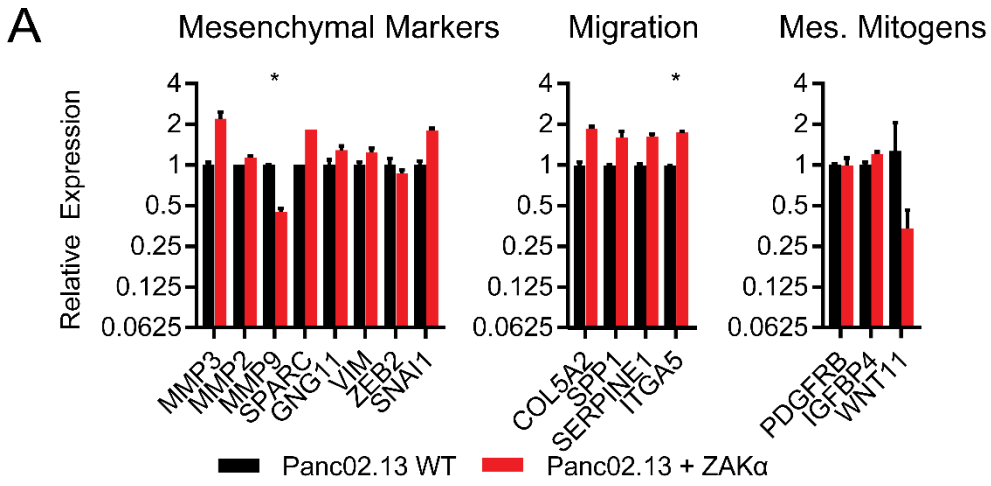

Figure 2.2.4.2 Mesenchymal marker expression in ZAKα expressing cells
A. Relative expression of epithelial to mesenchymal transition marker mRNAs in Panc02.13 cells overexpressing ZAKα versus un-transfected control (WT). Significance was calculated using Student's T-test (* denotes p-value < 0.05).

2.2.5 ZAK expression is independent of YAP-TEAD

Having established a correlative link between nuclear YAP activity and ZAK expression, I began to investigate the mechanistic relationship linking the two. Dr. Frank Szulzewsky *et al.* have

recently described a set of YAP fusion proteins that are implicated in the oncogenesis of several human cancers[180]. These fusion proteins maintain a large portion of YAP's transcriptional activity, while simultaneously destroying or impairing the cytoplasmic shuttling and degradation of the fusion protein through Hippo signaling and other mechanisms, resulting in constitutive nuclear YAP activity[180]. Dr. Szulzewsky had recently established mouse 3T3 cell lines stably expressing one such fusion, YAP-FAM118b, which I used to measure ZAK expression response to hyperactive YAP that was independent of the YAPS6A mutation. Mouse ZAK has three different splice isoforms[181]. The domain structures of mouse ZAK1 and ZAK3 closely mirror that of human ZAKα and ZAKβ respectively[181]. Mouse ZAK2 uniquely does not contain the leucine zipper or SAM domain[181]. Transfection of wild type YAP modestly but significantly increased expression of mouse *ZAK1* (log2 fold change: 0.68, p-value: 2.14×10^{-2}) and *ZAK3* (log fold change: 0.34, p-value: 3.03×10^{-2}) when transfected into mouse 3T3 cells (Figure 2.2.5A). Wild type FAM118b had a similar effect in increasing *ZAK1* expression (log2 fold change: 0.57, p-value: 3.32×10^{-2}) and *ZAK3* (log2 fold change: 0.28, p-value: 4.14×10^{-2}) (Figure 2.2.5A). Transfection of YAP-FAM118b fusions however, greatly increased the expression of all three isoforms of mouse *ZAK: ZAK1* (log2 fold change: 1.45, p-value: 1.04×10^{-3}), *ZAK2* (log2 fold change: 1.10, p-value: 1.5×10^{-3}), and *ZAK3* (log2 fold change: 0.86, p-value: 1.04×10^{-3}) (Figure 2.2.5A). This result provides additional support that YAP activity increases *ZAK* transcription.

In searching for YAP transcriptional partners that increase ZAK expression I first suspected TEADs due to their well characterized role in cell transformation and in promoting EMT[16,75,115]. Confirming this relationship, YAP knockdown (log 2 fold change: -4.01, p-value: 6.89×10^{-11}) was able to reduce the expression of key YAP-TEAD response genes *CTGF* (log2 fold change: -0.86, p-value: 1.51×10^{-3}) and *CYR61* (log2 fold change: -1.28, p-value: 1.84×10^{-4}), however, this same knockdown was not able to reduce the expression of either *ZAKA* or *ZAKB* (Figure 2.2.5B). I was surprised by this and sought further confirmation that TEAD was dispensable for transcriptional

regulation of *ZAK* in response to YAP hyperactivity. Verteporfin is a small molecule that is capable of disrupting the binding of YAP to TEADs, reducing YAP-TEAD target gene expression[76]. Treatment of Panc02.13 cells expressing YAPS6A or wild type FOCUS cells with verteporfin had no effect on *ZAKA/B* expression, despite significantly reducing expressing of *CTGF* and *CYR61* (Figure 2.2.5C, D). These data indicate that YAP mediated increases in *ZAK* expression are not dependent on TEAD transcription factors.

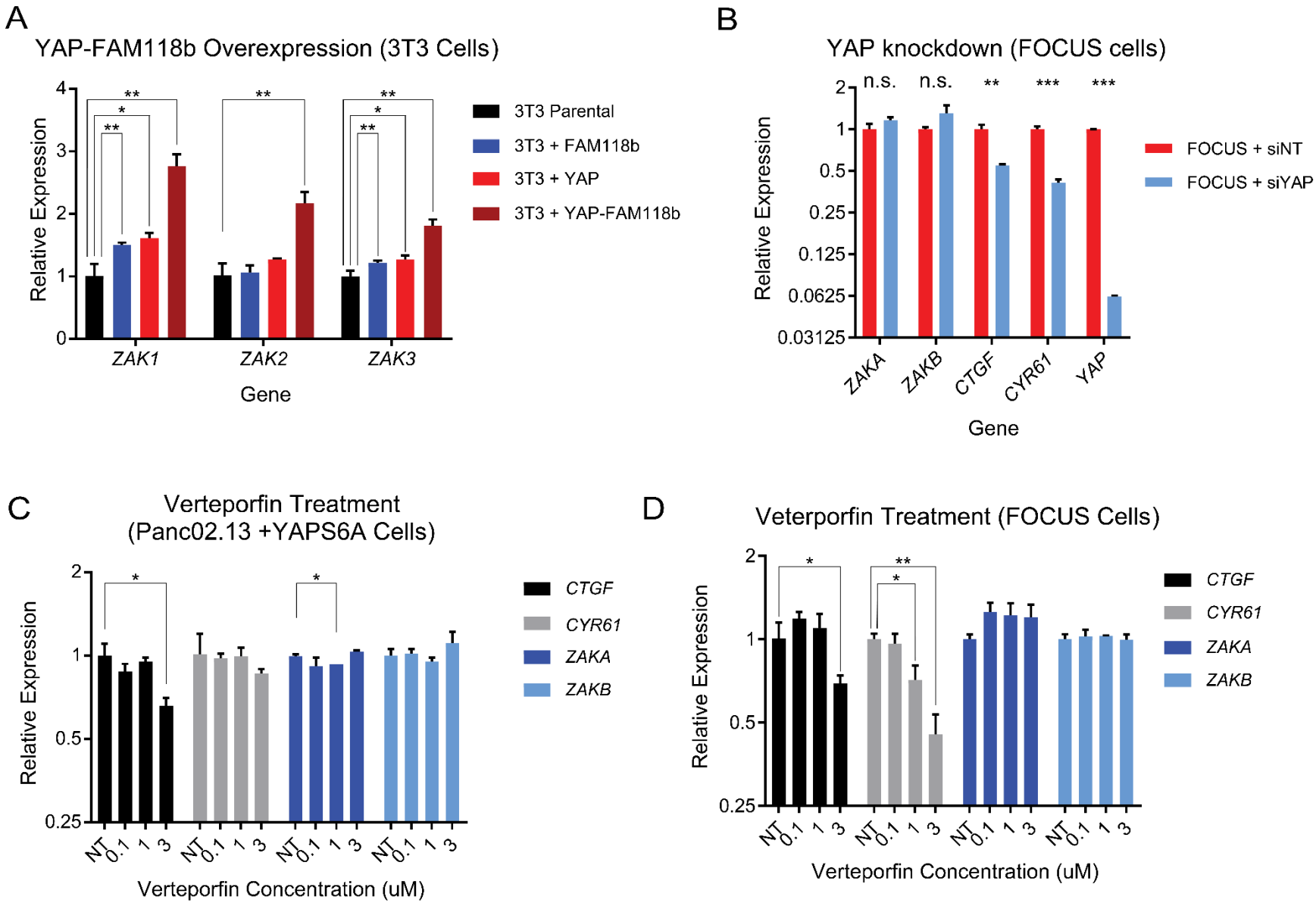

Figure 2.2.5 *Figure legend on following page*

Figure 2.2.5 ZAK expression is not mediated by YAP-TEAD
A) Relative expression of mouse ZAK isoforms ZAK1, ZAK2, ZAK3, in 3T3 cells overexpressing wild type FAM118b (3T3 + FAM118b), wild type YAP (3T3 + YAP), or YAP-FAM118b fusion (3T3 + YAP-FAM118b) versus un-transfected parental control (3T3 Parental). **B)** Relative mRNA expression of *ZAKA/B*, *CTGF* and *CYR61* in response to siRNA YAP knockdown (FOCUS + siYAP) versus non-targeting control (FOCUS + siNT). **C)** Relative mRNA expression of *ZAKA/B* and YAP-TEAD response genes *CTGF* and *CYR61* in Panc02.13 cells expressing YAPS6A in response to verteporfin treatment **D)** As in **C** with wild type FOCUS cells. Data shown are mean ± SEM. Significance was calculated using unpaired t test with Holm-Sidak correction method for multiple comparisons (* denotes p-value < 0.05, ** denotes p-value < 0.01 and *** denotes p-value < 0.001).

2.2.6 TCGA data reveals increased ZAK expression in mesenchymal and YAP active cell contexts

I next sought to establish the relationship between ZAK, EMT and the Hippo pathway in more clinically relevant samples. With the help of Andrew Xue, we made use of The Cancer Genome Atlas (TCGA)[182] to classify 17 patient sample cohorts into epithelial-like (E) or mesenchymal-like (M) sub-groups based on expression of epithelial and mesenchymal marker genes. We then compared ZAK expression between E and M and found significantly increased ZAK expression in the M sub-group in 13 out of 17 TCGA cohorts (Figure 2.2.6A). Similarly, we classified these same patient cohorts into high-Hippo or low-Hippo based on expression of a previously reported 22-gene Hippo signature[96]. Increased ZAK expression was strongly correlated with high-Hippo pathway output in every patient cohorts (n = 17) surveyed (Figure 2.2.6B). This analysis corroborates my findings in cell models and implicates a relationship between high YAP-activity, increased ZAK expression, and EMT in real-world patient samples.

A

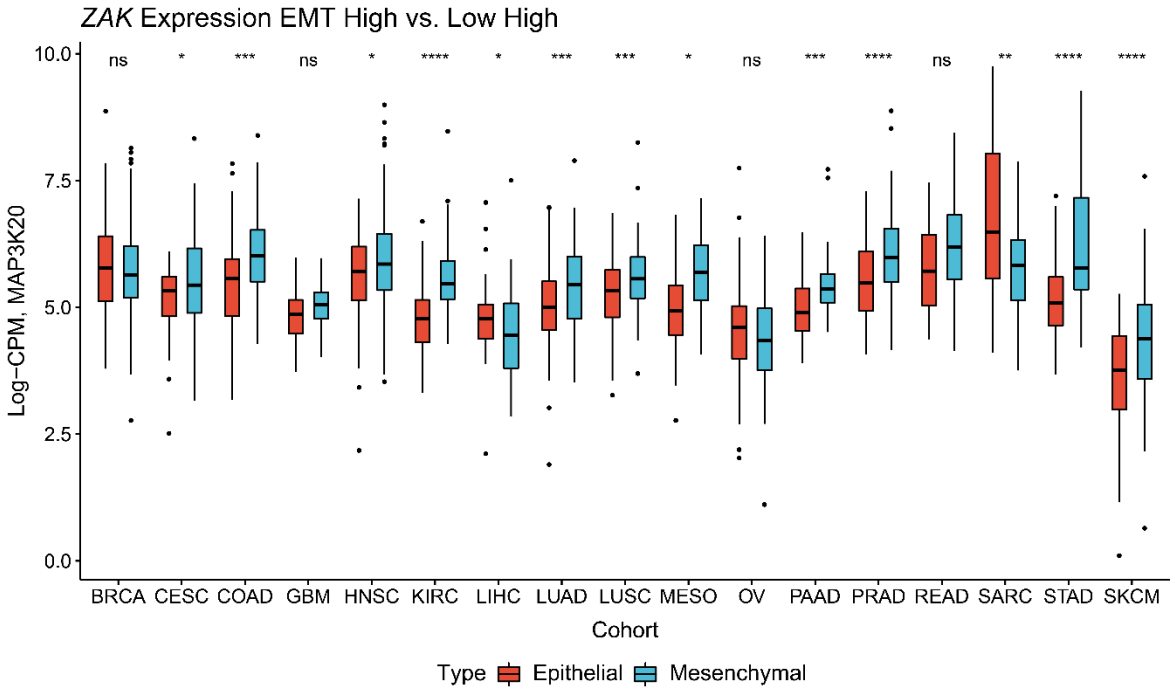

B

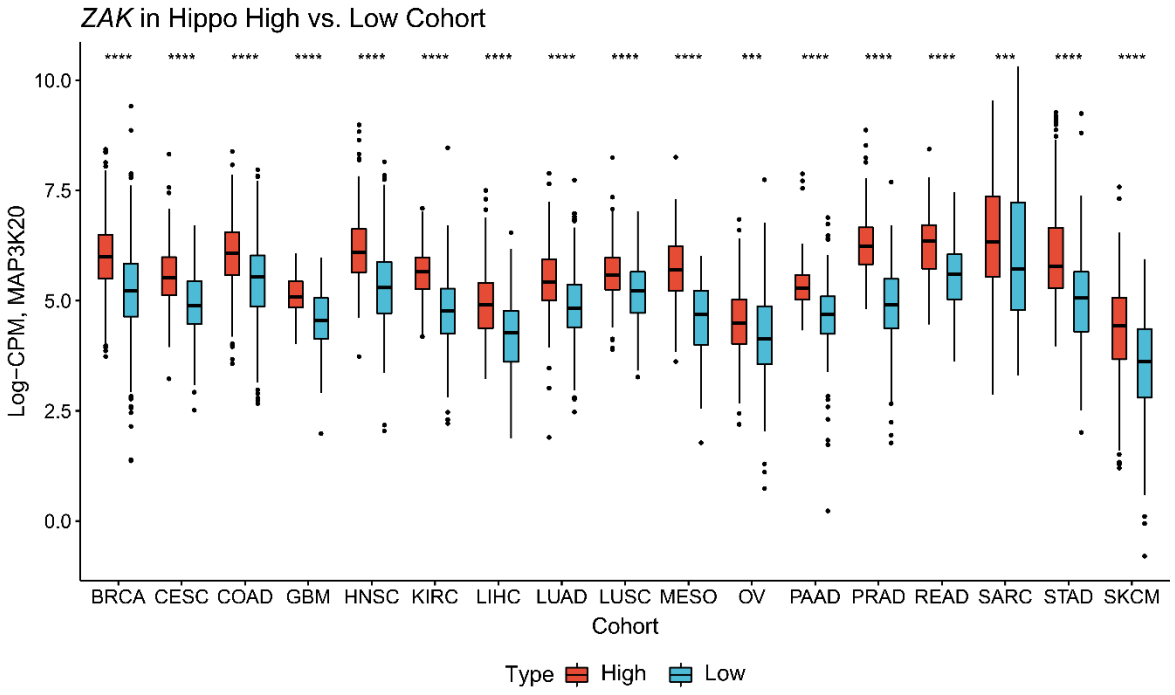

Figure 2.2.6 *Figure legend on following page*

Figure 2.2.6 ZAK is increased in mesenchymal and Hippo mutant clinical samples
A. Average ZAK expression level among 17 different cancer types segmented into epithelial- or mesenchymal-like based on epithelial/mesenchymal marker expression. B. Average ZAK expression level among 17 different cancer types classified based on Hippo pathway activity status. (BRCA: breast invasive carcinoma, CESC: cervical squamous cell carcinoma and endocervical adenocarcinoma, COAD: colon adenocarcinoma, GBM: glioblastoma multiforme, HNSC: head and neck squamous cell carcinoma, KIRC: kidney renal clear cell carcinoma, LIHC: liver hepatocellular carcinoma, LUAD: lung adenocarcinoma, LUSC: lung squamous cell carcinoma, MESO: mesothelioma, OV: ovarian serous cystadenocarcinoma, PAAD: pancreatic adenocarcinoma, PRAD: prostate adenocarcinoma, READ: rectum adenocarcinoma, SARC: sarcoma, STAD: stomach adenocarcinoma, SKCM: skin cutaneous melanoma) Significance was calculated using Wilcoxon rank-sum test (* denotes p-value < 0.05, ** denotes p-value < 0.01, *** denotes p-value < 0.001, **** denotes p-value < 0.00001,).

2.3 Discussion

Although much research has been done on downstream effects of YAP signaling, to our knowledge this is the first to describe the activity state of the kinome in response to YAP hyper-activity, an important next step in characterizing the signaling landscape downstream of YAP. Our kinobead/LC-MS profiling provides an intricate view of kinase activation state in YAP driven cells, a key window into their function[183]. For example, phosphorylation on Thr-1079 of LATS2, as well as increased phosphorylation/expression of MST2 and NUAK1 confirm previous reports of Hippo-coordinated negative feedback loops on YAP activity (Figure 2.2.2)[184,185]. The large amount of Hippo activation observed here speaks to the activation of aggressive negative compensatory pathways in response to hyper-active YAP. Additionally one of the most highly downregulated kinases, MARK2, has been implicated in regulating cell polarity and microtubule dynamics[186] and may be connected to some of the morphological changes associated with YAP activity. Of all quantified kinases however, ZAK had the largest number of increased phosphorylation sites with 12 in total (Figure 2.2.3B). Interestingly, this increased phosphorylation is primarily restricted to the C-terminal region of the ZAKα isoform (Figure 2.2.7A, B). These differing phosphorylations may play a role in subcellular localization differences observed between the ZAK kinase isoforms, with ZAKα primarily located in the cytosol and ZAKβ localizing to the both the cytosol and the nucleus (Figure 2.2.4C).

EMT is a complex process that is important in normal cell development and is intricately tied to cancer metastasis[101-103]. The Hippo pathway has primarily been implicated in cancer related EMT through the action of TEADs[75,115], however, other mechanisms have been proposed, including through direct interaction with FOS1[116], through interaction with ZEB1 via YAPs WW1 domain[92] and by direct binding to SNAIL/SLUG[187]. The disparity in these various cell processes hint that YAP and EMT coordination may occur through differing mechanisms depending on cellular context. Our study provides the first evidence linking EMT to the Hippo pathway through upregulation of the ZAK kinase. Previously, Korkina *et al.* have implicated ZAKβ as the primary mediator of EMT and migration induction of the two ZAK isoforms[164] although, Rey *et al.* suggest both isoforms of ZAK are involved[163]. I primarily see these effects resulting from overexpression of the ZAKβ isoform. Indeed, the effects on transcription and mesenchymal morphology observed by overexpression of ZAKα were not nearly as strong as that of ZAKβ (Figure 2.2.4.1D-F, Figure 2.2.4.2). The differential phosphorylation among the two isoforms may contribute to an isoform specific regulatory mechanism that may explain the differing EMT promoting potential of ZAKα versus ZAKβ in our experimental context.

Here I also present the first evidence that ZAK is a transcriptional target of YAP. Despite much data supporting TEAD as the primary effector of YAP transcription, our data suggest that ZAK is regulated independently of TEAD (Figure 2.2.5)[94]. Outside of TEAD1-4, YAP binds to other transcription factors via its WW domains including P73, ERBB4, ERB-1, RUNX1/2, TBX5, AMOTs and SMADS [54,188]. Furthermore, chromatin occupancy profiling of YAP-FAM118b fusions using CUT&RUN[189] indicate binding in regions enriched for BATF, RUNX and SOX2 binding motifs, which add to the pool of potential YAP-binding transcriptional partners influencing ZAK expression[180].

In clarifying the YAP-ZAK relationship in TCGA data, Andrew Xue and I designed our approach to incorporate YAP activity rather than Hippo mutation because although nuclear YAP is common in human cancer, mutations in the Hippo pathway are nevertheless rare[100]. Our findings

show that the correlation between high YAP activity and high ZAK expression is consistent across every tumor type surveyed, indicating the ubiquity of this relationship (Figure 2.2.6). In contrast to this, the relationship between ZAK expression and epithelial mesenchymal status is variegated and dependent on tumor type. This suggests that ZAK's influence on EMT may be restricted to specific cell or tumor contexts, which is informative when considering potential kinase targets in treating YAP-driven cancers. Although inhibitors exist that can target ZAK, these would potentially be more effective in the subset of cancers where EMT (and presumably metastasis) are indeed correlated with ZAK activity[190,191]. In summary, I have provided the first comprehensive survey of the kinome signaling landscape downstream of YAP and have added the ZAK kinase as a new player in connecting the Hippo pathway with cellular phenotypic change.

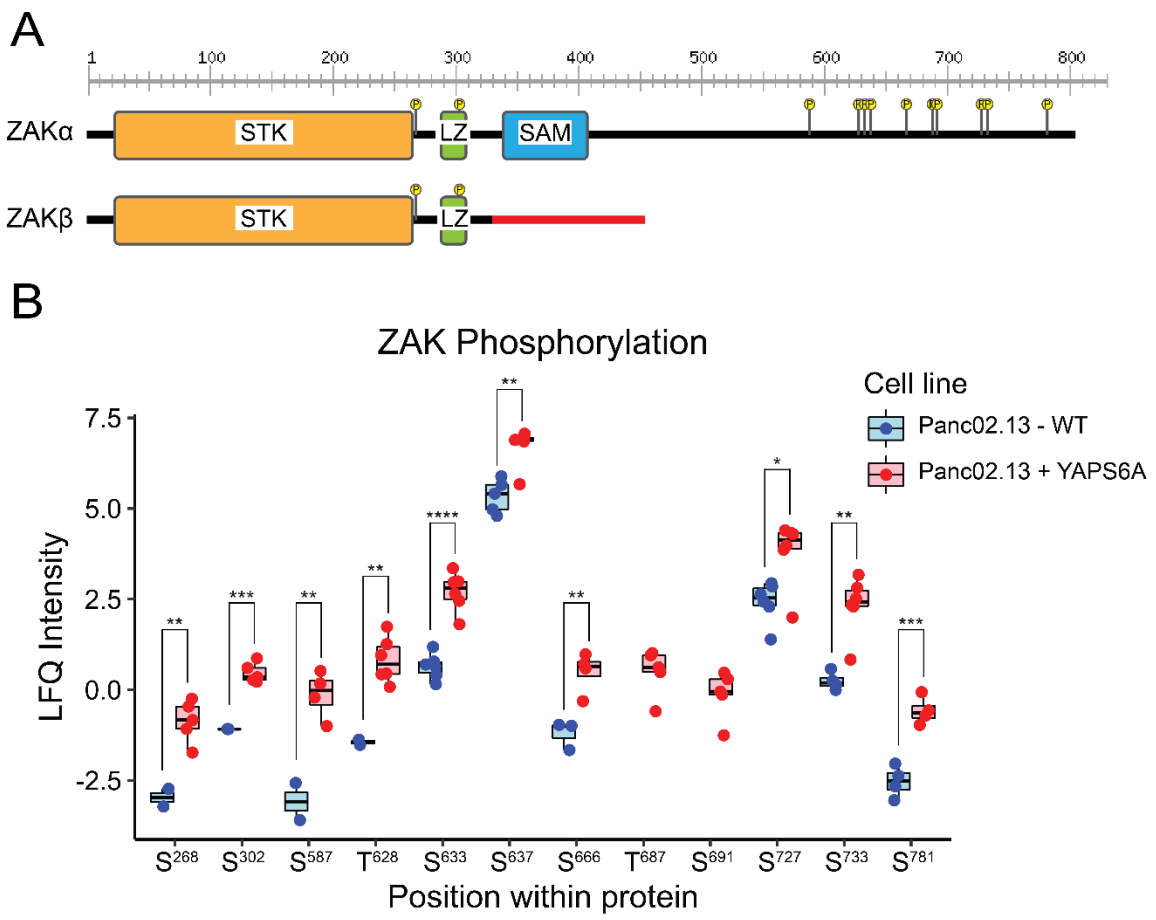

Figure 2.2.7 YAP-mediated phosphorylation is primarily restricted to ZAKα.
A) Domain structure of ZAK showing serine-threonine kinase domain (STK), leucine-zipper (LZ), sterile-alpha-motif (SAM) and significantly increased phosphorylation sites (yellow P's). Red indicates ZAKβ unique region. **B)** LFQ intensity ratios of significantly increased phosphorylation sites on total ZAK. Significance was calculated using Student's T-test (* denotes p-value < 0.05, ** denotes p-value < 0.01, *** denotes p-value < 0.001)

2.4 Materials and methods

Cell lines and reagents

Panc02.13 cells were obtained from American Type Culture Collection (ATCC). FOCUS cells have been described previously [151]. Panc02.13 cells were cultured in RPMI1640 supplemented with 10% (v/v) fetal bovine serum (FBS), 100 IU/ml penicillin, and 100 µg/ml streptomycin. FOCUS cells were culture in DMEM supplemented with 10% (v/v) fetal bovine serum (FBS), 100 IU/ml penicillin, and 100 µg/ml streptomycin.

Western blotting

Cells were lysed in SDS-based lysis buffer (50 mM Tris-HCl, 2% SDS, 5% Glycerol, 5 mM EDTA, 1 mM NaF, 1xProtease/Phosphatase inhibitor cocktail, 10 mM β-GP, 1 mM PMSF, 1 mM Na3VO4, 1 mM DTT). Monolayer cells were washed twice with PBS and suspended into the SDS lysis buffer. The remaining debris were removed by centrifuge filtration. Protein concentration was measured by BCA assay with bovine serum albumin as a standard. Protein samples were then suspended in nuPAGE LDS sample buffer (Invitrogen) denaturing at 95°C for 5 min in reducing condition by nuPAGE sample reducing agent (Invitrogen). 10-20 μg of protein per lane were separated with 4-12% Bis-Tris gradient gels (Invitrogen) in MOPS SDS running buffer (Invitrogen). The proteins were transferred by tank blotting system to nitrocellulose membrane. The membrane was blocked with LICOR blocking buffer (PBS) for 1 h at ambient temperature, followed by primary antibody at 1:1000 in the blocking buffer at 4°C for 12-18 h (Li-cor, Lincoln, Nebraska, USA). After washing with PBS, the membrane was incubated with infra-red-conjugated antibodies at 1:5000 for 1 h at room temperature (Li-cor, Lincoln, Nebraska, USA). The signal was imaged by Odyssey imaging system, and the band intensities were quantified with the Odyssey imaging analysis software (Li-cor, Lincoln, Nebraska, USA). The signal intensities of each protein were normalized with that of β-Actin.

Confocal Microscopy

Cells were seeded 1.25 x 10^5 cells/well onto 24-well No. 1.5 coverslip glass bottom plates (MatTek Corporation, Ashland, MA, USA Cat #: P24G-1.5-13-F) pre-coated with 1:10 dilution of 0.01% Poly-lysine in PBS for 1 hour at RT (manufacturer?). After 24 hours, cells were fixed with 4% para-formaldehyde (Fisher Scientific Cat #: 50-259-99) in PBS for 15 min on an orbital shaker at room temperature. Cells were then permeabilized with 100% ice-cold methanol for 10 minutes at -20° C. Cells were then blocked with IF-blocking buffer (3% bovine serum albumin + 0.3% Triton-X-100 in PBS (w/v)) for 1 hour, shaking at room temp. Primary antibodies were diluted 1:400 in IF-blocking buffer and applied to cells for 12-18 hours at 4° C before washing with PBS. Cells were

then incubated with Alexa-fluor-568 conjugated goat-anti-mouse or donkey-anti-rabbit secondary antibodies (Invitrogen, Cat #s: A-11004, A10042) at 1:400 dilution in IF-blocking buffer for 1 hour, shaking at room temperature. Cells were counter-stained with Hoechst 33342 (Sigma-Aldrich, St. Louis, MO). Cells were then washed and imaged using a Zeiss LSM 780 laser scanning confocal microscope at 40x magnification. Images were processed, channels were overlaid and signal intensities were normalized using Image J software (National Institutes of Health, Bethesda, MD).

Purified Antibodies

Antibodies used were anti-ZAKα (Bethyl Laboratories, Montgomery, TX, USA, Cat #: A301-993A), anti-V5 (Invitrogen, Cat #: 46-0705), anti-β-Actin (Santa Cruz Biotechnology, Cat #: sc-47778), anti-ECAD (Santa Cruz Biotechnology, Cat #: 21794), anti-OCLN (Invitrogen, Cat #: 33-1500), anti-NCAD (Cell Signaling Technology, Danvers, MA, USA, Cat #: 4061), anti-VIM (Santa Cruz Biotechnology, Cat #: sc-32322), anti-YAP (Cell Signaling Technology, Danvers, MA, USA, Cat #: 14074).

Quantitative PCR

RNA was extracted by RNeasy Mini Kit according to the manufacturers instructions (QIAGEN, Santa Clara, CA, USA). RNA concentration was measured with a NanoDrop Spectrophotometer (Thermo Scientific), 1ug was transcribed into cDNA using RT2 HT first strand kit according to the manufacturers instructions (QIAGEN, Santa Clara, CA, USA) and run in a qPCR with SYBR green-based reagent (BioRad, Hercules, CA, USA) with primers purchased from BioRad or RealTime Primer. The qPCR reaction was performed with an initial denaturation step of 2 min at 95°C, followed by 5s (Biorad) or 10 s (Realtime) at 95°C, and 30 s at 60°C (Biorad) or 45 s at 58°C (Realtime) for 40 cycles using C1000 Touch Thermal Cycler (BioRad, Hercules, CA, USA).
MRNA Expression levels were normalized relative to GAPDH or ACTB using the 2-ΔΔCt method. Normalized level of mRNA, X, is thus:

$$X = 2^{-Ct(GOI)}/2^{-Ct(CTL)}$$

where Ct is the threshold at which fluorescence of the reporter (SYBR green) becomes detectable above the background at a given baseline. GOI refers to gene of interest, CTL refers to a control housekeeping gene. Using this method, Ct values are thus inversely proportional to the mRNA concentration in the sample, and product doubles with every thermal cycle.

TCGA data analysis

RNA-Seq raw counts data and clinical information for 17 TCGA patient cohorts (BRCA, CESC, COAD, GBM, HNSC, KIRC, LIHC, LUAD, LUSC, MESO, OV, PAAD, PRAD, READ, SARC, STAD, SKCM) were downloaded through the Genomic Data Commons data portal[192]. Files were processed using edgeR[193], with patients missing clinical data removed, and raw counts were converted to logCPM values. To assess co-expression between EMT and ZAK, we used previously reported epithelial and mesenchymal marker genes[172] to rank patients in each TCGA cohort by calculating the mean-rank of their epithelial marker expression and mesenchymal marker expression, giving an E-score and M-score respectively. Patients with above median E-score and below median M-score were labelled as the epithelial-like group, while patients with above median M-score and below median E-score were labelled as mesenchymal-like. The expression of Zak between these two groups was compared per TCGA cohort using a Wilcoxon rank-sum test. Similarly, to assess co-expression between the Hippo pathway and Zak, patients in each TCGA cohort were assigned a Hippo-expression score based on a previously reported 22-gene Hippo signature[96] by calculating each patients' mean-rank of Hippo signature expression. Patients with above median/below median Hippo-expression score were assigned to high Hippo/low Hippo groups respectively. Zak expression between the two groups for each TCGA cohort were also compared using a Wilcoxon rank-sum test.

RNA sequencing

Total cellular RNA was isolated with RNeasy Mini Kit (QIAGEN, Santa Clara, CA). Library preparation, sequencing, and alignment were performed by Genomics Core Facility at the Fred

Hutchinson Cancer Research Center. Briefly, pair-end sequencing was performed on an Illumina HiSeq 2500 machine with the poly-A capturing protocol and a read length of 43 base pairs. Library preparation was performed using the TruSeq Stranded Sample Preparation Kit (Illumina, RS-122-2201) starting from 1000 ng of total RNA. cDNA libraries were amplified and sequenced with HiSeq2500 from Illumina. The dataset is accessible through GEO Series accession number GSE138380 for the RNA-Seq dataset. RNA-Seq data were filtered and normalized with the edgeR Bioconductor package in R. DEGs were calculated between the 2 cell-line groups with the standard generalized linear model workflow in edgeR using the following parameters: log fold change > 3 (absolute fold change > 8) and $P < 0.05$.

Kinase affinity enrichment and on-bead digestion

Kinase affinity enrichment and on-bead digestion was performed as previously described[149]. Briefly, three micro tubes containing 35 µl of a 50% slurry of the in-house-made, optimized kinobead mixture in 20% aq. ethanol were prepared for each pulldown experiment. The beads were washed twice with 300 µl modified RIPA buffer (50 mM Tris, 150 mM NaCl, 0.25% Na-deoxycholate, 1% NP-40, 1 mM EDTA and 10 mM NaF, pH 7.8). 1 mg of protein extract in mod. RIPA buffer containing HALT protease inhibitor cocktail (100x, Thermo Fisher Scientific, Waltham, MA) and phosphatase inhibitor cocktail II and III (100x, Sigma-Aldrich, St Louis, MO) were added to the first tube. The mixture was incubated on a tube rotator for 1h at 4°C and then the beads were spun down rapidly at 2000 rpm on a benchtop centrifuge (5s). The supernatant was pipetted into the next tube with kinobeads for the second round of affinity enrichment. The procedure was repeated once more for a total of three rounds of affinity enrichment. After removal of the supernatant, the beads were rapidly washed twice with 300 µl of ice-cold mod. RIPA buffer and three times with 300 µl ice-cold tris-buffered saline (TBS, 50 mM tris, 150 mM NaCl, pH 7.8) to remove detergents. 100 µl of the denaturing buffer (20% trifluoroethanol (TFE)[96], 25 mM Tris containing 5 mM tris(2-carboxyethyl)phosphine hydrochloride (TCEP*HCl) and 10 mM chloroacetamide (CAM), pH 7.8),

were added and the slurry vortexed at low speed briefly. At this stage, kinobeads from the three tubes are combined and heated at 95°C for 5 min. The mixture was diluted 2-fold with 25 mM triethylamine bicarbonate (TEAB), the pH adjusted to 8-9 by addition 1 N aq. NaOH; 5 µg LysC were added and the mixture agitated on a thermomixer at 700 rpm at 37°C for 2 h. Then 5 µg MS-grade trypsin (Thermo Fisher Scientific, Waltham, MA) were added, and the mixture agitated on a thermomixer at 700 rpm at 37°C overnight. 600 µl of 1% formic acid was added and the mixture acidified by addition of another 6 µl of formic acid to yield 1.2 ml peptide solution in total. An aliquot of 120 µl (10%) of the peptide solution was desalted using StageTips and analyzed in single nanoLC-MS/MS runs for protein quantification. The remaining peptide solution (90%) was dried under vacuum at RT on a SpeedVac. 300 µl of 70% aq. ACN + 0.1 % TFA was added to each tube, the mixture vortexed, and sonicated in a bath sonicator until dried peptide residue dissolved. In case the dried residue could not be fully resuspended, additional 0.1% aq. TFA can be added in 10 µl increments until dissolved. The solution was subjected to IMAC phosphopeptide enrichment protocol and desalted using StageTips (see 'IMAC phosphopeptide enrichment' and 'Peptide and phosphopeptide desalting with StageTips' above).

nanoLC-MS/MS analyses

The LC-MS/MS analyses were performed as described previously with the following minor modifications[149,150]. Peptide samples were separated on a Thermo-Dionex RSLCNano UHPLC instrument (Sunnyvale, CA) using 20 cm long fused silica capillary columns (100 µm ID) packed with 3 µm 120 Å reversed phase C18 beads (Dr. Maisch, Ammerbuch, DE). For whole peptide samples the LC gradient was 120 min long with 10–35% B at 300 nL/min. For phosphopeptide samples the LC gradient was 120 min long with 3–30% B at 300 nL/min. LC solvent A was 0.1% aq. acetic acid and LC solvent B was 0.1% acetic acid, 99.9% acetonitrile. MS data was collected with a Thermo Fisher Scientific Orbitrap Elite instrument. Data-dependent analysis was applied using Top15 selection with CID fragmentation.

Computation of MS raw files

Data .raw files were analyzed by MaxQuant/Andromeda [194] version 1.5.2.8 using protein, peptide and site FDRs of 0.01 and a score minimum of 40 for modified peptides, 0 for unmodified peptides; delta score minimum of 17 for modified peptides, 0 for unmodified peptides. MS/MS spectra were searched against the UniProt human database (updated July 22nd, 2015). MaxQuant search parameters: Variable modifications included Oxidation (M) and Phospho (S/T/Y). Carbamidomethyl (C) was a fixed modification. Max. missed cleavages was 2, enzyme was Trypsin/P and max. charge was 7. The MaxQuant "match between runs" feature was enabled. The initial search tolerance for FTMS scans was 20 ppm and 0.5 Da for ITMS MS/MS scans.

MaxQuant output data processing

MaxQuant output files were processed and statistically analyzed using the Perseus software package v1.5.6.0[195]. Human gene ontology (GO) terms (GOBP, GOCC and GOMF) were loaded from the 'Perseus Annotations' file downloaded on 01.08.2017. Expression columns (protein and phosphopeptide intensities) were log2 transformed and normalized by subtracting the median log2 expression value from each expression value of the corresponding data column. Potential contaminants, reverse hits and proteins only identified by site were removed. Reproducibility between LC-MS/MS experiments were analyzed by column correlation (Pearson's r) and replicates with a variation of $r > 0.25$ compared to the mean r-values of all replicates of the same experiment (cell line or knockdown experiment) were considered outliers and excluded from the analyses. Data imputation was performed using a modeled distribution of MS intensity values downshifted by 1.8 and having a width of 0.2. For statistical testing of significant differences in expression, a two-sample Student's T-test with Benjamini-Hochberg correction for multiple hypothesis testing was applied (FDR = 0.05).

Kinome dendrograms

Kinome dendrograms were prepared using the KinMap web application

(http://kinhub.org/kinmap/)[196]. For protein kinase abundance, all detected kinases are represented by an individual circle, size relative to log LFQ ratio and color relative to direction of change. Named kinases had absolute log2 LFQ ratio larger than 2. For kinase phosphorylation sites, only the largest absolute magnitude phosphorylation site per gene symbol was chosen for display, circle size relative to log LFQ ratio and color relative to direction of change. Within this set, phosphorylation sites that had log2 LFQ ratio larger than 2 display their associated gene symbol name.

Kinome volcano plots, "up-" and "downregulated" selection criteria

We considered a given kinase to be up- or downregulated when it displayed log2 LFQ ratio larger than 1 in the same direction in mass spec. I filtered for p-values less than 0.05 for both. I considered a given phosphorylation site to be significantly altered if the absolute $\log_2$ ratio was greater than 1 and the p-value was less than 0.05, or if that phosphorylation site was detected in at least 5/6 replicates in one cell line while simultaneously detecting that same site in less than 2/6 replicates in the other. These latter cases illustrate sites that are only detectable in one cell line and are thus labelled "mainly detected in" with their corresponding cell line.

Generation of stable cells lines

Panc02.13 expressing YAPS6A, Panc02.13 cells expressing depleted levels of YAP (Panc02.13-Yapsh) and FOCUS cells expressing depleted levels of Fzd2 (FOCUS-shFZd2) have been described previously[197,198]. Stably transduced NIH3T3 cells (untransduced control, wtYAP1, wtFAM188B, or YAP1-FAM118B) have been described previously[199]. The ZAKα and V5-ZAKβ plasmids were purchased from Genecopoeia (Cat #s: EX-X0399-Lv1-5-B, EX-OL03382-LX304-B respectively) and transfected into Panc02.13 cells in a reverse transfection using Lipofectamine 2000 (Thermo Fisher Scientific, Cat #: 11668030) according to the manufacturer's instructions. ZAKsh2, ZAKsh3 and non-targeting control (GIPZ) short hairpin constructs were acquired from OpenBiosystems and transfected into FOCUS cells in a reverse transfection using Lipofectamine

2000 (Thermo Fisher Scientific, Cat #: 11668030) according to the manufacturer's instructions.

Cell migration assay

Cells were seeded 2.5 x 10^4 cells/well in Incucyte Imagelock 96-well plates (Essen Biosciences, Cat #: 4379). Scratch wounds were made after 24 h cell growth using an Incucyte Woundmaker (Essen Biosciences, Cat #: 4493). Cells were then imaged for 2-3 days in an Incucyte Zoom Live-Cell Analysis System (Essen Biosciences) and analyzed using Incucyte software (Essen Biosciences). Relative wound density was measured every two hours for the duration of the experiment, comparisons were made by taking mean relative wound density of at least four biological replicates per experiment.

Verteporfin treatment

Cells were plated 5.0 x 10^5 cells/well in Cyto-One, 6-well tissue culture treated plates (USA Scientific, Ocala, FL, USA, Cat#: CC7682-7506). Verteporfin was then added to media at the appropriate concentration for 48 hours. RNA extraction, cDNA preparation and qPCR were then performed as in "Quantitative PCR" described above.

Statistical analysis

The statistics were performed using GraphPad Prism

Chapter 3: Investigations in mechanisms of Hippo-pathway mediated drug resistance

3.1 Introduction

Drug resistance is a major problem in the treatment of cancer. In both cytotoxic and targeted therapies, cancers that initially respond well to treatment often relapse with acquired resistance[124]. Acquired resistance to targeted therapy often occurs through mutation or amplification of the drug target, modification/activation of compensatory signaling either within the targeted pathway or in parallel signaling pathways[124,200]. Other mechanisms of resistance include increased tolerance and repair of drug-induced damage, deactivation of apoptosis and cell death signaling, altered interaction with tumor microenvironments, and alterations in drug uptake and efflux[124]. There is a critical need to understand further the signaling landscape involved in such resistances in order to clarify the nature of failed clinical trials and in helping to design novel treatment strategies.

The Hippo pathway is comprised of a kinase cascade that controls the activity of the transcriptional co-activator YAP[15,23]. Hippo mediated phosphorylation of YAP causes its nuclear exclusion, followed by cytoplasmic retention and degradation[15,23]. Excess YAP activity has been associated with several cellular processes known to promote tumor formation and metastasis, and increased nuclear YAP is seen in a variety of solid tumors[100,201]. YAP is also thoroughly involved in mediating diverse drug responses and has been implicated in increasing and decreasing resistance to various targeted and chemotherapeutic agents[127,133]. Gujral and Kirschner have previously identified a specific role for YAP in altering cellular response to the antimetabolite Gemcitabine[133]. I sought to expand on these findings by performing a larger scale drug screen using the Mechanism Interrogation Plate (MIPE) library of compounds with Dr. Michelle Ceribelli of the National Institute for the Advancement of Translational Science (NCATS)[202,203]. MIPE library drugs are well-annotated in terms of their target and mechanism of action, allowing for detailed pharmacogenetic probing

and improved hypothesis generation. Here, I have employed the MIPE library to screen for YAP-driven alterations to drug response.

The MIPE library drug screen identified both resistance and sensitivities to drugs targeting specific signaling nodes and cellular processes, and I confirmed YAP-driven resistance to drugs targeting the MAP kinase (MAPK) pathway member MEK (MAP2K1/MAP2K2). The MAPK signaling pathway is one of the most frequently mutated signaling pathways in cancer, with some cancers such as pancreatic ductal adenocarcinoma (PDAC) showing greater than 90% mutation rates in the GTPase KRAS[204,205]. Other mutations in the MAP kinase cascade are common in many other cancers and typically result in constitutive activation of mitogenic growth and proliferative signaling[206]. MEK kinases are commonly targeted in treating MAPK mutant cancers due to their status as watershed signaling nodes[207]. Indeed, MEK inhibition (MEKi) with Cobimetinib in combination with the BRAF inhibitor Vemurafenib has become standard of care in the treatment of BRAF and NRAS mutant melanoma, and clinical trials are ongoing evaluating their effectiveness in BRAF mutant non-small cell lung cancer and colorectal cancer[208]. However, despite initial response, MEKi treatment is almost invariably followed by resistance[200]. Additionally, not all MAPK driven cancers respond to MEKi treatment, and MEK inhibitors have failed in clinical trials treating KRAS-driven pancreatic cancer[209-211]. Mechanistically, resistance to MEKi is thought to occur through the induction of compensatory mitogenic signaling due to kinome re-programming[212,213]. Two prominent paths implicated in this regard are parallel activation of PI3K-AKT-MTOR signaling and feedback activation of upstream receptor tyrosine kinases (RTKs)[212,213]; however, the molecular underpinnings of kinome re-wiring underlying MEKi resistance are still being elucidated.

In this study, I confirmed AKT's activation in response to MEKi in YAP-driven cells but could not restore sensitivity through combined MEK and AKT inhibition. Moreover, although I saw large increases in the RTK AXL in response to YAP activity, I could not restore sensitivity to MEKi through combinatorial inhibition of AXL either. However, I discovered changes in the expression of four

apoptotic genes and increased expression of epithelial to mesenchymal transition (EMT) transcription factors. I thus postulate that MEKi resistance driven by YAP activity is mediated through a broad cellular state change that incorporates pro-survival and anti-apoptotic gene expression changes downstream of EMT that are highly resilient to perturbation of the traditionally expected kinase-centered survival mechanisms.

3.2 Results

3.2.1 High throughput drug screen identifies acquired resistances and sensitivities in YAP-driven cells

Dr. Ceribelli began our screen for Hippo-mediated alterations to drug response using the MIPE library in Panc02.13 cells expressing YAPS6A—a non-phosphorylatable, constitutively active mutant—as a positive control for YAP activity[214]. The MIPE library contains 2154 well-documented compounds, collectively encompassing 850 uniquely annotated mechanisms of action and/or protein targets (Figure 3.2.1.1A)[202,203]. YAPS6A caused widespread changes in drug response, increasing resistance to 16% of compounds (n = 342 drugs) and increasing sensitivity to 6% (n = 136 drugs) (Figure 3.2.1.1B). Previously Gujral and Kirschner have identified 14 drugs where YAPS6A increases sensitivity[133]. We were able to confirm increased sensitivity to ten out of fourteen of these drugs including Gemcitabine, Clofarabine, Cladribine, Tioguanine, Etoposide, Teniposide, Mitoxantrone, Methotrexate, Mitomycin, and Epirubicin (average $\log10AC_{50}$ (YAPS6A – WT): -0.85); increased resistance to three including 6-mercaptopurine, Topotecan, and Imatinib (average $\log10AC_{50}$ (YAPS6A – WT): 0.42); and no change in sensitivity to Cytarabine (Figure 3.2.1.2A)[133]. In addition to these findings, we observed consistent increases in sensitivity to 4 drugs targeting Topoisomerase-2A (TOP2A) (average $\log10AC_{50}$ (YAPS6A – WT): -0.86), 4 targeting dihydrofolate reductase (DHFR) (average $\log10AC_{50}$ (YAPS6A – WT): -0.91), 2 targeting DNA-methyltransferase (DNMT) (average $\log10AC_{50}$ (YAPS6A – WT): -1.225) 2 targeting 3-Hydroxy-3-Methylglutaryl-CoA Reductase (HMGCR) (average $\log10AC_{50}$ (YAPS6A – WT):- 0.6) and 2 targeting the CHK1/2 kinases (CHK1/2) (average $\log10AC_{50}$ (YAPS6A – WT): -0.79) (Figure 3.2.1.2B). In

contrast, we observed increases in resistance to drugs targeting the Aurora kinases (AURKi) (12, average log10AC_{50} (YAPS6A – WT): 6.06), tubulin depolymerization inhibitors (7, average log10AC_{50} (YAPS6A – WT): 1.423) and drugs targeting the MEK kinases (MEKi) (15, average log10AC_{50} (YAPS6A – WT): 1.75) (Figures 3.2.1.1D, 3.2.1.2C). YAP has previously been implicated in driving resistance to all three of these targets/processes supporting the validity of our screen[127].

To gain insight into signaling pathways underlying these drug responses, I subjected the subset of drugs with increased resistance (red in Figure 3.2.1.1A) to molecular enrichment analysis using Targetmine, a web-based data warehouse and integration tool for drug target prediction[215]. This analysis revealed drug targets involved in "MAPK signaling" as the most significant ($-\log_{10}(p\text{-value}) = 14.99$) followed by "PI3K-AKT" signaling ($-\log_{10}(p\text{-value}) = 14.00$), "RAP1 signaling" ($-\log_{10}(p\text{-value}) = 13.35$), "Interleukin signaling" ($-\log_{10}(p\text{-value}) = 12.64$), "Ras signaling" ($-\log_{10}(p\text{-value}) = 12.36$), "Focal adhesion" ($-\log_{10}(p\text{-value}) = 11.67$), "Endocrine resistance" ($-\log_{10}(p\text{-value}) = 11.59$), "Fluid shear stress" ($-\log_{10}(p\text{-value}) = 11.33$) and "Kaposi's Sarcoma" ($-\log_{10}(p\text{-value}) = 11.27$) (Figure 3.2.1.1C). I was intrigued to see MAPK signaling as a prominent hit because of the overwhelming resistance to MEK inhibitors seen in Panc02.13 cells expressing YAPS6A. AC50 values for all 15 members of these MEK inhibitors were on average more than four-fold higher in YAPS6A expressing cells (Figure 3.2.1.1D). Given such consistent resistance to MEK inhibitors, I decided to follow up in confirming YAP-mediated MEK inhibitor resistance.

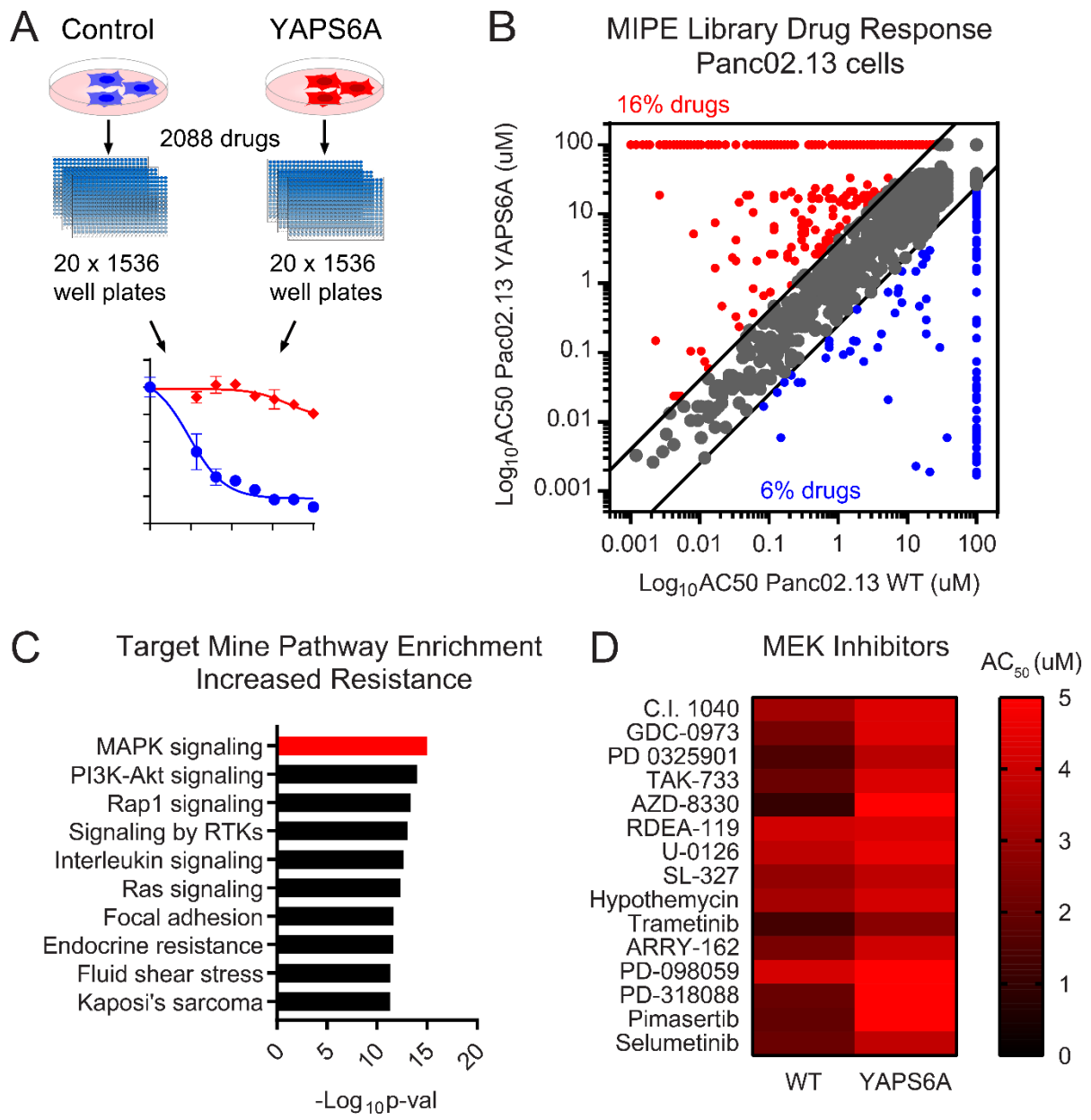

Figure 3.2.1.1 YAP-activity increases resistance to MEK inhibitors
A) Schematic of the MIPE screen. **B)** Scatter plot of AC_{50} values for all MIPE screen drugs. Red = increased resistance. Blue = increased sensitivity. **C)** Targetmine pathway enrichment profile for drugs where YAPS6A increases resistance (red in **B**). **D)** Heatmap of AC_{50} values for drugs targeting MEK in Panc02.13 cells expressing YAPS6A (+YAPS6A) versus wild type control (WT).

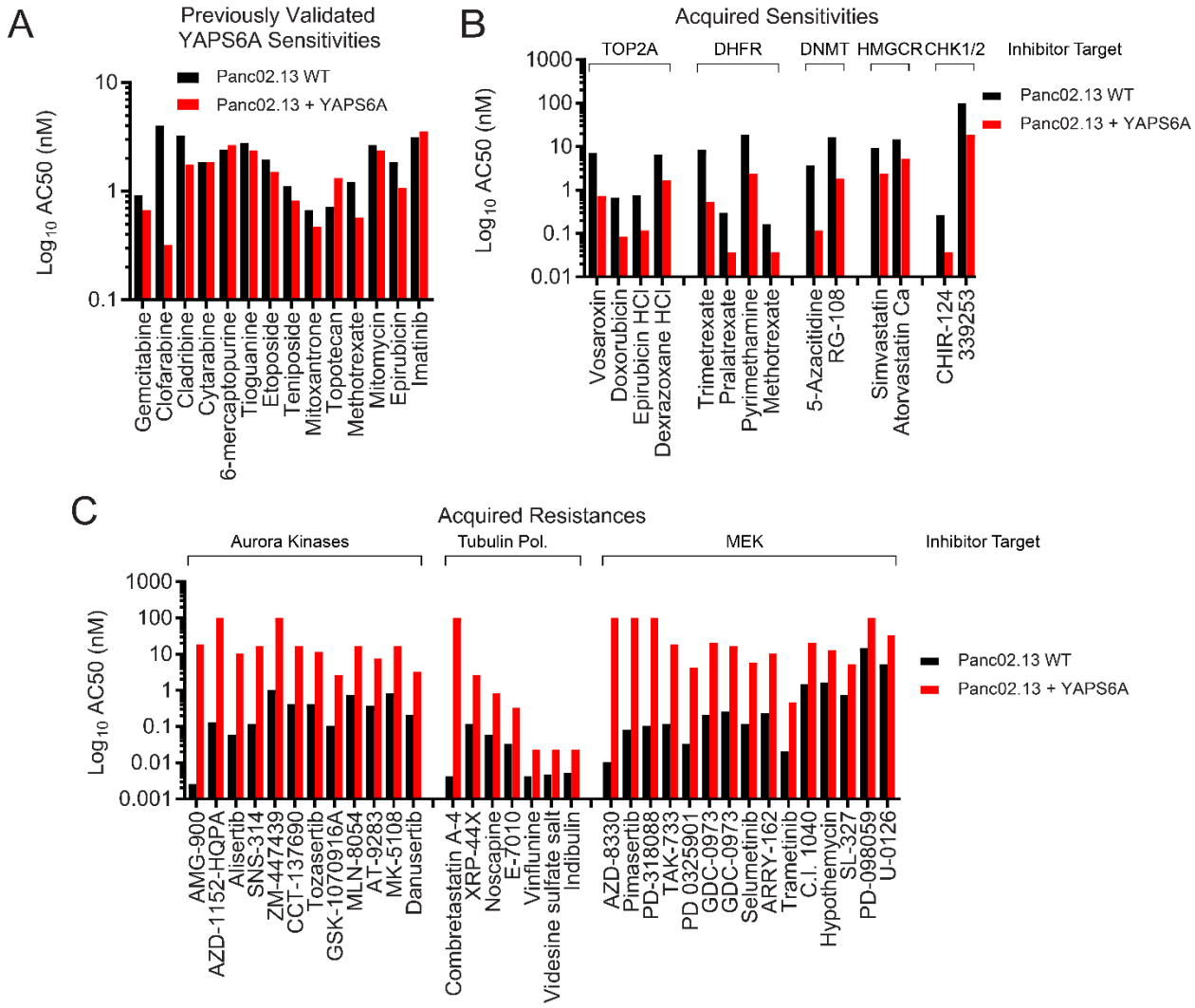

Figure 3.2.1.2 MIPE screen confirms the previously validated YAP-mediated drug sensitivities and identifies new acquired sensitivities and resistances.
A) AC_{50} values for drugs previously identified as having increased sensitivity in YAPS6A expressing cells[133]. **B)** AC_{50} values for MIPE drug targets/mechanisms of action with increased sensitivity. **C)** AC_{50} values for MIPE drug targets/mechanisms of action with increased resistance.

3.2.2 YAP activity confers resistance to MEK inhibitors

PD325901 and Selumetinib (hereafter termed MEKi) are two ATP-non-competitive MEK1/2 inhibitors with IC_{50} values against MEK1/2 of 1nm and 14nM, respectively[216]. With the help of Aya Miyaki, we confirmed these inhibitors both efficiently reduced MEK activity as measured by reduced phosphorylation of MEK1/2 activation loop residues S217/S221 (Figure 3.2.2A). Additionally, ERK1/2 kinases immediately downstream of MEK1/2 also showed reduced phosphorylation under MEKi treatment, demonstrating efficient inhibition of the MAPK signaling pathway and implicating MEK1/2 as primary mediators of MAPK signaling in Panc02.13 cells (Figure 3.2.2A). Interestingly, we did not observe any increase in cleaved caspase-3A, suggesting that apoptosis is not increased in response to MEKi in either WT or YAPS6A expressing Panc02.13 cells.

I next sought to confirm YAP-mediated MEKi resistance in density controlled cellular growth assays. Increases in cellular contact activate the Hippo pathway and decrease YAP nuclear localization, providing an experimental method to modulate wild-type YAP activity[23]. YAPS6A is insensitive to Hippo activation and therefore also to cellular contact[214]. Gujral and Kirschner have also previously confirmed this approach in validating Hippo-mediated alterations to Gemcitabine[133]. In high-density cell growth assays, expression of YAPS6A causes a profound increase in resistance to MEK inhibitors PD325901 and Selumetinib in Panc02.13 and Panc10.05 cancer lines (Figure 3.2.2A, B). Conversely, untransfected wild type parental cells show similar growth inhibition responses to cells with YAP knockdown, demonstrating MEK1/2 sensitivity in cells with reduced YAP activity (Figure 3.2.2A, B). Furthermore, low-density plating of cells—which promotes high endogenous YAP activity—increases MEKi resistance only in wild type cells; cells with YAP knockdown still maintain sensitivity (Figure 3.2.2A, B). These data confirm YAP involvement in conferring MEK inhibitor resistance.

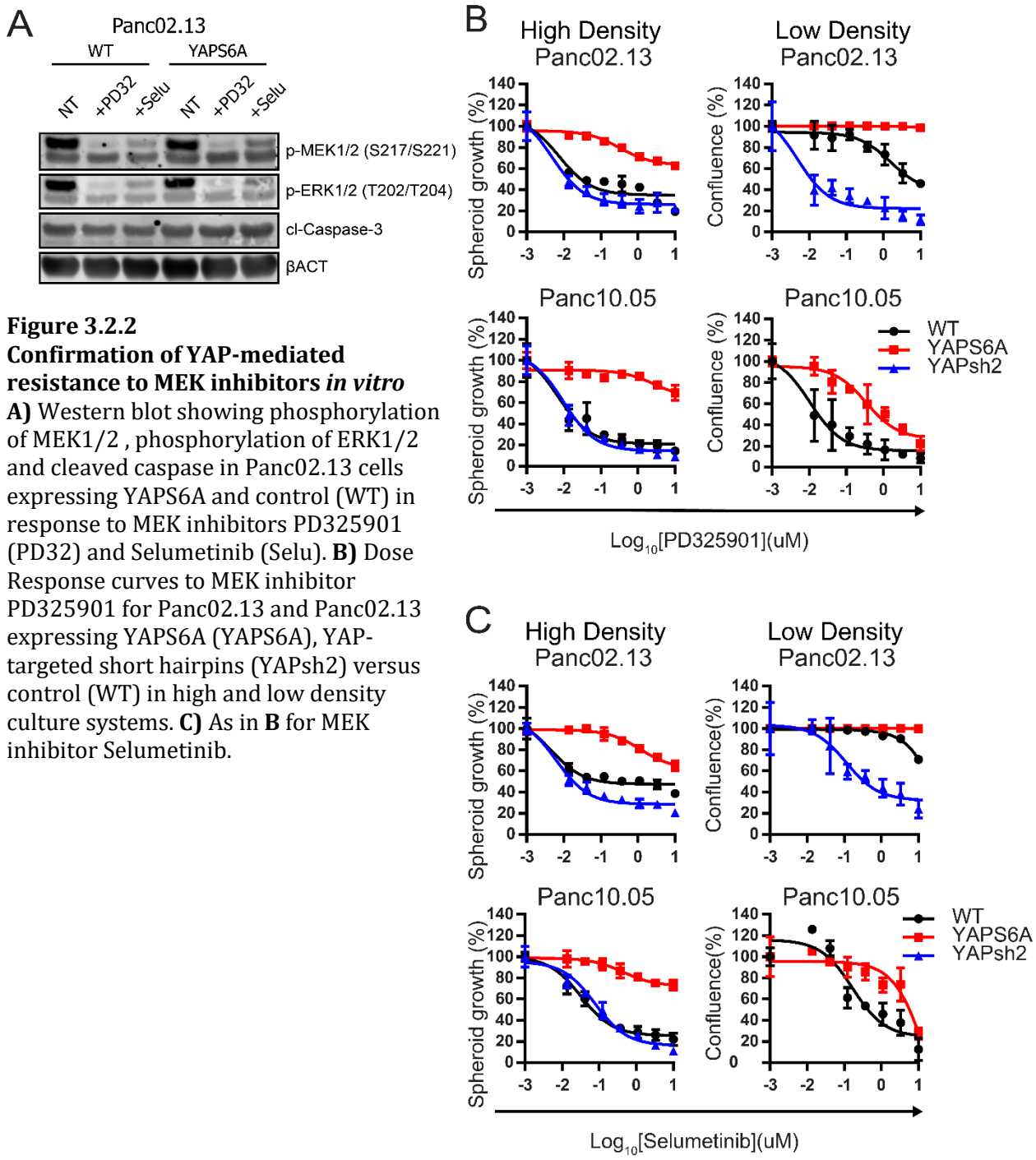

Figure 3.2.2
Confirmation of YAP-mediated resistance to MEK inhibitors *in vitro*
A) Western blot showing phosphorylation of MEK1/2 , phosphorylation of ERK1/2 and cleaved caspase in Panc02.13 cells expressing YAPS6A and control (WT) in response to MEK inhibitors PD325901 (PD32) and Selumetinib (Selu). **B)** Dose Response curves to MEK inhibitor PD325901 for Panc02.13 and Panc02.13 expressing YAPS6A (YAPS6A), YAP-targeted short hairpins (YAPsh2) versus control (WT) in high and low density culture systems. **C)** As in **B** for MEK inhibitor Selumetinib.

3.2.3 Resistance to MEK inhibitors is not mediated through compensatory AKT signaling

Upon observing this escape from MEKi treatment, I hypothesized that rewiring of the growth factor signaling networks might be responsible for the resistance. AKT is a cell-survival pathway that has been implicated as a MEKi resistance escape mechanism; however, the molecular determinants of this interaction are still being elucidated[200]. I observed increased AKT signaling at baseline in cells transformed with constitutively active YAPS6A and in cells with knockdown of Neurofibromatosis 2 (NF2), an upstream negative regulator of YAP (Figure 3.2.3A)[54]. I observed an increase in this YAP-mediated basal level of AKT activation in response to MEKi in both Panc02.13 and to a lesser extent in Panc10.05 (Figure 3.2.3B). I next sought to inhibit AKT compensatory signaling using the small molecule MK-2206 (hereafter AKTi), a potent and selective AKT inhibiting small molecule[217]. AKTi was able to completely abolish AKT phosphorylation even at very low (120 nM) doses (Figure 3.2.3C). However, treatment of Panc02.13 cells with MK-2206 did not drastically impair cell growth regardless of the YAPS6A expression or cell density conditions, indicating AKT activity is dispensable for growth of these cells (Figure 3.2.3C). To test for the ability of AKT to rescue MEKi sensitivity, I attempted a combination treatment of AKTi with MEKi in YAPS6A expressing cells, reasoning that AKT suppression should eliminate a YAP-driven MEKi escape mechanism. Surprisingly Panc02.13 cells with YAPS6A responded very mildly to combination treatment, exhibiting no increased efficacy over single-agent treatments (Figure 3.2.3D). These data indicate that AKTi is insufficient in restoring MEKi sensitivity in YAP-driven cells.

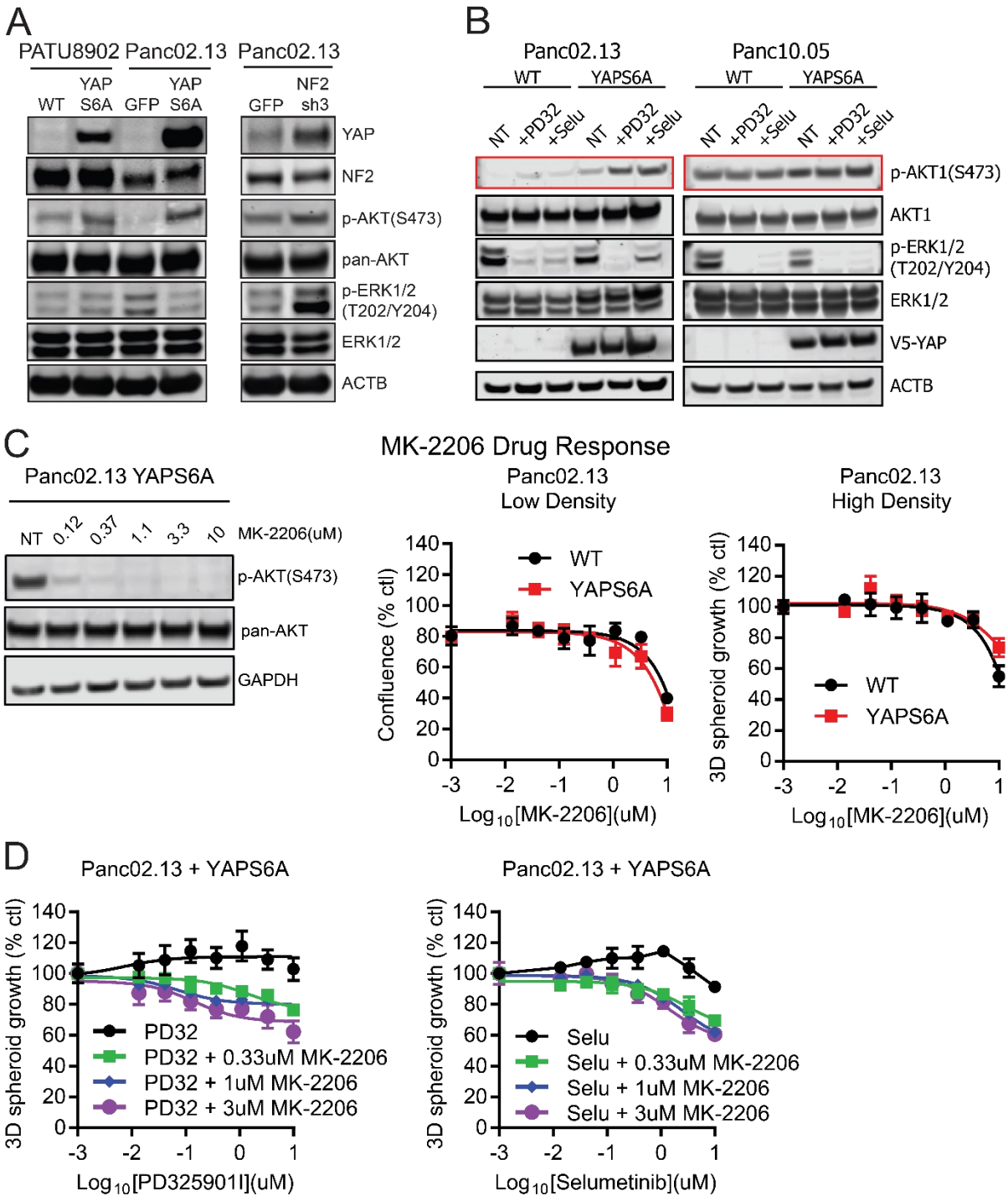

Figure 3.2.3 MEK inhibitor resistance is not mediated through compensatory activation of AKT

A) Western blot showing activation of AKT in response to elevated YAP activity. **B)** Western blot showing increased AKT activation in response to MEK inhibitors PD325901 (PD32) and Selumetinib (Selu) at 1uM **C)** *Left:* Western blot showing efficient inhibition of AKT phosphorylation with MK-2206 treatment. *Middle, right:* Dose response to MK-2206 treatment in Panc02.13 cells expressing YAPS6A versus control. **D)** Panc02.13 cells expressing YAPS6A dose

response to combination MEK inhibitor (Selumetinib and PD325901) and AKT inhibitor (MK-2206) treatment.

3.2.4 MEKi resistance is not mediated through upregulation of AXL

Having eliminated AKT activity as an essential mechanism for MEKi escape, I began an expanded search for potential upstream regulators. I chose to focus on receptor tyrosine kinases (RTKs) due to their ability to activate multiple downstream pathways and critical involvement in drug resistance[212,213,218]. YAPS6A caused significant changes in the expression of 27/58 selected RTKs (Figure 3.2.4A). I was intrigued by the increased expression of AXL (log2 fold change: 2.84, p-value: 3.44×10^{-8}) due to its large total expression, status as a *bona fide* YAP target, and the simultaneous increase in expression of its ligands GAS6 (log2 fold change: 4.55, p-value: 1.76×10^{-6}) and PROS1 (log2 fold change: 3.05, p-value: 1.70×10^{-6}) (Figure 3.2.4B)[96,219]. I confirmed increased expression at the protein level in Panc02.13 and RWP cell lines expressing YAPS6A, as well as in Panc02.13 cells with NF2 knockdown via western blot (Figure 3.2.4B). Therefore, I hypothesized that increased expression of AXL and its ligands functionally link YAP activity with increased AKT activation while simultaneously providing an alternative escape route to MEK inhibitors. I first evaluated Panc02.13 cell dependence on AXL activity using the AXL inhibitor R428[220,221] (hereafter termed AXLi). Treatment of YAPS6A expressing cells with AXLi did not reduce phosphorylation of the AXL transphosphorylation site T702[222] but was able to reduce phosphorylation of AKT, a downstream target of AXL, at higher doses (Figure 3.2.4C). Similar to AKTi, AXLi did not impair the growth of Panc02.13 WT or YAPS6A expressing cells at either high or low density (Figure 3.2.4C). Combination treatment of YAPS6A expressing cells with AXLi and MEKi did not enhance growth inhibition (Figure 3.2.4D). Collectively these results indicate that, like AKTi, AXLi is insufficient in restoring MEKi sensitivity in YAP-driven cells.

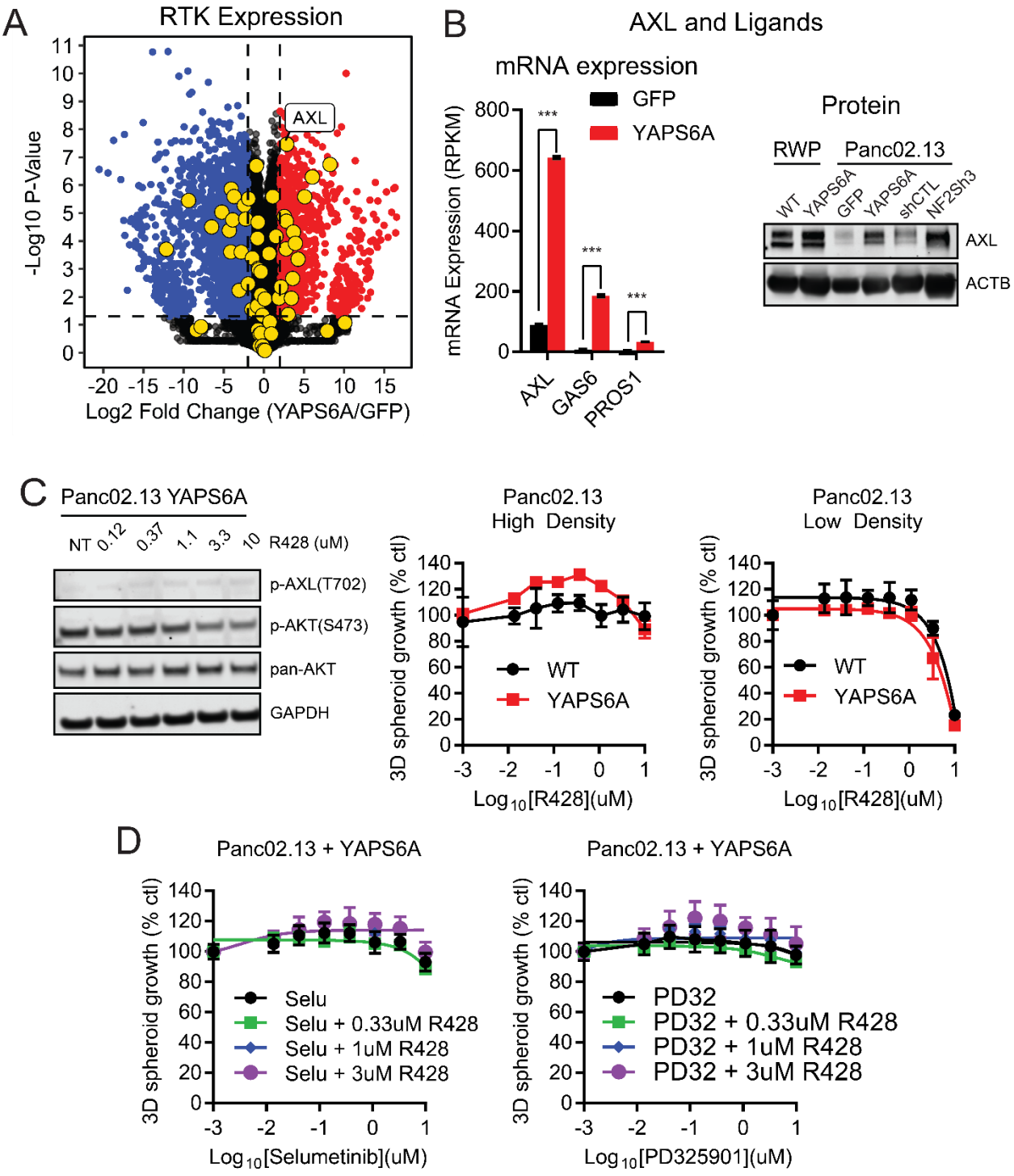

Figure 3.2.4 MEK inhibitor resistance induced by YAP is not mediated through AXL activity
A) *Left*: Volcano plot of whole transcriptome RNA sequencing in YAPS6A versus GFP transfected Panc02.13 cells. Highlighted yellow circles represent RTKs. Log2 fold change (YAPS6A/GFP) vs. -log10 P-values (two-sample T-test). *Middle*: mRNA expression of AXL and its ligands GAS6 and PROS1 in Panc02.13 cells transfected with YAPS6A versus GFP. *Right:* Western blot of AXL in RWP cells expressing YAPS6A versus un-transfected control (WT); in Panc02.13 cells expressing YAPS6A versus GFP control, or NF2 targeting short hairpin RNA (NF2sh3) versus non-targeting control

(shCTL) (*** denotes p-value < 0.001). **B)** *Left:* Western blot of AXL and AKT phosphorylation in response to AXL inhibitor R428 treatment in Panc02.13 cells expressing YAPS6A. *Middle, right:* Dose-response to R428 treatment in Panc02.13 cells expressing YAPS6A versus control at high and low-density growth conditions. **C)** Panc02.13 cells expressing YAPS6A dose-response to combination AXL inhibitor (Selumetinib and PD325901) and AXL inhibitor (R428) treatment.

3.2.5 YAP-driven changes to apoptosis may drive resistance to MEKi

After kinase-targeted approaches failed to reverse YAP-mediated MEKi resistance, I began to investigate YAP's effects on resistance mechanisms independent of the kinome. Previously, YAP has been implicated in both pro-[82] and anti-apoptotic[214] signaling, and YAP-driven alterations to apoptosis have been specifically implicated in driving resistance to RAF[135], MEK[135], and EGFR inhibitors[139] in lung cancer contexts. Therefore, I surveyed YAP-driven changes to apoptotic regulators using RNAseq and found significant expression level changes in four separate regulators of the intrinsic apoptotic pathway (Figure 3.2.5A). Two members of the BCL-2 family of pro-survival proteins had alternately increased (*BCL2A1* encoding BFL1, log2 fold change: -3.62, *p*-value: 7.91×10^{-5}) and decreased (*BCL2* encoding BCL2, log2 fold change: 2.89, *p*-value: 1.40×10^{-4}). Expression of two members of the BH-3 only family of apoptotic activators/sensitizers were also affected by YAPS6A with *BMF* (encoding BMF, log2 fold change: -2.47, *p*-value: 7.49×10^{-5}) decreasing in expression and *HRK* (encoding HRK, log2 fold change: 5.47, *p*-value: 2.44×10^{-3}) increasing in expression.

It has been suggested that the underlying relationship between YAP and apoptotic-factor-based resistance to MEK inhibitors is accomplished in coordination with the SLUG transcription factor, a major promoter of EMT[101,140]. In support of this hypothesis, I have confirmed a significant enrichment in the EMT hallmark gene set in YAPS6A transfected cells, implicating a clear shift towards a mesenchymal cell state (Figure 3.2.5B,C). Among these transcriptional changes, I observed large upregulation in the expression of *SNAI1* (log2 fold change: 1.38, p-value: 9.80×10^{-5}) and *SNAI2* (log2 fold change: 1.27, p-value: 4.72×10^{-4}) and *ZEB1* (log2 fold change: 2.56, p-value: 1.39×10^{-7})and *ZEB2* (log2 fold change: 2.30, p-value: 7.19×10^{-6}), EMT promoting transcription

factors which have both been previously reported to bind to YAP[92,93]. I, thus, hypothesize that in Panc02.13/Panc10.05 parental cells with functioning Hippo pathway, MEK inhibition of the MAPK pathway is sufficient to impair cellular growth (Figure 3.2.6A). However, in cells experiencing excess YAP activity, YAP cooperation with SLUG or other EMT transcription factors promotes a pro-survival state mediated by the upregulation of BCL2 and the downregulation of BMF, allowing sustained growth and survival despite MEKi treatment (Figure 3.2.6B).

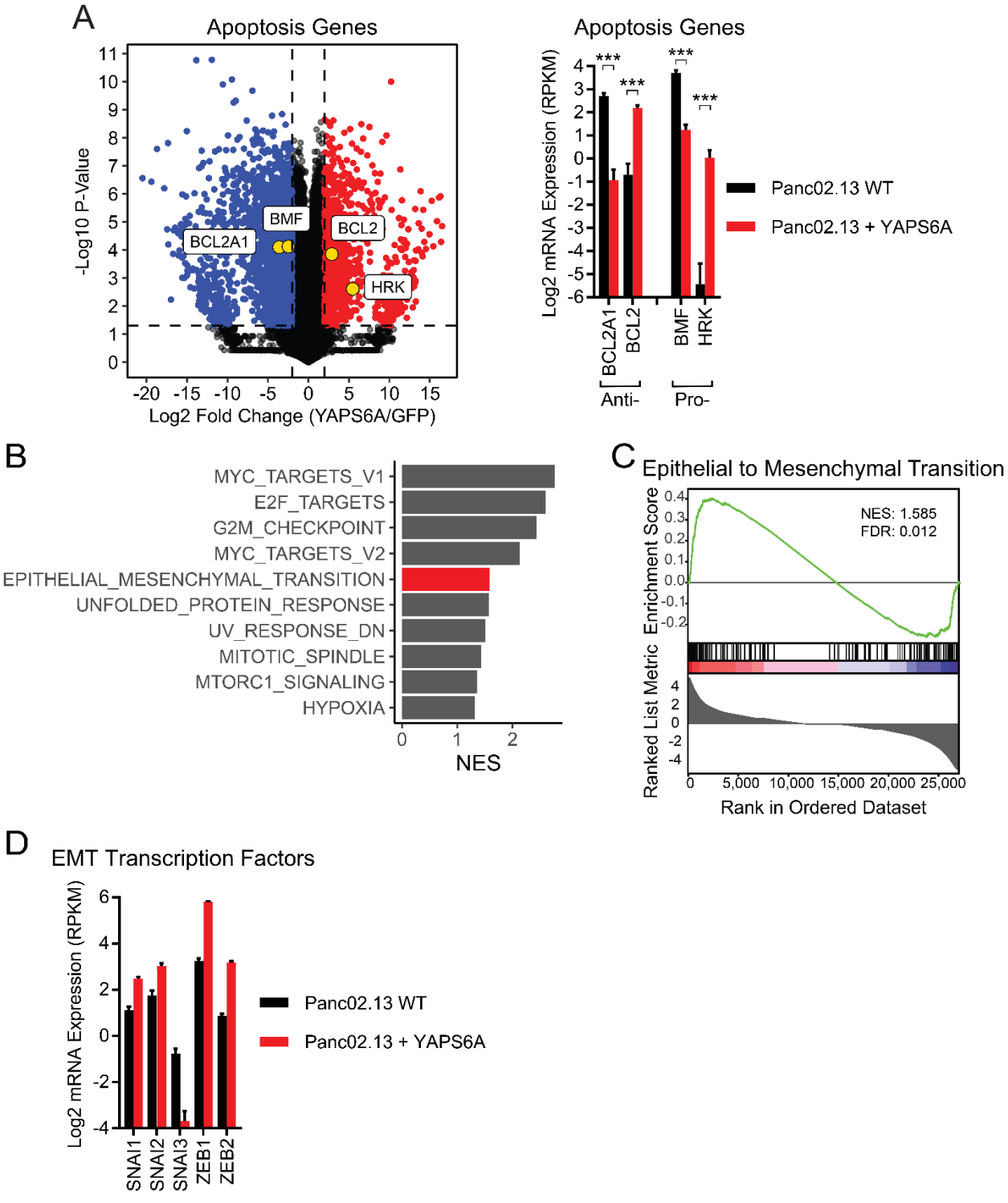

Figure 3.2.5 YAPS6A alters transcription of apoptosis regulators and increases EMT
A) *Left:* Whole transcriptome sequencing of Panc02.13 cells transfected with YAPS6A versus control. Members of the intrinsic apoptosis pathway with significantly altered expression are highlighted. *Right* MRNA expression values for significantly altered intrinsic apoptosis regulators (*** denotes p-value < 0.001). **B)** Gene set enrichment analysis normalized enrichment score (NES) values for Hallmark gene sets. **C)** The Hallmark Epithelial Mesenchymal Transition gene set

enrichment plot. NES: normalized enrichment score, FDR: false discovery ratio. **D)** MRNA expression values for common EMT promoting transcription factors in Panc02.13 cells transfected with YAPS6A versus control (WT) (*** denotes p-value < 0.001).

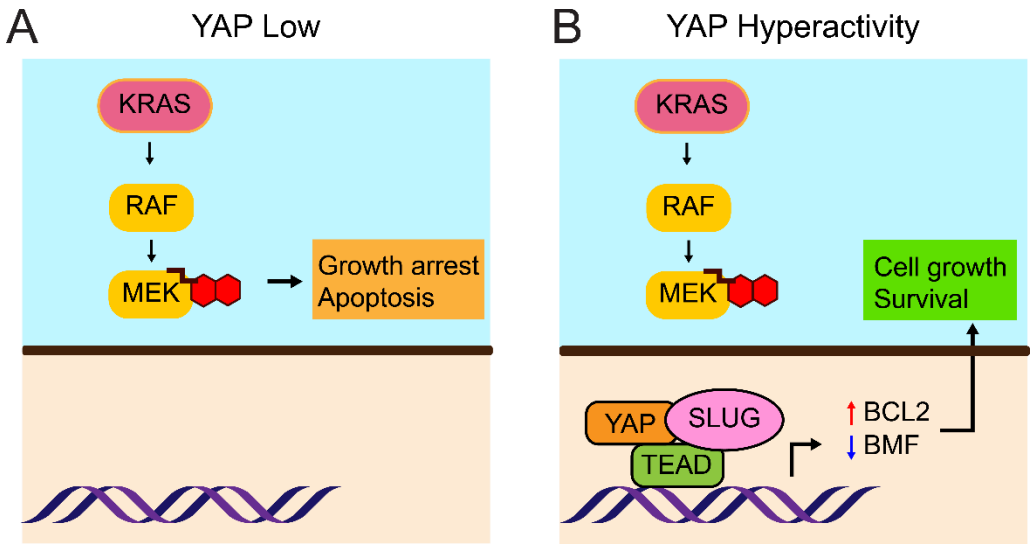

Figure 3.2.6 YAP activity allows MEK inhibitor escape via apoptotic gene regulation
A) In normal KRAS driven pancreatic cells, MEK inhibitors are sufficient to block cell growth. **B)** When YAP is hyperactive, cooperation with TEADs and EMT transcription factors (SLUG here) promote the upregulation of pro-survival BCL2 and the downregulation of pro-apoptotic BMF resulting in MEK inhibitor escape.

3.3 Discussion

Yap activity has a complex relationship with drug resistance, at times increasing and at other times decreasing resistance. Here, with Michelle Ceribelli, we have performed a drug screen with the MIPE library of compounds to offer expanded insight into the compounds and processes affected by YAP activity. The MIPE screen confirmed that YAP activity alters the cellular response to 428 drugs, or 22% of the library. Among drug targets with increased sensitivity driven by YAP, TOP2A and DHFR inhibitors have paradoxically been found to have YAP-driven resistance in other cell systems[127]. It is tempting to assume that the higher growth rate induced by YAP raises the threshold of replication stress causing these drugs to be more effective; however, previous work has shown that, in the case of certain chemotherapeutic agents such as gemcitabine, the increased sensitivity in YAP expressing cells is more likely a result of altered expression of drug metabolizing enzymes and drug efflux pumps[133]. Similar effects may be occurring here in regard to TOP2A, DNMT and DHFR inhibitors[133]. HMGCR inhibitors (also known as statins) have been noted to inhibit YAP by reducing upstream positive regulation through RHO[223]. Increased sensitivity here may indicate oncogenic addiction to YAP within Panc02.13 cells. Among increased sensitivities in our screen, CHK1/2 inhibitors were the only kinase inhibitors identified. CHK1 signaling contributes to control of cell entry into the S and G2/M while CHK2 contributes to the G1 checkpoint[224]. In this case, YAP-mediated increases to cell cycle progression may induce a cellular state that is heavily reliant on the CHK kinases to properly control pre-mature cell cycle entry, e.g. when the CHK kinases are non-functioning, excess replication stress induced by YAP is enough to induce cell death in YAP-driven cells, whereas in wild type contexts, the reduced replicative burden is manageable even in the absence of CHK signaling. More research is needed to determine the mechanistic nature of these specific drug sensitivities, but they present themselves as potential selective agents to target YAP-driven cancers.

In addition to sensitivities, the MIPE screen identified several YAP-mediated resistances to

drugs that target specific kinases (AUR, MEK) or cellular processes (tubulin polymerization). YAP has been previously implicated in increasing resistance microtubule targeting drugs; however, there is debate about the mechanism promoting tubulin drug resistance[127]. Due to the diverse chemical nature of drug structures within the drug classification "tubulin polymerization inhibitors" in our screen it is likely that YAP activates resistance to the mechanism of tubulin depolymerization itself, rather than the metabolism of individual drugs. Contrary to tubulin inhibitors, MIPE drugs targeting the Aurora and MEK kinases are primarily comprised of serine-threonine kinase inhibitors. It is interesting to note that both tubulin polymerization and aurora kinases are intricately involved in mitosis, suggesting YAP causes an intrinsic resistance to drugs targeting the mitotic checkpoint. MEK kinases on the other hand are important transducers of MAPK signaling.

Previously, YAP activity was identified as a driver of MAPKi resistance through promoting AKT activity[138] and through promoting RTK expression such as AXL[138]. Here, I have directly tested compensatory signaling through the activation of AKT and the expression of AXL through combinatorial drug treatments in pancreatic cells, yet I found that inhibition of AXL or AKT in combination with MEKi provides little to no increased effectiveness compared to single agent treatment (Figures 3.2.3D, 3.2.4D). Thus, it is unlikely that YAP's influence on MEKi resistance is mediated solely through kinome re-programming of AKT and AXL signaling. These results are in agreement with similar failures in the efficacy of MEK and PI3K/AKT combination therapy in KRAS driven cell models[225] and clinical trials[226]. It is, therefore, likely that in KRAS-driven cancers in general and in YAP-activated contexts in particular, there exists an arsenal of survival pathways that allow for escape from targeted inhibition of kinase oncogenic drivers.

In 2014 Hata *et. al.* made the discovery that differential activation of apoptosis may underly the heterogeneity in response to MAPKi therapy in non-small cell lung cancer (NSCLC)[225]. Since then, YAP activity has been implicated as a primary mediator of this effect in NSCLC, although there

is still debate as to the specific apoptotic genes involved[135,140]. Several groups have also investigated YAP's involvement in MAPKi resistance in pancreatic ductal adenocarcinoma and have arrived at differing conclusions: Kapoor *et. al.*[137] identify YAP-TEAD cooperation with E2F was able to drive cell cycle progression allowing for MEKi escape. Alternatively, Shao *et. al.*[116] implicate a TEAD independent mechanism based on YAP cooperation with FOS1 that drives EMT to promote survival. Here I have provided evidence supporting the latter hypothesis: that YAP drives resistance to MAPK inhibition through an EMT transcriptional paradigm that promotes an altered apoptotic response. Although this study was conducted in PDAC cell lines, due to the similarities seen in YAP-driven MEKi resistance seen in NSCLC[135,225], it is tempting to suggest that these findings may be generally extendable to KRAS driven tumor contexts. EMT involves a complex change of cell state and has been implicated in many areas of cancer progression, including metastasis, the establishment of cancer stem cells and drug resistance[227,228]. Mechanistically, EMT has variously been described to increase resistance to therapy by altering drug metabolism and efflux, reduce proliferation and by increasing survival through modifying cellular apoptosis[227]. Indeed, the EMT transcription factors ZEB1 and TWIST have been linked to increased resistance to EGFR inhibitors via decreasing the expression of BIM, a critical positive regulator of apoptosis[229,230]. YAP's influence on EMT has been well established, and the above work in this dissertation underscores this fact[54,75]. Here, I have identified increased transcription of *SNAI1/2* and *ZEB1/2,* which are likely to be responsible for promoting a pro-survival cellular state in the face of MEKi. Therefore, I hypothesize that the key link between YAP and MEK inhibitor resistance lies in the EMT/apoptosis axis generated as a result of YAP activity. Further work is needed in clarifying the relationship between YAP, EMT and modifications to apoptosis. Given the ubiquity of oncogenic mutations in the MAPK pathway and YAP's commonality in exacerbating resistance to therapies targeting these drivers, I hope this study will add to the understanding of YAP's relationship in driving resistance to targeted therapy.

3.4 Materials and Methods

MIPE screen

The MIPE screen was carried out by Michele Ceribelli as described previously[202]. Cells were seeded onto 1536 well microtitre plates and MIPE drugs were applied at the appropriate concentrations. Cell viability was measured with CellTiter-Glo (Promega Corporation, Madison, WI, USA) and used to generate dose response curves. Curves were fit using the NCGC curve fit tool (https://tripod.nih.gov/curvefit/[202]). Dose response curves were then used to interpolate AC_{50} values for each compound.

Cell lines and reagents

Panc02.13, RWP and Panc10.05 cancer cell lines were obtained from American Type Culture Collection (ATCC). FOCUS cells were obtained from J. Wands (Brown University) and have been previously described[173]. Panc02.13 and Panc10.05 cells were cultured in RPMI1640 supplemented with 10% (v/v) fetal bovine serum (FBS), 100 IU/ml penicillin, and 100 µg/ml streptomycin. FOCUS cells were culture in DMEM supplemented with 10% (v/v) fetal bovine serum (FBS), 100 IU/ml penicillin, and 100 µg/ml streptomycin.

Western blotting

Cells were lysed in SDS-based lysis buffer (50 mM Tris-HCl, 2% SDS, 5% Glycerol, 5 mM EDTA, 1 mM NaF, 1xProtease/Phosphatase inhibitor cocktail, 10 mM β-GP, 1 mM PMSF, 1 mM Na3VO4, 1 mM DTT). Monolayer cells were washed twice with PBS and suspended into the SDS lysis buffer. The remaining debris were removed by centrifuge filtration. Protein concentration was measured by BCA assay with bovine serum albumin as a standard. Protein samples were then suspended in nuPAGE LDS sample buffer (Invitrogen) denaturing at 95°C for 5 min in reducing condition by nuPAGE sample reducing agent (Invitrogen). 10-20 µg of protein per lane were separated with 4-12% Bis-Tris gradient gels (Invitrogen) in MOPS SDS running buffer (Invitrogen). The proteins were transferred by tank blotting system to nitrocellulose membrane. The membrane

was blocked with LICOR blocking buffer (PBS) for 1 h at ambient temperature, followed by primary antibody at 1:1000 in the blocking buffer at 4°C for 12-18 h (Li-cor, Lincoln, Nebraska, USA). After washing with PBS, the membrane was incubated with infra-red-conjugated antibodies at 1:5000 for 1 h at room temperature (Li-cor, Lincoln, Nebraska, USA). The signal was imaged by Odyssey imaging system, and the band intensities were quantified with the Odyssey imaging analysis software (Li-cor, Lincoln, Nebraska, USA). The signal intensities of each protein were normalized with that of β-Actin or GAPDH.

Purified Antibodies

Antibodies used were anti-YAP (Cell Signaling Technology, Danvers, MA, USA, Cat #: 12395), anti-Merlin (*NF2*, Cell Signaling Technology, Danvers, MA, USA, Cat #: 12896), anti-phospho-AKT(S473) (Cell Signaling Technology, Danvers, MA, USA, Cat #: 9271), anti-AKT(pan) (Cell Signaling Technology, Danvers, MA, USA, Cat #: 4691), anti-phospho-ERK1/2(T202/Y204) (Cell Signaling Technology, Danvers, MA, USA, Cat #: 4376), anti-ERK1/2 (Cell Signaling Technology, Danvers, MA, USA, Cat #: 9102), anti-AKT1 (Cell Signaling Technology, Danvers, MA, USA, Cat #: 2938), anti-V5 (Invitrogen, Cat #: 46-0705), anti-β-Actin (Santa Cruz Biotechnology, Cat #: sc-47778), anti-AXL (Cell Signaling Technology, Danvers, MA, USA, Cat #: 4939), anti-phospho-AXL(Y702) (Cell Signaling Technology, Danvers, MA, USA, Cat #: 5724).

Cell growth assays

Low density cell growth assays: Cells were seeded 2-4 x 10^3 cells/well in Cyto-One, 96-well, flat-bottom, tissue culture treated plates (USA Scientific, Ocala, FL, USA, Cat#: CC7682-7506). After 24 hours, small molecules were then added at the appropriate concentration and cell growth was tracked using Incucycte Live-Cell Imaging System and accompanying software (Essen Biosciences). Confluence was measured every hour for 48-96 hours or until control (DMSO-only) samples had reached 100% confluence.

High density cell growth assays: Cells were seeded 5 x 10^3 cells/well in Corning, round

bottom ultra-low attachment microplates (Corning Cat #: 7007). Immediately after seeding, plates were spun in a tabletop centrifuge for 10 min at 1000 RPM to form spheroids. 24 hours after spinning spheroids had formed. We then added small molecules at the appropriate concentration to the media and cells were allowed to grow for 72-96 hours. Total cell viability was then measured using CellTiter-Glo (Promega Corporation, Madison, WI, USA) according to the manufacturers instructions.

Small molecules

PD325901 (cat #: S1036), Selumetinib (cat #: S1008), and R428 (cat #: S2841) were purchased from Sellekchem (Houston, TX, USA). MK-2206 was purchased from Cayman Chemical (Ann Arbor, Michigan, USA).

Gene set enrichment analysis

We used software version 4.0.3 downloaded from http://www.gsea-msigdb.org/gsea/index.jsp using RNAseq data generated from Panc02.13 cells expressing YAPS6A versus untransfected control. We used the Hallmark gene sets[168], permutations were set at 1000 and permutation type was set to phenotype.

Expression constructs and RNAi knockdown

Panc02.13 and Panc10.05 cells expressing YAPS6A or GFP were previously generated[133]. Panc02.13 cells expressing GIPZ lentiviral shRNAmir cloens targeting human YAP, NF2 or scrambled control were generated previously[133].

Statistical analysis

The statistics were performed using GraphPad Prism

Chapter 4: Conclusions and future directions

The Hippo pathway is an important signaling pathway with multi-faceted effects in development and oncogenesis. Chapter 1 introduces the research done in flies that led to the discovery of the Hippo pathway as a critical mediator of organ size determination. Subsequently, a boom in Hippo studies revealed 35+ upstream regulators variously involved in cell junctional complexes, apico-basal polarity complexes, actin cytoskeletal dynamics, and many others. Generally, the Hippo pathway is activated in epithelial organized tissue experiencing high cell contact and properly determined apical-basal polarity. Conversely, The Hippo pathway is antagonized by loss or disruption of cell-cell contact or disruption of polarity. Despite this progress in defining the upstream regulators of the Hippo pathway, there is still a need for a mechanistic understanding of the mediators of YAP-driven phenotypes. I then described the Hippo pathway's output, focusing on studies that characterize how YAP transcriptional activity is involved in carcinogenesis. These studies have indicated that YAP activity induces cell proliferation and survival, cancer stem cell traits, increased growth factors, and metastasis via EMT[98]. However, this transcriptional information falls short in elucidating specific mediators of YAP function, something that may be particularly useful in targeting YAP's effects in the context of cancer.

After this description of Hippo pathway inputs and outputs, I focused specifically on YAP-driven effects on EMT and drug resistance. Similar to YAPs involvement in cancer, YAP involvement in EMT and drug resistance is well-documented, yet specific mediators of YAP's effects on EMT and drug resistance are lacking. While these two sections are presented separately in the introduction, they are intimately related to each other at the molecular level. EMT has long been known to alter drug resistance and has even been implicated as a specific mechanism employed by YAP to escape targeted therapy. YAP's position at the center of a signaling module that activates both of these phenomena hints at a likely relationship between the three. Chapter 2 explored YAP-driven effects on kinome re-wiring and how alterations in ZAK activity mediate YAP's influence on EMT. In

Chapter 3 I explored drug response changes driven by YAP, again focusing on the kinome. In both studies, the MAPK pathway is a central figure, indicating that YAP is reliant on MAPK as a secondary mediator of its effects on the cell and that this signaling is flexible in the face of inhibition. There are still many unanswered questions and future directions that warrant follow-up investigations.

In Chapter 2, I make the case for ZAK as a mediator of YAP's effects on inducing EMT. The ZAK kinase is upregulated in response to YAP activity and has a clear role in driving EMT. It would be worthwhile to investigate what proportion of YAPs effect on EMT is driven through ZAK specifically. My attempts to address this via knockdown of ZAK in YAP-driven cells were not successful due to inefficient knockdown of ZAK, likely because the S6A mutation on YAP may be powerful enough to overcome the knockdown (data not shown). However, ZAK expression is reduced at high cell density, a more physiologically relevant method for inducing YAP downregulation. Additionally, ZAK expression is well correlated with Hippo response genes in TCGA data, providing further evidence that the positive relationship between YAP activity and ZAK expression holds in clinical samples. The transcriptional machinery linking YAP to ZAK expression also requires further elucidation. ZAK is expressed ubiquitously and thus likely has many transcription factors controlling its expression. Genomic analysis of the ZAK promoter may provide a short-list of potential candidate transcription factors that YAP may cooperate with to drive ZAK expression. A systematic shRNA screen of these factors would then be able to further identify critical mediators of ZAK expression.

This study also brings up several questions regarding the function of the ZAK kinase. Notably, it is unclear how ZAK is influencing EMT in a YAP-active cellular context. Both ZAKα and ZAKβ are capable of signaling through the MAPK effectors ERK, p38, and JNK, and it has been hypothesized that ERK is the major signaling node responsible for ZAK dependent migration[153,163,164]. Therefore, it is a critical future task to identify which of these MAPK signaling arms is responsible for inducing EMT in a Hippo dysregulated context. Furthermore, there is likely involvement of EMT

transcription factors downstream of ZAK. Li and colleagues have identified several transcription factors that may regulate ZAK's effects on EMT including ZEB1, NFκB, SRE, AP-1 and others[165]. Notably, the upregulation of ZEB suggests positive feedback between YAP and ZAK activity, which may cooperate through ZEB to fully induce EMT in YAP driven cells. Deciphering this regulatory circuit may will help clarify YAP-driven EMT as mediated through ZAK.

I have identified specific differences in behavior between the two isoforms of ZAK. For example, IF imaging suggests that ZAKα is localized cytosolically, while ZAKβ resides in the nucleus (Figure 2.2.4.1C). Additionally, I found ZAKβ is much more potent of an inducer of EMT than ZAKα, at least in the transcription of EMT markers (Figure 2.2.4.1E). These differences are in slight disagreement with previous studies, showing equal cytosolic localization[153] and relatively similar induction of EMT[163] between the two isoforms. Interestingly, the major sites of differential phosphorylation in YAP-active versus parental cell contexts are restricted to the C-terminal tail of ZAKα. As yet, these phosphorylation sites have an unknown function. Further experiments are necessary to determine how these phosphorylations function in ZAKα, and whether they underly the differential effects between ZAKα and ZAKβ in promoting EMT. It would be especially informative to transfect phospho-mimetic and phospho-mutant versions of ZAKα to observe if these sites play a role in downregulating ZAKα's ability to induce EMT or in altering ZAKα's subcellular localization. Notably, SAM domains enable dimerization, which may underly some of the differences between ZAKα and ZAKβ. Moreover, mutations in the SAM domain are responsible for split-hand/split-foot malformation in mice and humans[231]. The involvement of EMT signaling in this phenotype is currently unknown, but it demonstrates the importance of the SAM domain in the proper regulation of ZAKα signaling.

Both Chapter 2 and Chapter 3 of this dissertation revolve around EMT, with Chapter 2 investigating a potential cause of this phenotype and Chapter 3 investigating a possible effect in drug resistance. ZAK is a member of the MAPK pathway, the same pathway targeted in Chapter 3,

and can activate MEK kinases[153]. There is potential that ZAK confers some of the drug resistance seen in YAP driven cells. While this is hypothetical, it remains an intriguing research direction to investigate how involved ZAK is in conferring drug resistance.

While the work for these two Chapters was performed separately, future work should aim to integrate these experiments to better model and predict drug response in Hippo mutant contexts. The union of drug response data (particularly responses to kinase inhibitors) and a simultaneous snapshot of the kinome's activation state via phosphoproteomic data presents an unprecedented landscape in which to evaluate signaling pathway flexibility in the face of drug treatment. The availability of specific kinase activation states may help predict or explain how YAP-driven cells coordinate such a resilient growth-promoting signaling paradigm. An eventual goal should also be to evaluate ZAK, EMT, and drug resistance *in vivo*. YAP is known to promote metastasis in animal models, and ZAK inhibition reduces metastatic burden in animal models[165], justifying it as a potential target in reducing the metastatic burden of YAP-driven tumors. This is especially considerable in the context of EMT as a driver of drug resistance, particularly because data within this dissertation suggests EMT as a primary mechanism allowing escape from targeted therapies. Finally, this work lays the foundation for discovering new tools to fight YAP-driven cancer, and for future investigations exploring the clinical relevance of these findings.

References

1 Justice, R. W., Zilian, O., Woods, D. F., Noll, M. & Bryant, P. J. The Drosophila tumor suppressor gene warts encodes a homolog of human myotonic dystrophy kinase and is required for the control of cell shape and proliferation. *Genes Dev* **9**, 534-546, doi:10.1101/gad.9.5.534 (1995).

2 Xu, T., Wang, W., Zhang, S., Stewart, R. A. & Yu, W. Identifying tumor suppressors in genetic mosaics: the Drosophila lats gene encodes a putative protein kinase. *Development* **121**, 1053-1063 (1995).

3 Kango-Singh, M. *et al.* Shar-pei mediates cell proliferation arrest during imaginal disc growth in Drosophila. *Development* **129**, 5719-5730, doi:10.1242/dev.00168 (2002).

4 Tapon, N. *et al.* salvador Promotes both cell cycle exit and apoptosis in Drosophila and is mutated in human cancer cell lines. *Cell* **110**, 467-478, doi:10.1016/s0092-8674(02)00824-3 (2002).

5 Harvey, K. F., Pfleger, C. M. & Hariharan, I. K. The Drosophila Mst ortholog, hippo, restricts growth and cell proliferation and promotes apoptosis. *Cell* **114**, 457-467 (2003).

6 Wu, S., Huang, J., Dong, J. & Pan, D. hippo encodes a Ste-20 family protein kinase that restricts cell proliferation and promotes apoptosis in conjunction with salvador and warts. *Cell* **114**, 445-456 (2003).

7 Jia, J., Zhang, W., Wang, B., Trinko, R. & Jiang, J. The Drosophila Ste20 family kinase dMST functions as a tumor suppressor by restricting cell proliferation and promoting apoptosis. *Genes & development* **17**, 2514-2519 (2003).

8 Pantalacci, S., Tapon, N. & Léopold, P. The Salvador partner Hippo promotes apoptosis and cell-cycle exit in Drosophila. *Nature cell biology* **5**, 921-927 (2003).

9 Udan, R. S., Kango-Singh, M., Nolo, R., Tao, C. & Halder, G. Hippo promotes proliferation arrest and apoptosis in the Salvador/Warts pathway. *Nature cell biology* **5**, 914-920 (2003).

10 Lai, Z.-C. *et al.* Control of cell proliferation and apoptosis by mob as tumor suppressor, mats. *Cell* **120**, 675-685 (2005).

11 Huang, J., Wu, S., Barrera, J., Matthews, K. & Pan, D. The Hippo signaling pathway coordinately regulates cell proliferation and apoptosis by inactivating Yorkie, the Drosophila Homolog of YAP. *Cell* **122**, 421-434 (2005).

12 Goulev, Y. *et al.* SCALLOPED interacts with YORKIE, the nuclear effector of the hippo tumor-suppressor pathway in Drosophila. *Current Biology* **18**, 435-441 (2008).

13 Wu, S., Liu, Y., Zheng, Y., Dong, J. & Pan, D. The TEAD/TEF family protein Scalloped mediates transcriptional output of the Hippo growth-regulatory pathway. *Developmental cell* **14**, 388-398 (2008).

14 Zhang, L. *et al.* The TEAD/TEF family of transcription factor Scalloped mediates Hippo signaling in organ size control. *Developmental cell* **14**, 377-387 (2008).

15 Yu, F.-X., Zhao, B. & Guan, K.-L. Hippo pathway in organ size control, tissue homeostasis, and cancer. *Cell* **163**, 811-828 (2015).

16 Zhao, B. *et al.* TEAD mediates YAP-dependent gene induction and growth control. *Genes & development* **22**, 1962-1971 (2008).

17 Zhao, B., Li, L., Lei, Q. & Guan, K. L. The Hippo-YAP pathway in organ size control and tumorigenesis: an updated version. *Genes Dev* **24**, 862-874, doi:10.1101/gad.1909210 (2010).

18 Zhou, D. *et al.* Mst1 and Mst2 maintain hepatocyte quiescence and suppress hepatocellular carcinoma development through inactivation of the Yap1 oncogene. *Cancer cell* **16**, 425-438 (2009).

19 Song, H. *et al.* Mammalian Mst1 and Mst2 kinases play essential roles in organ size control and tumor suppression. *Proceedings of the National Academy of Sciences* **107**, 1431-1436

(2010).
20 Lu, L. *et al.* Hippo signaling is a potent in vivo growth and tumor suppressor pathway in the mammalian liver. *Proceedings of the National Academy of Sciences* **107**, 1437-1442 (2010).
21 Camargo, F. D. *et al.* YAP1 increases organ size and expands undifferentiated progenitor cells. *Current biology* **17**, 2054-2060 (2007).
22 Dong, J. *et al.* Elucidation of a universal size-control mechanism in Drosophila and mammals. *Cell* **130**, 1120-1133 (2007).
23 Zhao, B. *et al.* Inactivation of YAP oncoprotein by the Hippo pathway is involved in cell contact inhibition and tissue growth control. *Genes & development* **21**, 2747-2761 (2007).
24 Zhao, B., Li, L., Tumaneng, K., Wang, C.-Y. & Guan, K.-L. A coordinated phosphorylation by Lats and CK1 regulates YAP stability through SCFβ-TRCP. *Genes & development* **24**, 72-85 (2010).
25 Yu, F.-X. & Guan, K.-L. The Hippo pathway: regulators and regulations. *Genes & development* **27**, 355-371 (2013).
26 Genevet, A. & Tapon, N. The Hippo pathway and apico–basal cell polarity. *Biochemical Journal* **436**, 213-224 (2011).
27 Hamaratoglu, F. *et al.* The tumour-suppressor genes NF2/Merlin and Expanded act through Hippo signalling to regulate cell proliferation and apoptosis. *Nature cell biology* **8**, 27-36 (2006).
28 Yu, J. *et al.* Kibra functions as a tumor suppressor protein that regulates Hippo signaling in conjunction with Merlin and Expanded. *Developmental cell* **18**, 288-299 (2010).
29 Yin, F. *et al.* Spatial organization of Hippo signaling at the plasma membrane mediated by the tumor suppressor Merlin/NF2. *Cell* **154**, 1342-1355 (2013).
30 Ling, C. *et al.* The apical transmembrane protein Crumbs functions as a tumor suppressor that regulates Hippo signaling by binding to Expanded. *Proceedings of the National Academy of Sciences* **107**, 10532-10537 (2010).
31 Robinson, B. S., Huang, J., Hong, Y. & Moberg, K. H. Crumbs regulates Salvador/Warts/Hippo signaling in Drosophila via the FERM-domain protein Expanded. *Current Biology* **20**, 582-590 (2010).
32 Varelas, X. *et al.* The Crumbs complex couples cell density sensing to Hippo-dependent control of the TGF-β-SMAD pathway. *Developmental cell* **19**, 831-844 (2010).
33 Moleirinho, S. *et al.* Regulation of localization and function of the transcriptional co-activator YAP by angiomotin. *Elife* **6**, e23966 (2017).
34 Paramasivam, M., Sarkeshik, A., Yates III, J. R., Fernandes, M. J. & McCollum, D. Angiomotin family proteins are novel activators of the LATS2 kinase tumor suppressor. *Molecular biology of the cell* **22**, 3725-3733 (2011).
35 Wang, W., Huang, J. & Chen, J. Angiomotin-like proteins associate with and negatively regulate YAP1. *Journal of Biological Chemistry* **286**, 4364-4370 (2011).
36 Zhao, B. *et al.* Angiomotin is a novel Hippo pathway component that inhibits YAP oncoprotein. *Genes & development* **25**, 51-63 (2011).
37 Bossuyt, W. *et al.* An evolutionary shift in the regulation of the Hippo pathway between mice and flies. *Oncogene* **33**, 1218-1228 (2014).
38 Cordenonsi, M. *et al.* The Hippo transducer TAZ confers cancer stem cell-related traits on breast cancer cells. *Cell* **147**, 759-772 (2011).
39 Grzeschik, N. A., Parsons, L. M., Allott, M. L., Harvey, K. F. & Richardson, H. E. Lgl, aPKC, and Crumbs regulate the Salvador/Warts/Hippo pathway through two distinct mechanisms. *Current biology* **20**, 573-581 (2010).
40 Liu, J. *et al.* Loss of DLG5 promotes breast cancer malignancy by inhibiting the Hippo signaling pathway. *Scientific reports* **7**, 1-11 (2017).
41 Mohseni, M. *et al.* A genetic screen identifies an LKB1–MARK signalling axis controlling the

Hippo–YAP pathway. *Nature cell biology* **16**, 108-117 (2014).
42 Gumbiner, B. M. & Kim, N.-G. The Hippo-YAP signaling pathway and contact inhibition of growth. *Journal of cell science* **127**, 709-717 (2014).
43 Kim, N.-G., Koh, E., Chen, X. & Gumbiner, B. M. E-cadherin mediates contact inhibition of proliferation through Hippo signaling-pathway components. *Proceedings of the National Academy of Sciences* **108**, 11930-11935 (2011).
44 Garcia, M. A., Nelson, W. J. & Chavez, N. Cell–cell junctions organize structural and signaling networks. *Cold Spring Harbor perspectives in biology* **10**, a029181 (2018).
45 Oka, T. *et al.* Functional complexes between YAP2 and ZO-2 are PDZ domain-dependent, and regulate YAP2 nuclear localization and signalling. *Biochemical Journal* **432**, 461-478 (2010).
46 Chan, S. W. *et al.* Hippo pathway-independent restriction of TAZ and YAP by angiomotin. *Journal of Biological Chemistry* **286**, 7018-7026 (2011).
47 Li, Y. *et al.* Angiomotin binding-induced activation of Merlin/NF2 in the Hippo pathway. *Cell research* **25**, 801-817 (2015).
48 Schlegelmilch, K. *et al.* Yap1 acts downstream of α-catenin to control epidermal proliferation. *Cell* **144**, 782-795 (2011).
49 Silvis, M. R. *et al.* α-catenin is a tumor suppressor that controls cell accumulation by regulating the localization and activity of the transcriptional coactivator Yap1. *Science signaling* **4**, ra33-ra33 (2011).
50 Dupont, S. *et al.* Role of YAP/TAZ in mechanotransduction. *Nature* **474**, 179-183 (2011).
51 Wada, K.-I., Itoga, K., Okano, T., Yonemura, S. & Sasaki, H. Hippo pathway regulation by cell morphology and stress fibers. *Development* **138**, 3907-3914 (2011).
52 Zhao, B. *et al.* Cell detachment activates the Hippo pathway via cytoskeleton reorganization to induce anoikis. *Genes & development* **26**, 54-68 (2012).
53 Aragona, M. *et al.* A mechanical checkpoint controls multicellular growth through YAP/TAZ regulation by actin-processing factors. *Cell* **154**, 1047-1059 (2013).
54 Piccolo, S., Dupont, S. & Cordenonsi, M. The biology of YAP/TAZ: hippo signaling and beyond. *Physiol Rev* **94**, 1287-1312, doi:10.1152/physrev.00005.2014 (2014).
55 Kim, N.-G. & Gumbiner, B. M. Adhesion to fibronectin regulates Hippo signaling via the FAK–Src–PI3K pathway. *Journal of Cell Biology* **210**, 503-515 (2015).
56 Lachowski, D. *et al.* FAK controls the mechanical activation of YAP, a transcriptional regulator required for durotaxis. *The FASEB Journal* **32**, 1099-1107 (2018).
57 Hu, J. K.-H. *et al.* An FAK-YAP-mTOR signaling axis regulates stem cell-based tissue renewal in mice. *Cell stem cell* **21**, 91-106. e106 (2017).
58 Fan, R., Kim, N.-G. & Gumbiner, B. M. Regulation of Hippo pathway by mitogenic growth factors via phosphoinositide 3-kinase and phosphoinositide-dependent kinase-1. *Proceedings of the National Academy of Sciences* **110**, 2569-2574 (2013).
59 Yu, F. X. *et al.* Regulation of the Hippo-YAP pathway by G-protein-coupled receptor signaling. *Cell* **150**, 780-791, doi:10.1016/j.cell.2012.06.037 (2012).
60 Miller, E. *et al.* Identification of serum-derived sphingosine-1-phosphate as a small molecule regulator of YAP. *Chemistry & biology* **19**, 955-962 (2012).
61 Mo, J.-S., Yu, F.-X., Gong, R., Brown, J. H. & Guan, K.-L. Regulation of the Hippo–YAP pathway by protease-activated receptors (PARs). *Genes & development* **26**, 2138-2143 (2012).
62 Zhou, X. *et al.* Estrogen regulates Hippo signaling via GPER in breast cancer. *The Journal of clinical investigation* **125**, 2123-2135 (2019).
63 Wennmann, D. *et al.* The Hippo pathway is controlled by Angiotensin II signaling and its reactivation induces apoptosis in podocytes. *Cell death & disease* **5**, e1519-e1519 (2014).
64 Yu, F.-X. *et al.* Protein kinase A activates the Hippo pathway to modulate cell proliferation and differentiation. *Genes & development* **27**, 1223-1232 (2013).
65 Kim, M. *et al.* cAMP/PKA signalling reinforces the LATS–YAP pathway to fully suppress YAP

in response to actin cytoskeletal changes. *The EMBO journal* **32**, 1543-1555 (2013).
66 Reddy, B. & Irvine, K. D. Regulation of Hippo signaling by EGFR-MAPK signaling through Ajuba family proteins. *Developmental cell* **24**, 459-471 (2013).
67 Straßburger, K., Tiebe, M., Pinna, F., Breuhahn, K. & Teleman, A. A. Insulin/IGF signaling drives cell proliferation in part via Yorkie/YAP. *Developmental biology* **367**, 187-196 (2012).
68 Sorrentino, G. *et al.* Glucocorticoid receptor signalling activates YAP in breast cancer. *Nature communications* **8**, 1-14 (2017).
69 Park, H. W. *et al.* Alternative Wnt signaling activates YAP/TAZ. *Cell* **162**, 780-794 (2015).
70 Azzolin, L. *et al.* YAP/TAZ incorporation in the β-catenin destruction complex orchestrates the Wnt response. *Cell* **158**, 157-170 (2014).
71 Azzolin, L. *et al.* Role of TAZ as mediator of Wnt signaling. *Cell* **151**, 1443-1456 (2012).
72 Wang, X. *et al.* YAP/TAZ orchestrate VEGF signaling during developmental angiogenesis. *Developmental cell* **42**, 462-478. e467 (2017).
73 Azad, T. *et al.* A LATS biosensor screen identifies VEGFR as a regulator of the Hippo pathway in angiogenesis. *Nature communications* **9**, 1-15 (2018).
74 Pan, D. The hippo signaling pathway in development and cancer. *Developmental cell* **19**, 491-505 (2010).
75 Lamar, J. M. *et al.* The Hippo pathway target, YAP, promotes metastasis through its TEAD-interaction domain. *Proceedings of the National Academy of Sciences* **109**, E2441-E2450 (2012).
76 Liu-Chittenden, Y. *et al.* Genetic and pharmacological disruption of the TEAD-YAP complex suppresses the oncogenic activity of YAP. *Genes Dev* **26**, 1300-1305, doi:10.1101/gad.192856.112 (2012).
77 Zhao, B., Kim, J., Ye, X., Lai, Z.-C. & Guan, K.-L. Both TEAD-binding and WW domains are required for the growth stimulation and oncogenic transformation activity of yes-associated protein. *Cancer research* **69**, 1089-1098 (2009).
78 Guo, T. *et al.* A novel partner of Scalloped regulates Hippo signaling via antagonizing Scalloped-Yorkie activity. *Cell research* **23**, 1201-1214 (2013).
79 Koontz, L. M. *et al.* The Hippo effector Yorkie controls normal tissue growth by antagonizing scalloped-mediated default repression. *Developmental cell* **25**, 388-401 (2013).
80 Jiao, S. *et al.* A peptide mimicking VGLL4 function acts as a YAP antagonist therapy against gastric cancer. *Cancer cell* **25**, 166-180 (2014).
81 Strano, S. *et al.* Physical interaction with Yes-associated protein enhances p73 transcriptional activity. *Journal of Biological Chemistry* **276**, 15164-15173 (2001).
82 Levy, D., Adamovich, Y., Reuven, N. & Shaul, Y. Yap1 phosphorylation by c-Abl is a critical step in selective activation of proapoptotic genes in response to DNA damage. *Mol Cell* **29**, 350-361, doi:10.1016/j.molcel.2007.12.022 (2008).
83 Chan, S. W. *et al.* WW domain-mediated interaction with Wbp2 is important for the oncogenic property of TAZ. *Oncogene* **30**, 600 (2011).
84 McDonald, C. B. *et al.* Biophysical analysis of binding of WW domains of the YAP2 transcriptional regulator to PPXY motifs within WBP1 and WBP2 adaptors. *Biochemistry* **50**, 9616-9627 (2011).
85 Yagi, R., Chen, L. F., Shigesada, K., Murakami, Y. & Ito, Y. A WW domain-containing yes-associated protein (YAP) is a novel transcriptional co-activator. *The EMBO journal* **18**, 2551-2562 (1999).
86 Cui, C. B., Cooper, L. F., Yang, X., Karsenty, G. & Aukhil, I. Transcriptional coactivation of bone-specific transcription factor Cbfa1 by TAZ. *Molecular and cellular biology* **23**, 1004-1013 (2003).
87 Vitolo, M. I. *et al.* The RUNX2 transcription factor cooperates with the YES-associated

protein, YAP65, to promote cell transformation. *Cancer biology & therapy* **6**, 856-863 (2007).
88 Komuro, A., Nagai, M., Navin, N. E. & Sudol, M. WW domain-containing protein YAP associates with ErbB-4 and acts as a co-transcriptional activator for the carboxyl-terminal fragment of ErbB-4 that translocates to the nucleus. *Journal of Biological Chemistry* **278**, 33334-33341 (2003).
89 Omerovic, J. *et al.* Ligand-regulated association of ErbB-4 to the transcriptional co-activator YAP65 controls transcription at the nuclear level. *Experimental cell research* **294**, 469-479 (2004).
90 Fujii, M. *et al.* TGF-β synergizes with defects in the Hippo pathway to stimulate human malignant mesothelioma growth. *Journal of Experimental Medicine* **209**, 479-494 (2012).
91 Varelas, X. *et al.* TAZ controls Smad nucleocytoplasmic shuttling and regulates human embryonic stem-cell self-renewal. *Nature cell biology* **10**, 837-848 (2008).
92 Lehmann, W. *et al.* ZEB1 turns into a transcriptional activator by interacting with YAP1 in aggressive cancer types. *Nature communications* **7**, 1-15 (2016).
93 Tang, Y., Feinberg, T., Keller, E. T., Li, X. Y. & Weiss, S. J. Snail/Slug binding interactions with YAP/TAZ control skeletal stem cell self-renewal and differentiation. *Nat Cell Biol* **18**, 917-929, doi:10.1038/ncb3394 (2016).
94 Zanconato, F. *et al.* Genome-wide association between YAP/TAZ/TEAD and AP-1 at enhancers drives oncogenic growth. *Nature cell biology* **17**, 1218-1227 (2015).
95 Stein, C. *et al.* YAP1 exerts its transcriptional control via TEAD-mediated activation of enhancers. *PLoS Genet* **11**, e1005465 (2015).
96 Wang, Y. *et al.* Comprehensive molecular characterization of the Hippo signaling pathway in cancer. *Cell reports* **25**, 1304-1317. e1305 (2018).
97 Totaro, A., Panciera, T. & Piccolo, S. YAP/TAZ upstream signals and downstream responses. *Nature cell biology* **20**, 888-899 (2018).
98 Zheng, Y. & Pan, D. The Hippo signaling pathway in development and disease. *Developmental cell* **50**, 264-282 (2019).
99 Hanahan, D. & Weinberg, R. A. The hallmarks of cancer. *cell* **100**, 57-70 (2000).
100 Harvey, K. F., Zhang, X. & Thomas, D. M. The Hippo pathway and human cancer. *Nature Reviews Cancer* **13**, 246 (2013).
101 Lamouille, S., Xu, J. & Derynck, R. Molecular mechanisms of epithelial-mesenchymal transition. *Nat Rev Mol Cell Biol* **15**, 178-196, doi:10.1038/nrm3758 (2014).
102 Kalluri, R. & Weinberg, R. A. The basics of epithelial-mesenchymal transition. *The Journal of clinical investigation* **119**, 1420-1428 (2009).
103 Ye, X. & Weinberg, R. A. Epithelial-Mesenchymal Plasticity: A Central Regulator of Cancer Progression. *Trends Cell Biol* **25**, 675-686, doi:10.1016/j.tcb.2015.07.012 (2015).
104 Gilbert, S. F. (2008).
105 Thiery, J. P., Acloque, H., Huang, R. Y. & Nieto, M. A. Epithelial-mesenchymal transitions in development and disease. *cell* **139**, 871-890 (2009).
106 Puisieux, A., Brabletz, T. & Caramel, J. Oncogenic roles of EMT-inducing transcription factors. *Nature cell biology* **16**, 488-494 (2014).
107 Polyak, K. & Weinberg, R. A. Transitions between epithelial and mesenchymal states: acquisition of malignant and stem cell traits. *Nature Reviews Cancer* **9**, 265-273 (2009).
108 Huang, R. Y.-J., Guilford, P. & Thiery, J. P. (The Company of Biologists Ltd, 2012).
109 Nelson, W. J. Remodeling epithelial cell organization: transitions between front–rear and apical–basal polarity. *Cold Spring Harbor perspectives in biology* **1**, a000513 (2009).
110 Moreno-Bueno, G., Portillo, F. & Cano, A. Transcriptional regulation of cell polarity in EMT and cancer. *Oncogene* **27**, 6958-6969 (2008).
111 Xu, J., Lamouille, S. & Derynck, R. TGF-β-induced epithelial to mesenchymal transition. *Cell*

research **19**, 156-172 (2009).
112 Hao, Y., Chun, A., Cheung, K., Rashidi, B. & Yang, X. Tumor suppressor LATS1 is a negative regulator of oncogene YAP. *Journal of Biological Chemistry* **283**, 5496-5509 (2008).
113 Overholtzer, M. *et al.* Transforming properties of YAP, a candidate oncogene on the chromosome 11q22 amplicon. *Proceedings of the National Academy of Sciences* **103**, 12405-12410 (2006).
114 Zhang, X., Milton, C. C., Humbert, P. O. & Harvey, K. F. Transcriptional output of the Salvador/warts/hippo pathway is controlled in distinct fashions in Drosophila melanogaster and mammalian cell lines. *Cancer research* **69**, 6033-6041 (2009).
115 Diepenbruck, M. *et al.* Tead2 expression levels control the subcellular distribution of Yap and Taz, zyxin expression and epithelial–mesenchymal transition. *J Cell Sci* **127**, 1523-1536 (2014).
116 Shao, D. D. *et al.* KRAS and YAP1 converge to regulate EMT and tumor survival. *Cell* **158**, 171-184, doi:10.1016/j.cell.2014.06.004 (2014).
117 Chabner, B. A. & Roberts, T. G. Chemotherapy and the war on cancer. *Nature Reviews Cancer* **5**, 65-72 (2005).
118 Perez, E. A. Microtubule inhibitors: Differentiating tubulin-inhibiting agents based on mechanisms of action, clinical activity, and resistance. *Molecular cancer therapeutics* **8**, 2086-2095 (2009).
119 Binenbaum, Y., Na'ara, S. & Gil, Z. Gemcitabine resistance in pancreatic ductal adenocarcinoma. *Drug Resistance Updates* **23**, 55-68 (2015).
120 Longley, D. B., Harkin, D. P. & Johnston, P. G. 5-fluorouracil: mechanisms of action and clinical strategies. *Nature reviews cancer* **3**, 330-338 (2003).
121 Dasari, S. & Tchounwou, P. B. Cisplatin in cancer therapy: molecular mechanisms of action. *European journal of pharmacology* **740**, 364-378 (2014).
122 Carvalho, C. *et al.* Doxorubicin: the good, the bad and the ugly effect. *Current medicinal chemistry* **16**, 3267-3285 (2009).
123 Bhullar, K. S. *et al.* Kinase-targeted cancer therapies: progress, challenges and future directions. *Molecular cancer* **17**, 1-20 (2018).
124 Holohan, C., Van Schaeybroeck, S., Longley, D. B. & Johnston, P. G. Cancer drug resistance: an evolving paradigm. *Nat Rev Cancer* **13**, 714-726, doi:10.1038/nrc3599 (2013).
125 Lai, D., Ho, K. C., Hao, Y. & Yang, X. Taxol resistance in breast cancer cells is mediated by the hippo pathway component TAZ and its downstream transcriptional targets Cyr61 and CTGF. *Cancer research* **71**, 2728-2738 (2011).
126 Xia, Y., Zhang, Y.-L., Yu, C., Chang, T. & Fan, H.-Y. YAP/TEAD co-activator regulated pluripotency and chemoresistance in ovarian cancer initiated cells. *PloS one* **9**, e109575 (2014).
127 Nguyen, C. D. K. & Yi, C. YAP/TAZ Signaling and Resistance to Cancer Therapy. *Trends Cancer* **5**, 283-296, doi:10.1016/j.trecan.2019.02.010 (2019).
128 Xiao, L. *et al.* YAP induces cisplatin resistance through activation of autophagy in human ovarian carcinoma cells. *OncoTargets and therapy* **9**, 1105 (2016).
129 Yoshikawa, K. *et al.* The Hippo pathway transcriptional co-activator, YAP, confers resistance to cisplatin in human oral squamous cell carcinoma. *International journal of oncology* **46**, 2364-2370 (2015).
130 Ciamporcero, E. *et al.* YAP activation protects urothelial cell carcinoma from treatment-induced DNA damage. *Oncogene* **35**, 1541-1553 (2016).
131 Huo, X. *et al.* Overexpression of Yes-associated protein confers doxorubicin resistance in hepatocellullar carcinoma. *Oncology reports* **29**, 840-846 (2013).
132 Kim, M. H. & Kim, J. Role of YAP/TAZ transcriptional regulators in resistance to anti-cancer therapies. *Cellular and Molecular Life Sciences* **74**, 1457-1474 (2017).

133 Gujral, T. S. & Kirschner, M. W. Hippo pathway mediates resistance to cytotoxic drugs. *Proceedings of the National Academy of Sciences* **114**, E3729-E3738 (2017).
134 Shalem, O. *et al.* Genome-scale CRISPR-Cas9 knockout screening in human cells. *Science* **343**, 84-87, doi:10.1126/science.1247005 (2014).
135 Lin, L. *et al.* The Hippo effector YAP promotes resistance to RAF-and MEK-targeted cancer therapies. *Nature genetics* **47**, 250-256 (2015).
136 Kim, M. H. *et al.* Actin remodeling confers BRAF inhibitor resistance to melanoma cells through YAP/TAZ activation. *Embo j* **35**, 462-478, doi:10.15252/embj.201592081 (2016).
137 Kapoor, A. *et al.* Yap1 activation enables bypass of oncogenic Kras addiction in pancreatic cancer. *Cell* **158**, 185-197 (2014).
138 Zhao, X. *et al.* A combinatorial strategy using YAP and pan-RAF inhibitors for treating KRAS-mutant pancreatic cancer. *Cancer Lett* **402**, 61-70, doi:10.1016/j.canlet.2017.05.015 (2017).
139 Lee, T. F. *et al.* Enhanced YAP expression leads to EGFR TKI resistance in lung adenocarcinomas. *Sci Rep* **8**, 271, doi:10.1038/s41598-017-18527-z (2018).
140 Kurppa, K. J. *et al.* Treatment-induced tumor dormancy through YAP-mediated transcriptional reprogramming of the apoptotic pathway. *Cancer Cell* **37**, 104-122. e112 (2020).
141 Kitajima, S. *et al.* Overcoming resistance to dual innate immune and MEK inhibition downstream of KRAS. *Cancer cell* **34**, 439-452. e436 (2018).
142 Scott, D. E., Bayly, A. R., Abell, C. & Skidmore, J. Small molecules, big targets: drug discovery faces the protein–protein interaction challenge. *Nature Reviews Drug Discovery* **15**, 533 (2016).
143 Meng, Z. *et al.* MAP4K family kinases act in parallel to MST1/2 to activate LATS1/2 in the Hippo pathway. *Nature communications* **6**, 1-13 (2015).
144 Mo, J. S. *et al.* Cellular energy stress induces AMPK-mediated regulation of YAP and the Hippo pathway. *Nat Cell Biol* **17**, 500-510, doi:10.1038/ncb3111 (2015).
145 Azad, T. *et al.* A gain-of-functional screen identifies the Hippo pathway as a central mediator of receptor tyrosine kinases during tumorigenesis. *Oncogene* **39**, 334-355, doi:10.1038/s41388-019-0988-y (2020).
146 Yuan, W. C. *et al.* NUAK2 is a critical YAP target in liver cancer. *Nat Commun* **9**, 4834, doi:10.1038/s41467-018-07394-5 (2018).
147 Manning, G., Whyte, D. B., Martinez, R., Hunter, T. & Sudarsanam, S. The protein kinase complement of the human genome. *Science* **298**, 1912-1934, doi:10.1126/science.1075762 (2002).
148 Fleuren, E. D. G., Zhang, L., Wu, J. & Daly, R. J. The kinome 'at large' in cancer. *Nature Reviews Cancer* **16**, 83-98, doi:10.1038/nrc.2015.18 (2016).
149 Golkowski, M. *et al.* Kinobead/LC-MS Phosphokinome Profiling Enables Rapid Analyses of Kinase-Dependent Cell Signaling Networks. *J Proteome Res* **19**, 1235-1247, doi:10.1021/acs.jproteome.9b00742 (2020).
150 Golkowski, M. *et al.* Kinobead and Single-Shot LC-MS Profiling Identifies Selective PKD Inhibitors. *Journal of proteome research* **16**, 1216-1227, doi:10.1021/acs.jproteome.6b00817 (2017).
151 Golkowski, M. *et al.* Pharmacoproteomics Identifies Kinase Pathways that Drive the Epithelial-Mesenchymal Transition and Drug Resistance in Hepatocellular Carcinoma. *Cell Syst* **11**, 196-207 e197, doi:10.1016/j.cels.2020.07.006 (2020).
152 Gross, E. A., Callow, M. G., Waldbaum, L., Thomas, S. & Ruggieri, R. MRK, a mixed lineage kinase-related molecule that plays a role in γ-radiation-induced cell cycle arrest. *Journal of Biological Chemistry* **277**, 13873-13882 (2002).
153 Gotoh, I., Adachi, M. & Nishida, E. Identification and characterization of a novel MAP kinase kinase kinase, MLTK. *J Biol Chem* **276**, 4276-4286, doi:10.1074/jbc.M008595200 (2001).

154 Liu, T. C. *et al.* Cloning and expression of ZAK, a mixed lineage kinase-like protein containing a leucine-zipper and a sterile-alpha motif. *Biochem Biophys Res Commun* **274**, 811-816, doi:10.1006/bbrc.2000.3236 (2000).
155 Cho, Y. Y. *et al.* A novel role for mixed-lineage kinase-like mitogen-activated protein triple kinase alpha in neoplastic cell transformation and tumor development. *Cancer Res* **64**, 3855-3864, doi:10.1158/0008-5472.CAN-04-0201 (2004).
156 Liu, J. *et al.* Integrated exome and transcriptome sequencing reveals ZAK isoform usage in gastric cancer. *Nat Commun* **5**, 3830, doi:10.1038/ncomms4830 (2014).
157 Vinayagam, A. *et al.* A directed protein interaction network for investigating intracellular signal transduction. *Sci Signal* **4**, rs8, doi:10.1126/scisignal.2001699 (2011).
158 Vin, H. *et al.* Sorafenib suppresses JNK-dependent apoptosis through inhibition of ZAK. *Mol Cancer Ther* **13**, 221-229, doi:10.1158/1535-7163.Mct-13-0561 (2014).
159 Sauter, K. A., Magun, E. A., Iordanov, M. S. & Magun, B. E. ZAK is required for doxorubicin, a novel ribotoxic stressor, to induce SAPK activation and apoptosis in HaCaT cells. *Cancer Biol Ther* **10**, 258-266, doi:10.4161/cbt.10.3.12367 (2010).
160 Yang, J. J. *et al.* ZAK inhibits human lung cancer cell growth via ERK and JNK activation in an AP-1-dependent manner. *Cancer Sci* **101**, 1374-1381, doi:10.1111/j.1349-7006.2010.01537.x (2010).
161 Yang, J.-J. Mixed lineage kinase ZAK utilizing MKK7 and not MKK4 to activate the c-Jun N-terminal kinase and playing a role in the cell arrest. *Biochemical and biophysical research communications* **297**, 105-110 (2002).
162 Tosti, E., Waldbaum, L., Warshaw, G., Gross, E. A. & Ruggieri, R. The stress kinase MRK contributes to regulation of DNA damage checkpoints through a p38gamma-independent pathway. *J Biol Chem* **279**, 47652-47660, doi:10.1074/jbc.M409961200 (2004).
163 Rey, C. *et al.* The MAP3K ZAK, a novel modulator of ERK-dependent migration, is upregulated in colorectal cancer. *Oncogene* **35**, 3190-3200 (2016).
164 Korkina, O. *et al.* The MLK-related kinase (MRK) is a novel RhoC effector that mediates lysophosphatidic acid (LPA)-stimulated tumor cell invasion. *J Biol Chem* **288**, 5364-5373, doi:10.1074/jbc.M112.414060 (2013).
165 Li, L. *et al.* Mixed lineage kinase ZAK promotes epithelial–mesenchymal transition in cancer progression. *Cell death & disease* **9**, 1-14 (2018).
166 Pobbati, A. V. & Hong, W. A combat with the YAP/TAZ-TEAD oncoproteins for cancer therapy. *Theranostics* **10**, 3622-3635, doi:10.7150/thno.40889 (2020).
167 Subramanian, A. *et al.* Gene set enrichment analysis: a knowledge-based approach for interpreting genome-wide expression profiles. *Proceedings of the National Academy of Sciences* **102**, 15545-15550 (2005).
168 Liberzon, A. *et al.* The Molecular Signatures Database (MSigDB) hallmark gene set collection. *Cell Syst* **1**, 417-425, doi:10.1016/j.cels.2015.12.004 (2015).
169 Endicott, J. A., Noble, M. E. & Johnson, L. N. The structural basis for control of eukaryotic protein kinases. *Annual review of biochemistry* **81**, 587-613 (2012).
170 Nolen, B., Taylor, S. & Ghosh, G. Regulation of protein kinases: controlling activity through activation segment conformation. *Molecular cell* **15**, 661-675 (2004).
171 Furth, N. & Aylon, Y. The LATS1 and LATS2 tumor suppressors: beyond the Hippo pathway. *Cell Death & Differentiation* **24**, 1488-1501 (2017).
172 Barretina, J. *et al.* The Cancer Cell Line Encyclopedia enables predictive modelling of anticancer drug sensitivity. *Nature* **483**, 603-607 (2012).
173 Gujral, T. S. *et al.* A noncanonical Frizzled2 pathway regulates epithelial-mesenchymal transition and metastasis. *Cell* **159**, 844-856 (2014).
174 Mamuya, F. A. & Duncan, M. K. aV integrins and TGF-β-induced EMT: a circle of regulation. *J Cell Mol Med* **16**, 445-455, doi:10.1111/j.1582-4934.2011.01419.x (2012).

175 Nam, E. H., Lee, Y., Park, Y. K., Lee, J. W. & Kim, S. ZEB2 upregulates integrin α5 expression through cooperation with Sp1 to induce invasion during epithelial-mesenchymal transition of human cancer cells. *Carcinogenesis* **33**, 563-571, doi:10.1093/carcin/bgs005 (2012).
176 Taube, J. H. *et al.* Core epithelial-to-mesenchymal transition interactome gene-expression signature is associated with claudin-low and metaplastic breast cancer subtypes. *Proc Natl Acad Sci U S A* **107**, 15449-15454, doi:10.1073/pnas.1004900107 (2010).
177 Steller, E. J. *et al.* PDGFRB promotes liver metastasis formation of mesenchymal-like colorectal tumor cells. *Neoplasia* **15**, 204-217, doi:10.1593/neo.121726 (2013).
178 Praveen Kumar, V. R. *et al.* Insulin like growth factor binding protein 4 promotes GBM progression and regulates key factors involved in EMT and invasion. *J Neurooncol* **116**, 455-464, doi:10.1007/s11060-013-1324-y (2014).
179 Cory, G. in *Cell Migration* 25-30 (Springer, 2011).
180 Szulzewsky, F. *et al.* Comparison of tumor-associated YAP1 fusions identifies a recurrent set of functions critical for oncogenesis. *Genes & Development* **34**, 1051-1064 (2020).
181 Carninci, P. *et al.* The transcriptional landscape of the mammalian genome. *Science* **309**, 1559-1563, doi:10.1126/science.1112014 (2005).
182 Weinstein, J. N. *et al.* The cancer genome atlas pan-cancer analysis project. *Nature genetics* **45**, 1113-1120 (2013).
183 Hornbeck, P. V. *et al.* PhosphoSitePlus, 2014: mutations, PTMs and recalibrations. *Nucleic Acids Res* **43**, D512-520, doi:10.1093/nar/gku1267 (2015).
184 Moroishi, T. *et al.* A YAP/TAZ-induced feedback mechanism regulates Hippo pathway homeostasis. *Genes Dev* **29**, 1271-1284, doi:10.1101/gad.262816.115 (2015).
185 Humbert, N. *et al.* Regulation of ploidy and senescence by the AMPK-related kinase NUAK1. *The EMBO journal* **29**, 376-386 (2010).
186 Wu, Y. & Griffin, E. E. Regulation of Cell Polarity by PAR-1/MARK Kinase. *Curr Top Dev Biol* **123**, 365-397, doi:10.1016/bs.ctdb.2016.11.001 (2017).
187 Tang, Y., Feinberg, T., Keller, E. T., Li, X.-Y. & Weiss, S. J. Snail/Slug binding interactions with YAP/TAZ control skeletal stem cell self-renewal and differentiation. *Nature cell biology* **18**, 917-929 (2016).
188 Kim, M. K., Jang, J. W. & Bae, S. C. DNA binding partners of YAP/TAZ. *BMB Rep* **51**, 126-133, doi:10.5483/bmbrep.2018.51.3.015 (2018).
189 Skene, P. J. & Henikoff, S. An efficient targeted nuclease strategy for high-resolution mapping of DNA binding sites. *Elife* **6**, e21856 (2017).
190 Maruyama, T. *et al.* ZAK Inhibitor PLX4720 Promotes Extrusion of Transformed Cells via Cell Competition. *Iscience* **23**, 101327 (2020).
191 Karaman, M. W. *et al.* A quantitative analysis of kinase inhibitor selectivity. *Nature biotechnology* **26**, 127-132 (2008).
192 Grossman, R. L. *et al.* Toward a shared vision for cancer genomic data. *New England Journal of Medicine* **375**, 1109-1112 (2016).
193 Robinson, M. D., McCarthy, D. J. & Smyth, G. K. edgeR: a Bioconductor package for differential expression analysis of digital gene expression data. *Bioinformatics* **26**, 139-140 (2010).
194 Cox, J. *et al.* Andromeda: a peptide search engine integrated into the MaxQuant environment. *Journal of proteome research* **10**, 1794-1805, doi:10.1021/pr101065j (2011).
195 Tyanova, S. *et al.* The Perseus computational platform for comprehensive analysis of (prote)omics data. *Nat Methods* **13**, 731-740, doi:10.1038/nmeth.3901 (2016).
196 Eid, S., Turk, S., Volkamer, A., Rippmann, F. & Fulle, S. KinMap: a web-based tool for interactive navigation through human kinome data. *BMC Bioinformatics* **18**, 16, doi:10.1186/s12859-016-1433-7 (2017).
197 Gujral, T. S. *et al.* A noncanonical Frizzled2 pathway regulates epithelial-mesenchymal

transition and metastasis. *Cell* **159**, 844-856, doi:10.1016/j.cell.2014.10.032 (2014).
198 Gujral, T. S. & Kirschner, M. W. Hippo pathway mediates resistance to cytotoxic drugs. *Proc Natl Acad Sci U S A* **114**, E3729-E3738, doi:10.1073/pnas.1703096114 (2017).
199 Szulzewsky, F. *et al.* Comparison of tumor-associated YAP1 fusions identifies a recurrent set of functions critical for oncogenesis. *Genes Dev* **34**, 1051-1064, doi:10.1101/gad.338681.120 (2020).
200 Kakadia, S. *et al.* Mechanisms of resistance to BRAF and MEK inhibitors and clinical update of US Food and Drug Administration-approved targeted therapy in advanced melanoma. *Onco Targets Ther* **11**, 7095-7107, doi:10.2147/ott.S182721 (2018).
201 Zanconato, F., Cordenonsi, M. & Piccolo, S. YAP/TAZ at the roots of cancer. *Cancer cell* **29**, 783-803 (2016).
202 Mathews Griner, L. A. *et al.* High-throughput combinatorial screening identifies drugs that cooperate with ibrutinib to kill activated B-cell-like diffuse large B-cell lymphoma cells. *Proc Natl Acad Sci U S A* **111**, 2349-2354, doi:10.1073/pnas.1311846111 (2014).
203 Jansson, K. H. *et al.* High-throughput screens identify HSP90 inhibitors as potent therapeutics that target inter-related growth and survival pathways in advanced prostate cancer. *Sci Rep* **8**, 17239, doi:10.1038/s41598-018-35417-0 (2018).
204 Waters, A. M. & Der, C. J. KRAS: The Critical Driver and Therapeutic Target for Pancreatic Cancer. *Cold Spring Harb Perspect Med* **8**, doi:10.1101/cshperspect.a031435 (2018).
205 Braicu, C. *et al.* A Comprehensive Review on MAPK: A Promising Therapeutic Target in Cancer. *Cancers (Basel)* **11**, doi:10.3390/cancers11101618 (2019).
206 Burotto, M., Chiou, V. L., Lee, J. M. & Kohn, E. C. The MAPK pathway across different malignancies: a new perspective. *Cancer* **120**, 3446-3456, doi:10.1002/cncr.28864 (2014).
207 Roberts, P. J. & Der, C. J. Targeting the Raf-MEK-ERK mitogen-activated protein kinase cascade for the treatment of cancer. *Oncogene* **26**, 3291-3310, doi:10.1038/sj.onc.1210422 (2007).
208 Grimaldi, A. M. *et al.* MEK Inhibitors in the Treatment of Metastatic Melanoma and Solid Tumors. *Am J Clin Dermatol* **18**, 745-754, doi:10.1007/s40257-017-0292-y (2017).
209 Infante, J. R. *et al.* A randomised, double-blind, placebo-controlled trial of trametinib, an oral MEK inhibitor, in combination with gemcitabine for patients with untreated metastatic adenocarcinoma of the pancreas. *Eur J Cancer* **50**, 2072-2081, doi:10.1016/j.ejca.2014.04.024 (2014).
210 Bodoky, G. *et al.* A phase II open-label randomized study to assess the efficacy and safety of selumetinib (AZD6244 [ARRY-142886]) versus capecitabine in patients with advanced or metastatic pancreatic cancer who have failed first-line gemcitabine therapy. *Invest New Drugs* **30**, 1216-1223, doi:10.1007/s10637-011-9687-4 (2012).
211 Brauswetter, D. *et al.* Molecular subtype specific efficacy of MEK inhibitors in pancreatic cancers. *PLoS One* **12**, e0185687, doi:10.1371/journal.pone.0185687 (2017).
212 Ryan, M. B., Der, C. J., Wang-Gillam, A. & Cox, A. D. Targeting RAS-mutant cancers: is ERK the key? *Trends Cancer* **1**, 183-198, doi:10.1016/j.trecan.2015.10.001 (2015).
213 Samatar, A. A. & Poulikakos, P. I. Targeting RAS-ERK signalling in cancer: promises and challenges. *Nat Rev Drug Discov* **13**, 928-942, doi:10.1038/nrd4281 (2014).
214 Rosenbluh, J. *et al.* β-Catenin-driven cancers require a YAP1 transcriptional complex for survival and tumorigenesis. *Cell* **151**, 1457-1473 (2012).
215 Chen, Y. A., Tripathi, L. P. & Mizuguchi, K. TargetMine, an integrated data warehouse for candidate gene prioritisation and target discovery. *PLoS One* **6**, e17844, doi:10.1371/journal.pone.0017844 (2011).
216 Wu, P. K. & Park, J. I. MEK1/2 Inhibitors: Molecular Activity and Resistance Mechanisms. *Semin Oncol* **42**, 849-862, doi:10.1053/j.seminoncol.2015.09.023 (2015).
217 Hirai, H. *et al.* MK-2206, an allosteric Akt inhibitor, enhances antitumor efficacy by standard

chemotherapeutic agents or molecular targeted drugs in vitro and in vivo. *Mol Cancer Ther* **9**, 1956-1967, doi:10.1158/1535-7163.Mct-09-1012 (2010).
218 Ghiso, E. *et al.* YAP-Dependent AXL Overexpression Mediates Resistance to EGFR Inhibitors in NSCLC. *Neoplasia* **19**, 1012-1021, doi:10.1016/j.neo.2017.10.003 (2017).
219 Hafizi, S. & Dahlbäck, B. Signalling and functional diversity within the Axl subfamily of receptor tyrosine kinases. *Cytokine Growth Factor Rev* **17**, 295-304, doi:10.1016/j.cytogfr.2006.04.004 (2006).
220 Gay, C. M., Balaji, K. & Byers, L. A. Giving AXL the axe: targeting AXL in human malignancy. *Br J Cancer* **116**, 415-423, doi:10.1038/bjc.2016.428 (2017).
221 Holland, S. J. *et al.* R428, a selective small molecule inhibitor of Axl kinase, blocks tumor spread and prolongs survival in models of metastatic breast cancer. *Cancer Res* **70**, 1544-1554, doi:10.1158/0008-5472.Can-09-2997 (2010).
222 Lauter, M., Weber, A. & Torka, R. Targeting of the AXL receptor tyrosine kinase by small molecule inhibitor leads to AXL cell surface accumulation by impairing the ubiquitin-dependent receptor degradation. *Cell Commun Signal* **17**, 59, doi:10.1186/s12964-019-0377-8 (2019).
223 Sorrentino, G. *et al.* Metabolic control of YAP and TAZ by the mevalonate pathway. *Nat Cell Biol* **16**, 357-366, doi:10.1038/ncb2936 (2014).
224 Smith, H. L., Southgate, H., Tweddle, D. A. & Curtin, N. J. DNA damage checkpoint kinases in cancer. *Expert Rev Mol Med* **22**, e2, doi:10.1017/erm.2020.3 (2020).
225 Hata, A. N. *et al.* Failure to induce apoptosis via BCL-2 family proteins underlies lack of efficacy of combined MEK and PI3K inhibitors for KRAS-mutant lung cancers. *Cancer Res* **74**, 3146-3156, doi:10.1158/0008-5472.Can-13-3728 (2014).
226 Bedard, P. L. *et al.* A phase Ib dose-escalation study of the oral pan-PI3K inhibitor buparlisib (BKM120) in combination with the oral MEK1/2 inhibitor trametinib (GSK1120212) in patients with selected advanced solid tumors. *Clin Cancer Res* **21**, 730-738, doi:10.1158/1078-0432.Ccr-14-1814 (2015).
227 Shibue, T. & Weinberg, R. A. EMT, CSCs, and drug resistance: the mechanistic link and clinical implications. *Nat Rev Clin Oncol* **14**, 611-629, doi:10.1038/nrclinonc.2017.44 (2017).
228 Song, K. A. & Faber, A. C. Epithelial-to-mesenchymal transition and drug resistance: transitioning away from death. *J Thorac Dis* **11**, E82-e85, doi:10.21037/jtd.2019.06.11 (2019).
229 Song, K. A. *et al.* Epithelial-to-Mesenchymal Transition Antagonizes Response to Targeted Therapies in Lung Cancer by Suppressing BIM. *Clin Cancer Res* **24**, 197-208, doi:10.1158/1078-0432.Ccr-17-1577 (2018).
230 Yochum, Z. A. *et al.* Targeting the EMT transcription factor TWIST1 overcomes resistance to EGFR inhibitors in EGFR-mutant non-small-cell lung cancer. *Oncogene* **38**, 656-670, doi:10.1038/s41388-018-0482-y (2019).
231 Spielmann, M. *et al.* Exome sequencing and CRISPR/Cas genome editing identify mutations of ZAK as a cause of limb defects in humans and mice. *Genome research* **26**, 183-191 (2016).